DESIGN, CHARACTERIZATION AND MODELING OF HIGH TEMPERATURE PROTON EXCHANGE MEMBRANES IN DEAD ENDED ANODE OPERATED POLYMER ELECTROLYTE MEMBRANE FUEL CELL

A THESIS SUBMITTED TO THE GRADUATE SCHOOL OF ENGINEERING AND NATURAL SCIENCES

BY

LALE IŞIKEL ŞANLI

IN

PARTIAL FULFILLMENT OF

THE REQUIREMENTS FOR THE DEGREE

OF

DOCTOR OF PHILOSOPHY

SABANCI UNIVERSITY

SPRING 2013

DESIGN, CHARACTERIZATION AND MODELING OF HIGH TEMPERATURE PROTON EXCHANGE MEMBRANES IN DEAD ENDED ANODE POLYMER ELECTROLYTE MEMBRANE FUEL CELL
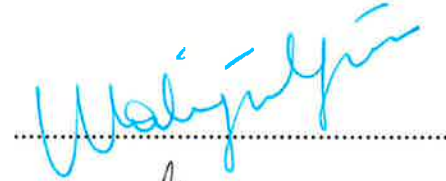
APPROVED BY

Assoc. Prof. Dr. Selmiye Alkan Gürsel
(Thesis Supervisor)
....

Assoc. Prof. Dr. Serhat Yeşilyurt
(Thesis Co-advisor)
....
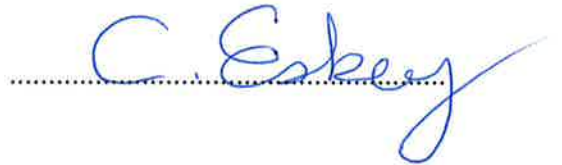
Prof. Dr. Mehmet Ali Gülgün
....

Assoc. Prof. Dr. Ahmet Onat
....

Prof. Dr. Can Erkey
....

DATE OF APPROVAL: 30/07/2013

DESIGN, CHARACTERIZATION AND MODELING OF HIGH TEMPERATURE PROTON EXCHANGE MEMBRANES IN DEAD ENDED ANODE OPERATED POLYMER ELECTROLYTE MEMBRANE FUEL CELL

LALE IŞIKEL ŞANLI
Mechatronics Engineering, Ph.D. Thesis, 2013
Thesis Advisor: Assoc. Prof. Dr. Selmiye Alkan Gürsel
Thesis Co-Advisor: Assoc. Prof. Dr. Serhat Yeşilyurt

Key words: Fuel Cell, Dead Ended Anode, High Temperature, Proton Exchange
Membrane, Degradation, Numerical Modeling

ABSTRACT

Polymer electrolyte membrane fuel cells (PEMFC) have the potential to reduce our pollutant emissions and dependence on fossil fuels. Factors such as complex balance-of-plant design and cost still remain as the major barriers to fuel cell. The eradication of the two main shortcomings of PEMFC has been targeted in this thesis study. The first shortcoming is high cost of the membrane and its water depended low operation temperature. The second one is the complex balance-of-plant design of PEMFC system.

The synthesized, radiation grafted, high temperature proton conducting membrane improves the operation temperature of conventional PEMFC (i.e., <80 °C) up to 120 °C. The novel, high temperature proton conducting membrane eliminates the electrochemical by product water and improves the overall performance of PEMFC. Moreover, the synthesized, high temperature proton conducting membrane is cost competitive and very well suited for bulk production in any defined size.

The dead ended anode (DEA) operation is considered as an alternative to the conventional PEMFC system. The operation with a DEA reduces fuel cell system cost, weight, and volume since the anode external humidification and recirculation hardware can be eliminated. Thus, the conventional PEMFC system is modified according to DEA operation in the study. The shortcomings of the commercial membrane in the DEA operation have been reduced with the synthesized, high temperature proton exchange membrane.
Additionally, a transient, one dimensional along the channel numerical model is developed. The model is used to understand the two phase water transport mechanism during a low temperature DEA operation.

YÜKSEK SICAKLIK PROTON DEĞİŞİM MEMBRANLARININ TASARIM, KARAKTERİZAYON, MODELLENMESİ VE ANOT ÇIKIŞ KAPALI POLİMER ELEKTROLİT YAKIT HÜCRESİ İÇERİSİNDE ÇALIŞTIRILMASI

LALE IŞIKEL ŞANLI
Mekatronik Mühendisliği, Ph.D Tezi, 2013
Tez Danışmanı: Doç. Dr. Selmiye Alkan Gürsel
Tez Yardımcı Danışmanı: Doç. Prof. Dr. Serhat Yeşilyurt

Polimer elektrolit membran yakıt hücreleri (PEMFC) artan kirlilik yayılımımızı ve fosil yakıtlara bağımlılığımızı azaltma noktalarında çok büyük potansiyele sahiptirler. Fakat, karmaşık sistem yapısı ve yüksek maliyet gibi faktörler yakıt hücrelerinin yaygınlaşması önündeki önemli engellerdir.Yakıt hücrelerindeki iki ana dezavantajın iyileştirilmesi ve geliştirilmesi bu tezin amacı olmuştur. Bunlaradan bir tanesi membran maliyeti ve membranın suya bağımlı iyonik iletlenliği nedeni ile hücresinin düşük çalışma sıcaklığıdır. İkincisi ise yakıt hücresi sisteminin karmaşık dizaynıdır.

Bu tez çalışmasında sentezlenen radyasyon başlatmalı aşı kopolimer membralar geleneksel yakıt pili çalışma sıcaklığını (< 80 °C) 100 °C üzerine çıkarabilmektedir. Bunun yanında sentezlenen yüksek sıcaklık membranların maliyetleri oldukça düşükdür ve istenilen boyutlarda kolaylıkla üretilebilmektedir.

Anot çıkış kapalı (AÇK) çalışma prensibi, geleneksel yakıt hücresinin karmaşık sistem dizaynına alternatif olarak düşünülmüştür. AÇK çalışma prensibi yakıt hücresinin maliyetini, ağırlığını ve hacmini azaltma konularında avantajlara sahiptir. Anot kısmının harici nemlendirmesi ve hidrojenin sirkülasyon komponentlerinin sistemden çıkarılması AÇK çalışma ile mümkündür. Bu nedenle, bu tez çalışmasında yakıt hücresi, AÇK çalışacak şekilde modifiye edilmiştir. Ayrıca, AÇK çalışma prensibinin ticari membrandan kaynaklanan dezavantajlarının, sentezlenen radyasyon başlatmalı aşı kopolimer, iyon değişim yüksek sıcaklık membranları ile giderilmesi de yine bu tezin konusudur.Bu çalışmalara ek olarak, zamana bağlı, bir boyutlu ve iki fazlı numerik model çalışması yapılmıştır. Numerik model, ticari membran ile düşük sıcaklık AÇK prensibinde çalışan iki fazlı suyun incelenmesi için kullanılmıştır. Ayrıca, numerik model sentezlenen yüksek sıcaklık membranının AÇK prensibinde çalışmasını incelemek için gelecek çalışmalarda kullanılabilecektir.

To my bellowed ones; Bahar, Güven and Ayşe for helping me find the light in my day.

ACKNOWLEDGEMETS

List of Contents

List of Tables

List of Figures

CHAPTER 1

INTRODUCTION

There are two key problems with the continued use of fossil fuels, which meet about 80% of the world energy demand today. The first problem is that they are limited in amount and sooner or later they will be depleted. Thus, there will be a gap between demand and production of fossil fuels. The second problem is that fossil fuels are causing serious environmental problems, such as global warming, environmental changes, rising sea levels. The hydrogen energy system has been proposed as a solution for these two interconnected global problems. Hydrogen can be converted to electricity in fuel cells with higher efficiencies than conversion of fossil fuels to mechanical energy in internal combustion engines. This unique property of hydrogen made the hydrogen fuel cells an alternative choice for car companies. The reason for higher efficiency of hydrogen fuel cell is that they are electrochemical engines and not limited with the Carnot Efficiency limits. Moreover, unlike the batteries a fuel cell does not need recharging as long as fuel supplied from an external source and anode and cathode are not consumed during the cell operation.

The electrolyte of hydrogen fuel cells defines the key properties, such as operating temperature and fuel type of the fuel cell so that fuel cell technologies are named by their electrolyte. There are five distinct types of fuel cells; polymer electrolyte membrane fuel cell (PEMFC), alkaline fuel cell (AFC), phosphoric acid fuel cell (PAFC), molten carbonate fuel cell (MCFC) and solid oxide fuel cell (SOFC). Among them, PEMFC has gained great attention due to its major advantages, including quick start-up time, pollution free operation and solid-compact construction.

1.1 WHAT IS A PEM FUEL CELL?

PEMFC is an electrochemical device that converts chemical energy to electricity. The device is composed of a membrane electrode assembly (MEA) covered by two porous gas diffusion layers (GDL) that are mostly carbon based cloth, paper or felt, placed between two current collector plates. Proton exchange membrane plays dual roles of gas separation and proton conduction in a PEMFC. Today's commercial proton exchange membrane Nafion® is a perfluorosulfonic acid membrane (PFSA). It has high proton conductivity that is strongly correlated with its water content. High water content results in low internal resistance to proton conductivity in PEMFC. On the other hand, high water content clogs the GDL pores resulting in mass transport losses on both anode and cathode. The basic structure of the PEMFC is shown in **Figure 1.1**. The fuel and oxygen are delivered across the active area through gas flow channels. These channels are typically CNC machined conductive graphite, allowing electron transfer to the current collectors and completion of the electric circuit. The ratio of channel width to rib (contact) width, and the channel flow-field pattern are important design parameters affecting fuel cell performance.
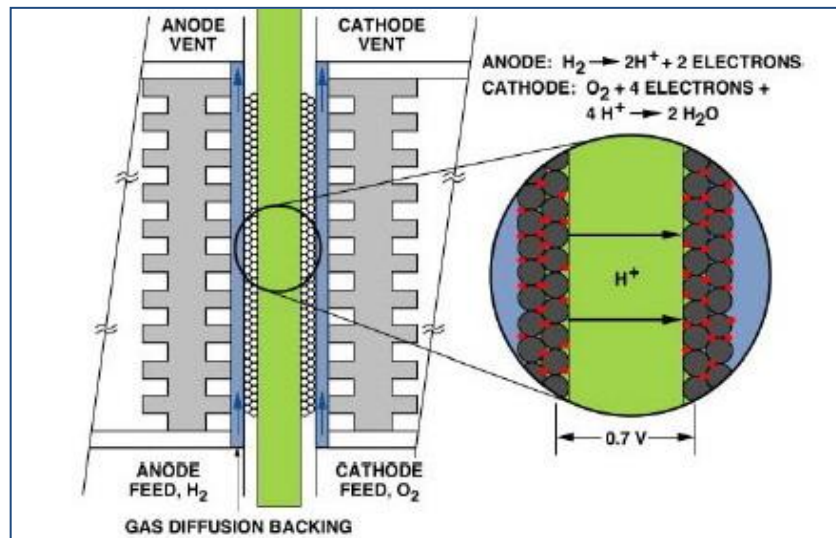
Figure 1.1: Basic PEMFC structure schematic [1]

The Gas Diffusion Layer (GDL) is used to evenly distribute the reactant gases from the channel to the catalyst surface in the area under the ribs and channels. It is also designed to remove the product water from the catalyst area, by treatment of the carbon

with a hydrophobic coating (such as PTFE). The catalyst layer where the reaction takes place contains platinum (Pt) particles supported on a powdered carbon structure (**Figure 1.2**).
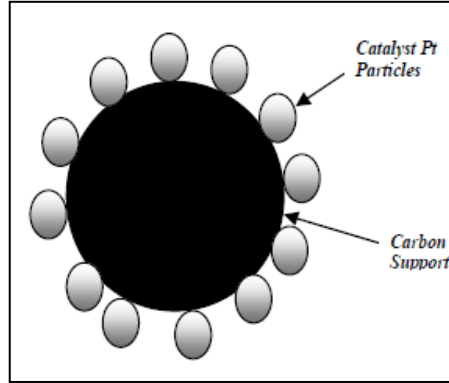
Figure 1.2: Idealized structure of catalyst layer

For the reaction to take place at the cathode, all three reactants, protons, oxygen, and electrons, must be able to reach the Pt catalyst. Protons are conducted through the proton exchange membrane, electrons through the carbon support structure, and oxygen gas through the pore space. Therefore, each Pt particle must be in contact with all three portions of the cell (three phase interface) [1]. A thin micro porous layer (MPL) can also be inserted between the GDL and catalyst layer to increase the water removal from the catalyst or membrane hydration [2]

1.2 OPERATING CELL VOLTAGE

The theoretical cell voltage of the hydrogen fuel cell in at a defined temperature and pressure is calculated with Nerst equation (Eq. 1.1).

$$\Delta G = \Delta G_0 - RT \ln \frac{p_A^a p_B^b}{p_C^c p_D^d} \tag{1.1}$$

where ΔG is the Gibbs free energy, T temperature, R universal gas constant and P is pressure. Since the Gibbs free energy is reversible electrical energy, i.e. Eq. (1.2)

$$\Delta G = W_e = -n_e FNVrev \tag{1.2}$$

Then for hydrogen fuel cells reversible cell voltage at a certain pressure and temperature can be written as in Eq. (1.3)

$$V_{rev} = V_{rev,0} + \frac{RT}{nF} \ln \frac{p_{H_2} p_{O_2}^{1/2}}{p_{H_2O}} \qquad (1.3)$$

For PEMFC Eq. (1.3) can be written as below Eq. (1.4) and gives the theoretical cell voltage at a certain pressure and temperature [3].

$$E_{T,P} = 1,482 - 0.000845T + 0.0000431\ln(P_{H2}P_{O2}^{0.5}) \qquad (1.4)$$

If the fuel cell is supplied with reactant gases, but no current is driven, the voltage is called open circuit voltage (OCV) will be lower than the calculated theoretical reversible cell voltage, i.e. Eq. (1.4). This suggests that there are some losses in the fuel cell even with no external current generated. There are different kinds of voltage losses (or polarizations) in PEMFC that are explained in below.

Activation Losses

When hydrogen reacts and splits into electrons and protons at the anode, energy is released; however, some energy must be supplied to get over the energy barrier. This energy is called activation energy, which is the amount of energy that must be subtracted from Gibbs free energy of reaction for the reaction to occur. Activation losses are expressed by Tafel equation, Eq. (1.5):

$$V_{act} = \frac{RT}{\alpha F} \ln(\frac{i}{i_0}) \qquad (1.5)$$

where α is the charge transfer coefficient. Its value depends on the reaction involved and the material the electrode is made from, and it is in range of 0-10. i_0 is called the exchange current density. If this current density is high, and then the surface of the electrode is more active. The exchange current density is critical in controlling the performance of fuel cell electrodes.

Internal Currents and Crossover Losses

Although the electrolyte is a polymer membrane and impermeable to reactant gases, some small amount of hydrogen diffuses from anode to cathode and some electrons may also find a shortcut through the membranes. Each hydrogen molecule that diffuses through the membrane and reacts with oxygen on the cathode results in two electrons generated. These losses may be insignificant however, when the fuel cell is at

open circuit potential or at low current densities these losses have a dramatic effect on the cell potential. The total electrical current is the sum of external (useful) current and current losses due to the crossover and internal currents, i.e., $i=i_{ext}+i_{loss}$, Eq. (1.5) can be rewritten in Eq. (1.6),

$$V_{act} = \frac{RT}{\alpha F}\ln(\frac{i_{ext}+i_{loss}}{i_0})$$ (1.6)

Ohmic Losses

Ohmic losses occur because of resistance to the flow of ions in the electrolyte and resistance to the flow of electrons through the electrically conductive fuel cell components. Ohmic losses follow the Ohm's Law and are expressed as in Eq. (1.7)

$$V_{ohm} = i_{ext}R_{int}$$ (1.7)

i_{ext} is the current density and R_i is the total internal resistance. The typical values for R_i are between 0.1 and 0.2 Ω cm^2 in a PEMFC. There are three ways of reducing the internal resistance: i) using highly conductive electrodes, ii) good cell design in bipolar plates and current collectors, iii) reducing the electrolyte thickness as much as possible.

Mass Transport (Concentration) Losses

Mass transport is the process of supplying reactants and removing products. In the operation, there are two phase transport in PEM fuel cell: i) gas phase transport which is the form of reactants ii) Liquid phase transport which is the form of products (i.e., water). Poor mass transport can be caused by a change in the concentration of reactant and product within the catalyst layer. And, it is know that the electrochemical reaction potential changes with partial pressure of the reactants, this relationship is given by the Nernst equation. The Nernst equation is modified according to the Fick's Law, the mass transport losses can be written as below Eq. (1.8),

$$V_{mass} = \frac{RT}{\alpha F}\ln(\frac{i_L}{i_L-i})$$ (1.8)

where i_L is the limiting current density in the catalyst layer, and is the maximum current density that can be used to obtain ideal electrode reaction without polarization.

Polarization Curve

A polarization curve is the most important characteristic of a fuel cell and its performance. **Figure 1.3** shows how the cell polarization curve is formed, by subtracting the activation losses, ohmic losses and concentration losses from the OCV. It should be noted that in this figure anode and cathode activation losses are lumped together, but a majority of the losses occur on the cathode because of the slow oxygen reduction reaction.
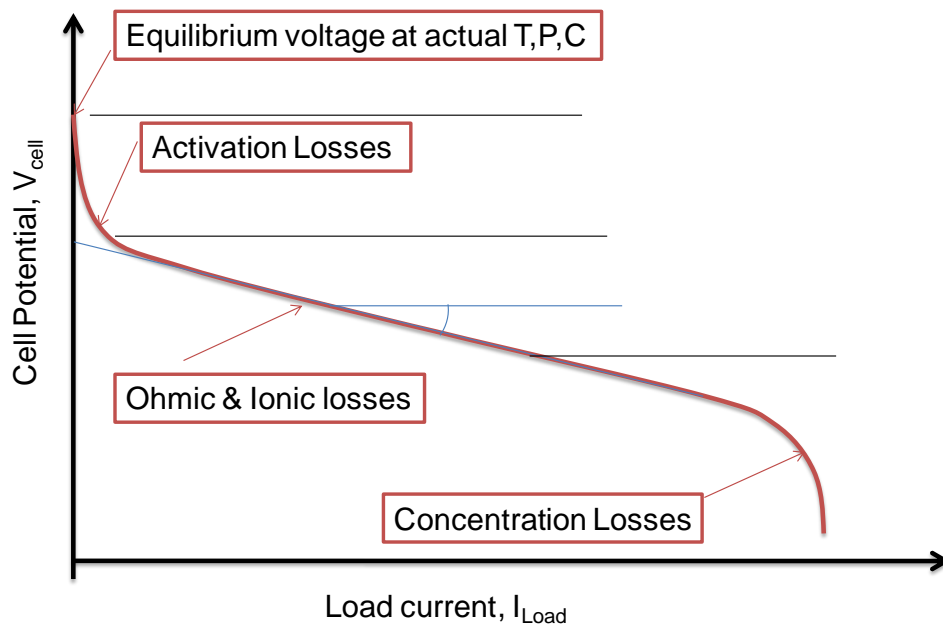
Figure 1.3: Voltage losses in the fuel cell and resulting polarization curve

1.3 FUEL MANAGEMENT AND DEAD ENDED ANODE OPERATION

Fuel managements of a PEMFC system can be classified as flow through mode (FTA), recirculation mode (RCA), and dead-end mode (DEA). In the FTA and RCA mode, excess hydrogen is supplied to the anode due to the electrochemical polarizations. Lower hydrogen flow rate may cause hydrogen starvation near the anode outlet. The hydrogen starvation could cause reverse-current, resulting in the carbon corrosion of the catalyst and degradation of the fuel cell. In the RCA, non-reacted residual hydrogen is re-circulated back to the supply line by a pump or an ejector.

There has been worldwide interest in the development and commercialization of PEMFC; however the conventional RCA operating system has drawbacks such as complex balance-of-plant design. The RCA requires hydrogen grade an ejector/blower, water separator, and hydrogen humidification. These components add weight, volume, and expense to the system. Moreover, the water must be removed from the hydrogen exiting the anode before it goes to the ejector and then the dry hydrogen supplied to the anode must be re-humidified to prevent over-drying of the membrane due to the higher flow rate.

Thus, the DEA operation is an alternative approach to reduce the complexity of overall system [4]. The advantages of this design are mostly due to the elimination of costly hardware for anode humidification and hydrogen recovery components that reduces power density of system by adding weight and volume.

In a typical DEA operation, dry hydrogen is fed to the anode by pressure regulator, thus channel pressure remains constant **(Figure 1.4)**. On the other hand, the cathode is operated in flow through conditions with a stoichiometry ratio (SR) greater than one. However, during a DEA operation, nitrogen and vapor/liquid water are accumulated in anode GDL and gas flow channels. In the driving mechanism, nitrogen is pushed toward the end of the anode channel by the flow of reactants and accumulates. The accumulating N_2 prevents hydrogen from reaching the catalyst layer [5]. Water vapor gradients between the humidified cathode and the dry anode also drive excess water into the anode, which can cause significant liquid water accumulation. This liquid water accumulation in the channel and GDL blocks the flow of reactants and stops the production of electricity in the affected active area of the cell. The gas velocity, driven by consumption of hydrogen, pulls nitrogen and water toward the bottom of the channel. Gravity helps to stabilize the system as heavier molecules get pushed toward the bottom. The mass accumulation physically blocks hydrogen gas from reaching the anode catalyst sites, which is the mechanism for the experimentally observed and recoverable voltage degradation [5,6,7]. Therefore, a cyclic purging that releases accumulated nitrogen and water is needed in a DEA operation. Purging is maintained by a solenoid valve at an anode downstream (exit). There are many studies for purge time optimization however, on average the purging event occurs between 20-900 ms. After the purge, the active area contributing to the reaction increases and hence the measured voltage increases.
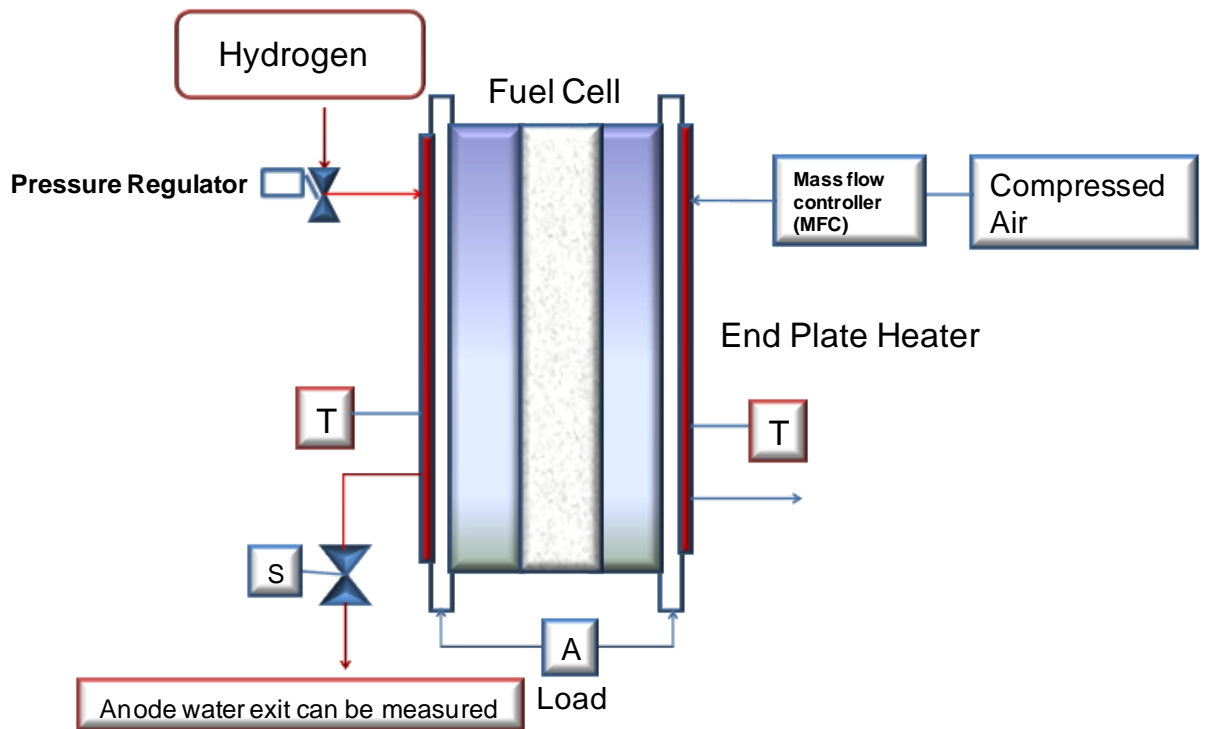
Figure 1.4: Schematic of DEA operated PEMFC

A proper water management in a DEA operation is essential in order to keep the membrane sufficiently humidified whilst ensuring that the anode does not flood due to water accumulation at low operation temperatures of PEMFC (<100 °C). The control of air flow rate, cathode pressure, cathode inlet relative humidity, and stack temperature are all tied to control the water management.

1.4 ADVANTAGES OF THE HIGH TEMPERATURE OPERATION

The shortcomings of the DEA operation might be correlated with the limit on its operation temperatures (60-80 °C). This limit largely arise from the current state-of-the-art PFSA membranes such as Nafion[®] because of its water dependence for proton transport and low glass transition temperature (T_g) that is below 100 °C. However, the water inside the PEMFC limits the expensive electrode life time by carbon corrosion. It blocks the electrochemical reaction areas and leads to severe voltage losses so that it is a major drawback on the PEMFC commercialization.

Higher operating temperatures mean that water management is simplified significantly as there is only a single (gaseous) phase present. This means that the

transport of water in the membrane, electrodes and diffusion layer is easier and flow field plate design can be simplified.

Another effect of the higher temperatures is that the reactant and product gases are expected to have increased diffusion rates and with no liquid water present to block the electrochemically active surface area thus reaction rate increases. The simplified water management means that much simpler flow field designs can be used which should help decrease the overall cost of the stack as machining plates should be cheaper. Moreover, operating at high temperatures brings another side advantage to the PEMFC. Since primary catalyst platinum in PEMFC has a significant affinity for carbon monoxide (CO) which is a byproduct of reformation, the catalyst layer is deformed that causes power losses in PEMFC. As a result, trace levels of carbon monoxide can cause a large decrease in the performance of the PEMFC that operates at temperatures below 80 °C due to poisoning effect. High temperature operation avoids this problem, at high temperatures, the affinity for carbon monoxide is reduced and CO tolerance is increased.

Even though higher operating temperatures have many advantages as listed above, there is a concern which could affect commercial viability for automobile applications. The concern is the increased start-up time (up to 40 min in some cases). The high temperature fuel cell must slowly be brought up to its operating temperature which could mean waiting for half an hour after start-up before any current can be drawn. As the average driving range is only around 23 miles per day in the UK this would rule out high temperature PEMFC use for any short distance driving. Thus, as the US Department of Energy (DOE) states there is a gap where the appropriate materials are missing for temperatures 80-120 °C so that high temperature proton conducting membrane synthesis study in this thesis aims to fill that open window.

1.5 SCOPE OF THE THESIS STUDY

The shortcomings of the conventional PEMFC system represented the point of take off for this research, which is to operate PEMFC in DEA mode at high temperatures (100-120 °C) with the synthesized high temperature proton exchange membranes. DEA operation at temperature above 100 °C will reduce the disadvantages of conventional PEMFC system complexity and low temperature listed above.

This thesis study has three parts; proton conducting membrane synthesis for high temperature operation, high temperature DEA operation of the synthesized membranes and the modeling studies.

In the membrane synthesis part, to create water free proton conducting mechanism, nitrogen containing monomers 4-vinyl pyridine (4VP), 2-vinyl pyridine (2VP) and *N*-vinyl-2-pyrrolidone (NVP) monomers are graft copolymerized into poly (ethylene-*alt*-tetrafluoroethylene) (ETFE) in an aqueous medium by radiation induced grafting. Subsequent phosphoric acid doping was carried out in order to introduce acidic functionality required for proton conduction. Due to the interaction between N-H sides, a proton hopping mechanism to mobilize the protons is created without any dependence of water inside the membrane. Because of the ability of water independent proton transport mechanism membranes can operate at high temperature conditions. From this point, the proton conduction mechanism differs from that of perflorosulfonic acid (PFSA) membranes, i.e., Nafion®. Since the radiation grafting method relatively simpler than other polymerization methods, alternative and cost competitive proton exchange membranes can be manufactured. The resultant high temperature proton exchange membranes in the thesis were studied in detail for fuel cell relevant properties including proton conductivity, water uptake, mechanical properties and thermal properties. Moreover, the phosphorous distribution is also investigated to obtain information about the homogeneity of the membranes.

In the second part; DEA operation of the synthesized membranes is the main focus. FTA and DEA single cell operation of commercial and synthesized high temperature proton exchange membranes have been conducted. The fuel cell test station Greenlight® FC G50 is modified and calibrated to control the applied load, pressure, flow, temperature and relative humidity of the gas streams. The DEA operation of both Nafion® membrane and synthesized high temperature proton exchange membrane were investigated.

In the last part of study, time-depended, one-dimensional, along the channel numerical model of DEA operated PEMFC is presented. The model is validated with Siegel et al. [8] physical experiment to understand the two phase transport of liquid/vapor water in a DEA operated PEMFC at low operating temperatures. The model exhibit very well agreement with the experiments. The accumulated liquid water amount at anode/cathode gas channels and GDL can be predicted by our two phase

transport model. Additionally, the time of onset hydrogen starvation due to the accumulated species can be predicted with our numerical model.

As summary, the thesis is motivated by the desire to improve the overall performance of PEMFC system by operating in DEA mode at temperatures 100-130 °C to contribute PEMFC adaptation.

The three main part of this thesis study can be summarized in **Table 1-1**,

| Membrane | Membrane Synthesis | Single Cell Testing | | Numerical Modeling |
		FTA operation	DEA operation	
Nafion® Membrane	Commercial Nafion® membrane was used.	Greenlight® FC G50 test station was modified and calibrated. FTA operated PEMFC tests of Nafion® membrane was conducted.	DEA operated PEMFC tests of Nafion® membrane were conducted	Time-depended, 1D along the channel numerical model of DEA operated PEMFC at low operation temperatures
High Temperature Membrane	Synthesis and characterization of the high temperature proton exchange membranes by radiation induced grafting were performed	FTA operated PEMFC tests of synthesized high temperature membranes were conducted.	DEA operated PEMFC tests of high temperature membranes were conducted.	Is the subject of our future study.

Table 1-1: Summary of the three main parts in the thesis study

CHAPTER 2

SYNTHESIS AND CHARACTERIZATION OF RADIATION INDUCED GRAFT COPOLYMERS

2.1. INTRODUCTION

One of the commonly used methods for modifying the surface and bulk properties of polymeric materials is to graft monomers onto them by using an irradiation technique known as radiation-induced grafting. Radiation- induced grafting method has the advantages such as simplicity, low cost, control over process, and adjustment of the materials composition and structure. In addition, this method assures the grafting of monomers that are difficult to polymerize by conventional methods without residues of initiators and catalyst 9. Radiation-induced grafting is simply based on the irradiation of a base polymer either in the presence of a monomer (simultaneous radiation grafting) or without a monomer (pre-irradiation grafting) to create active sites as shown schematically in **Figure 2.1**. Radiation grafting can also be used to combine the proton-conducting properties of a graft component with the thermal and chemical stability of the fluoropolymer base films together in membranes suitable for the application in PEMFC and other electrochemical devices. The attractiveness of this technique is based on the possibility to easily tune and control several parameters in a wide range. The radiation grafting involves the use of different radiation types (electron-beam, γ-rays and X-rays), and may be carried out using different methods.

The radiation grafting was directed towards the use of perfluorinated and partially fluorinated polymers in the preparation of proton exchange membranes for fuel cell, due to their outstanding and unique combination of useful properties [10, 11] such as high thermal stability, hydrophobicity, resistance to ageing and to oxidation,

chemical inertness, low permeability to gas, hydrolytic stability, low flammability, high surface energy. Several studies were carried out based on perfluorinated polymers such as PTFE [12,13,14] FEP [15-18], PFA [19, 20] and partially fluorinated base materials such as PVDF [21, 22], ETFE [10, 23,24] and others [25]. Nevertheless, there are similarities and differences between the perfluorinated and partially fluorinated polymers due to the existence of C-H bonds in the latter. The high polarity of the C-F bond contributes strongly to the observed stability of fluoropolymers [26]. When subjected to ionizing radiation, the fluoropolymers may undergo different changes in the chemical and physical properties. The mechanism and the extent of changes are relative to the nature of the fluoropolymers, their intrinsic properties, and to the irradiation conditions.

The irradiation of polymers in general leads to the formation of active species, which depending on the conditions may be radicals or ionic species [27]. The formed active species result from either homolytic or heterolytic bond scission reactions. The active sites formed in the long polymer chain tend to be highly selective in nature. Thus, the reaction of produced active species is either dominated by crosslinking, chain scission, or by other chemical changes (formation of oxidative degradation products (hydroperoxide, acid fluoride and many others) [27,28]. For the grafting process, the lifetime of the active species (radicals or ions) is of major importance and can be controlled easily, either by reducing the temperature or working under vacuum (e.g. irradiated ETFE, FEP and PVDF stored from -18 to -60 °C for a periods of 4 months to 1 year) [29].

It was previously reported that the favorable performance and durability of radiation-grafted membranes based on styrene and its derivatives for low-temperature PEMFC [30–32]. However, so far, only limited attention has been paid on the preparation of proton exchange membranes by radiation grafting for high-temperature fuel cell applications [33].
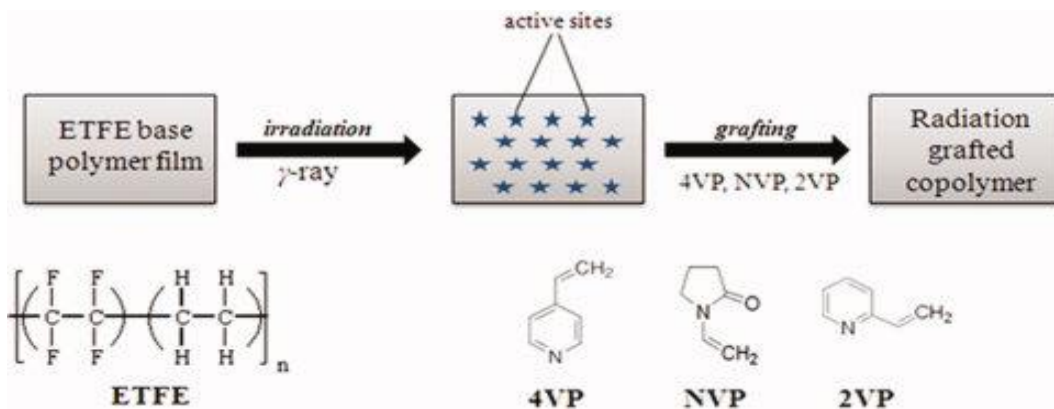
Figure 2.1: Radiation-induced grafting by pre-irradiation method

In this study, nitrogen containing vinyl monomers, *N*-vinyl-2-pyrrolidone (NVP), 4-vinyl pyridine (4VP), and 2-vinyl pyridine (2VP) have been proposed as alternative grafting monomers to establish strong hydrogen bonding between N-H atoms that highly contributes to both ionic conductivity and durability of the membranes that will be used in high-temperature PEMFC. Poly(ethylene-alt-tetrafluoroethylene) (ETFE) has been employed as the base polymer for the preparation of membranes by radiation-induced grafting method due to its higher radiation stability and superior mechanical properties compared with perfluorinated polymers and better compatibility with the graft component [31,34,35].

4VP has been studied previously due to its interesting property changes that can result from the presence of the polar pyridine ring. Much previous work was oriented toward radiation grafting of 4VP into various base polymers including polyethylene [36], polyvinylchloride [37], styrene-butadiene-styrene triblock polymer [38], poly(tetrafluoroethylene-*co*-hexafluoropropylene) [40] and there is only limited information available on the optimization of grafting and characterization [36–40]. Grafting of NVP onto poly(tetrafluoroethylene) [41], low density polyethylene [42] (tetrafluoroethylene- perfluorovinyl ether) copolymer [43], poly(tetrafluoroethylene-hexafluoropropylene-vinylidenefluoride) [44] and polypropylene [45] by radiation grafting was reported earlier only in a few studies. However, up to know, there are only two studies on radiation grafting of 2VP [46,47] both are about the grafting of 2VP onto isotactic polypropylene. However, no systematic research has been reported on the effect of grafting conditions. In addition, these monomers were not employed before for

the preparation of proton exchange membranes for fuel cells by radiation grafting except for a study in literature in which 4VP was used [37].

It is known that the use of solvents in radiation grafting enhances the accessibility of monomer to the grafting sites due to the ability of the solvent to swell the base polymer and the nature of the solvent may influence the grafting kinetics, the length of grafted chains, and the polymer microstructure. Correct choice of solvents is one of the essential elements toward the success of radiation-induced grafting process. There are only a few publications on the influence of solvents on radiation-induced grafting of different monomer/base film combinations [40,48-51]. However, research is still needed for understanding of the effect of solvents on grafting and properties of copolymers.

Consequently, not only the base polymer used but also grafting process (simultaneous radiation grafting, e-beam irradiation, high irradiation doses, grafting in aqueous media or bulk grafting, etc. were performed mostly in literature) are very different from our current process. Therefore, it is desirable to investigate both the grafting of these monomers onto ETFE and characterization of the resultant graft copolymers in detail. Preirradiation grafting, which is only suitable for the grafting of crystalline base polymers where radicals remain trapped for a long period, is employed. Grafting conditions especially the effect of solvents during radiation grafting is investigated in detail in this part of thesis study. Moreover, resultant graft copolymers are characterized *ex situ* by Fourier transform infrared (FTIR) spectroscopy, dynamic mechanical analysis (DMA), and scanning electron microscopy-energy dispersive spectroscopy (SEM-EDAX).

2.1. EXPERIMENTAL

2.1.1. Materials and Method

The base polymer poly(ethylene-*alt*-tetrafluoroethylene), or ETFE, was purchased in the form of a 25 μm thick film (Nowoflon ET-6235) from Nowofol GmbH (Siegsdorf, Germany). The reagents used during membrane preparation, monomers (NVP, 4VP, and 2VP), and solvents (Sigma Aldrich), were used without any further purification. The base polymer, ETFE was cut into 7 cm x 7 cm, washed with ethanol,

and then, dried in a vacuum oven at 80 °C for 1 h. The dried films were placed one by one in polyethylene zip-lock bags to prevent contamination.

Irradiation of the films was performed at γ-Pak Sterilization (Çerkezköy, Turkey) using gamma rays from a ^{60}Co source. The irradiation was carried out in air at room temperature with doses of 10–50 kGy. After exposure, the films were stored at -10 °C until used. Irradiated films were placed into glass tube reactors and then grafting solution composed of monomer and solvent was added to reactors which were then purged with dry nitrogen for 30 min. The reactors were subsequently sealed and placed in thermostated water bath, and grafting reactions were carried out for certain times to achieve reasonable grafting by irradiation dose. The grafted films were washed with the solvent used during grafting to remove residual monomer and/or polymer, which were not bonded to the base film, then dried at 70 °C and reweighed. The extent of graft polymerization, grafting percentage, or graft level (GL) is calculated as follows:

$$GL\ (\%) = \frac{w_g - w_i}{w_i} x100$$

where w_i and w_g are the weights of the film before and after grafting, respectively.

2.1.2 Fourier Transform Infrared Spectroscopy

The structure of both the base polymer film and the graft copolymer films was analyzed by FTIR spectroscopy. Measurements were carried out with a Bruker Equinox 55 FTIR spectrometer in absorbance mode in a wave number range of 4000 cm^{-1} to 500 cm^{-1}.

2.1.3 Dynamic Mechanical Analysis

Mechanical properties of the resultant graft copolymers were studied by a Netzsch 242C dynamic mechanical analyzer (DMA). The measurements were done in the tensile mode at an oscillation frequency of 1 Hz. The dimensions of the test films were 0.5 cm in width and 2 cm in length. The sinusoidal amplitude of strain was applied during the temperature sweep from 25 to 200 °C at a rate of 1 °C/min. The value of glass transition temperatures was evaluated from the loss tangent (tan δ) curve as the maximum of the peak.

$$\tan \delta = \frac{E''}{E'}$$

where E'' is loss modulus and E' is storage modulus of the graft copolymer.

2.1.4 Scanning Electron Microscopy-Energy Dispersive Spectroscopy

SEM-EDAX (Supra 35VP, Leo, Germany) measurement was conducted to investigate the nitrogen distribution on the surface of the copolymer films. An accelerating voltage of 10 kV was used during the measurements.

2.3 RESULTS AND DISCUSSION

2.3.1 Radiation Grafting

Radiation-grafted copolymers based on three different nitrogen containing vinyl monomers were synthesized in various solvents including; *n*-propanol, isoproponol, benzyl alcohol, methanol, ethanol, cyclohexanone, THF, nitromethane, 1,4-dioxane, and *n*-heptane. The resultant copolymers from 4VP/ETFE, NVP/ETFE, and 2VP/ETFE grafting were abbreviated as ETFE-*g*-P4VP, ETFE-*g*-PNVP, and ETFE-*g*-P2VP, respectively.

Figure 2.2 represents the variation of graft level for 4VP grafting onto ETFE in different solvents. Two different 4VP concentrations, 30% (v/v) and 50% (v/ v), were applied. Because of the high reactivity of 4VP, desired graft levels can be achieved by using short reaction time and low irradiation dose which has the advantage of reduced radiation damage to the base polymer. It is evident that higher monomer concentration yielded higher graft levels due to the availability of monomer at grafting sites. It was found that graft level of the copolymers was strongly dependent on the type of solvent used during grafting. Graft levels of ETFE-*g*-P4VP copolymers decrease in the order of cyclohexanone > *n*-propanol > isoproponol > ethanol > THF > benzyl alcohol > nitromethane > methanol > 1,4-dioxane > *n*-heptane.
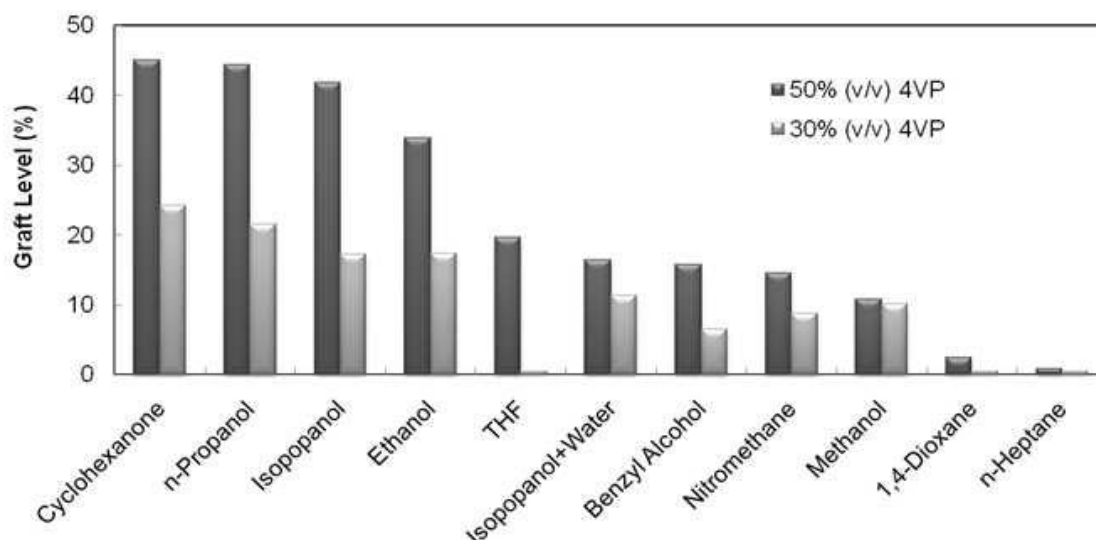
Figure 2.2: Effect of solvent on graft level (%) for 4VP grafting onto ETFE at different 4VP concentrations. Grafting conditions: 25μm ETFE, 10 kGy, 60 °C.

The radiation grafting reaction is governed by the diffusion of monomers into the base film, step growth reaction of the grafted chains, and termination reactions. Since the base polymer films are insoluble in all common solvents and barely swell, grafting takes place at the film surface and behaves as the grafting front. This grafted layer swells in the reaction medium and further grafting proceeds by the progressive diffusion of the monomer through this swollen layer and grafting front movement to the middle of the film. This mechanism is known as grafting front mechanism [51]. Grafting occurs uniformly and smoothly in a solvent which provides the swelling of grafting front. The diffusion of the monomer to the base polymer and swelling of grafting front are mainly determined by the solubility parameters of the grafting components (solvent, monomer/ polymer). As shown in **Figure 2.2**, high graft levels achieved in cyclohexanone, n-propanol, and isopropanol can be explained by the close proximity of solubility parameters of these solvents with 4VP and poly(4-vinyl pyridine) [53]. Similarly, *n*-heptane yielded the lowest graft level due to the large difference in solubility parameters. Higher graft levels obtained in ethanol compared with those in methanol could be also attributed to the much closer solubility parameter ethanol than that of methanol. Solubility parameters of solvents employed in this study are given in **Table 2-1**[56]. Although, benzyl alcohol, nitromethane, and 1,4-dioxane have similar solubility parameters with 4VP and poly(4-vinyl pyridine), graft levels obtained in these solvents were too low. This behavior can be accounted for chain

transfer to solvent. It is known that low graft levels are obtained with solvents having high chain transfer constants; hence, the growing chains will be readily terminated. Benzyl alcohol, nitromethane, and 1,4-dioxane have high chain transfer constants leading to lower graft levels. Moreover, significant amount of homopolymer formation due to the chain transfer reactions was observed for grafting of 4VP monomer in benzyl alcohol, 1,4-dioxane, and nitromethane. Therefore, the graft copolymers obtained in these solvents were subsequently washed with solvents and soaked overnight to remove homopolymer. On the other hand, as reported earlier [54] for 4VP and 2VP polymerizations, the chain transfer constants to aliphatic alcohols were found to be too low which can be another reason of high graft levels in *n*-propanol, isopropanol, and ethanol. According to previous findings of styrene/ETFE grafting, significantly enhanced graft levels were obtained with the addition of water to isopropanol [55]. Polar solvents such as alcohols in combination with water were found to yield high grafting rates. This means that the grafting times are short or the irradiation dose of the base polymer can be reduced which leads the less radiation damage of the material. However, no improvement was detected for 4VP/ETFE grafting in isopropanol–water system, since addition of water increases the difference in solubility parameters.

Solvent	Solubility Parameter δ (cal /cm³)$^{\frac{1}{2}}$
n-Heptane	7.40
Tetrahydrofuran(THF)	9.10
Acetone	9.90
Cyclohexanone	9.90
1,4- Dioxane	10.00
4-Vinyl Pyridine	**11.00**
Isopropanol	11.50
n-propyl alcohol	11.90
Benzyl alcohol	12.10
Nitromethane	12.70
Ethanol	12.70
Methanol	14.50
Isopropanol-Water	19.00

Table 2-1: Solubility parameters of the used solvents [56]

Same tendency of graft levels with respect to solvents was observed for both 4VP concentrations [30% (v/v) and 50% (v/v)] except for THF. Surprisingly, it was found that THF yielded reasonable graft levels for 50% (v/v) 4VP, whereas very low graft levels were obtained for 30% (v/v) 4VP. It was observed experimentally that at low 4VP concentrations [30% (v/v)] homopolymer formation was significant when monomer was introduced to THF. Consequently, most of the monomer was converted to homopolymer before grafting to base film; so, graft levels were too low in that case. At high 4VP concentration, homopolymer formation was still predominant but there may be some monomer remained for the grafting to the base film. It was reported previously the influence of various solvents on radiation-induced grafting of 4VP onto polyethylene [36] poly(vinyl chloride) [37] styrene-butadiene- styrene triblock copolymer [38] and poly(tetrafluoroethylene-*co*-hexafluoropropylene) (FEP) [40]. Compared with our work, the diversity of the results may be due to the differences of grafting method (simultaneous grafting used in literature) and base film type.

To the best of our knowledge, there were no previous studies on the synthesis of NVP-based copolymers by radiation-induced grafting of NVP onto ETFE. Therefore, NVP/ETFE grafting was more focused on in this study. Grafting in various solvents, several irradiation doses, and different NVP concentrations have been studied. As far as the different NVP concentrations are concerned, graft level increases as the monomer concentration increases, reaching a maximum value at 50% (v/v) NVP, and then decreases abruptly at higher monomer concentration [80% (v/v) NVP] **(Figure 2.3a)**. This may be due to the limited diffusion of the monomer into the film, which is low in the case of high monomer concentration. At high monomer concentrations, the complexity arising from the extensive homopolymerization during the grafting may hinder monomer diffusion to the radical sites and may lead to diminishing grafting. This may lead to the maxima at specific monomer concentrations, beyond which the grafting would decrease rapidly [9,56]. In such a case, the trapped radicals can recombine readily and homopolymerization which increases the viscosity of the solution occurs intensively. Eventually, the graft level decreases.

Figure 2.3a exhibits also that as the irradiation dose increases, graft levels of ETFE-*g*-PNVP copolymer increase dramatically owing to the increased concentration of free radicals on the base film [56]. Since desired graft levels were achieved with 50% (v/v) NVP concentration and ETFE films irradiated with 50 kGy, these conditions were selected as the optimum conditions at which the rest of experiments were performed.

Figure 2.3b indicates the variation of graft level of ETFE-*g*-PNVP copolymer with respect to solvents studied. It was found that graft levels decrease in the following sequence: THF > 1,4-dioxane > *n*-heptane > water > isopropanol > cyclohexanone > *n*-propanol > methanol > ethanol > benzyl alcohol > nitromethane. THF and 1,4-dioxane, having solubility parameters close to that of poly(*N*-vinyl 2-pyrrolidone) or PNVP (10.1–13.7) [53] are likely to be the suitable solvents for NVP grafting to ETFE. Isopropanol, cyclohexanone also yielded reasonable graft levels by the similar reason. However, high graft levels obtained in *n*-heptane and water or very low graft level obtained in nitromethane and benzyl alcohol cannot be explained by solubility parameters. High chain transfer constants of nitromethane and benzyl alcohol may be the reason of low graft levels as found in 4VP/ETFE. Moreover, water serves as a suitable solvent for NVP grafting may be due to its low chain transfer constant, which enhances graft level or its polarity, which aids the swelling of the grafted layer when the hydrophilic monomers were grafted onto ETFE.
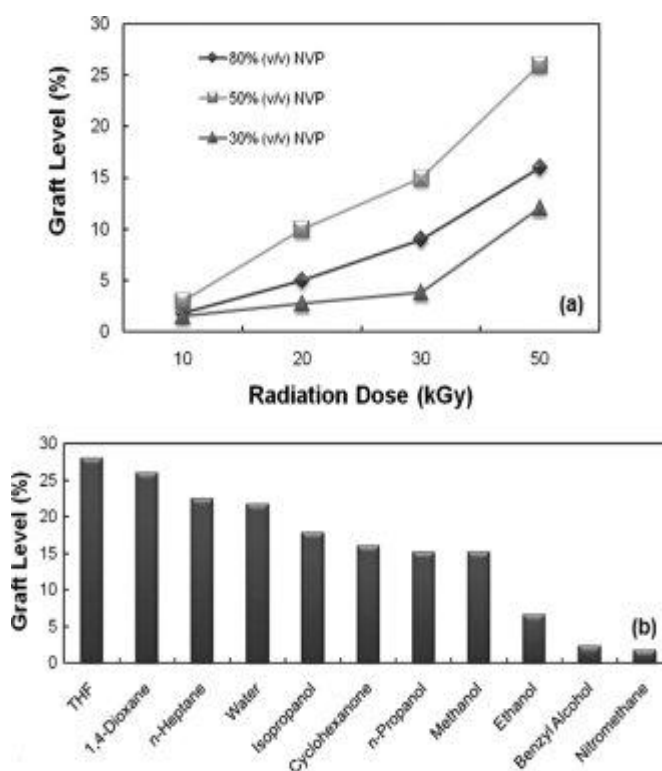
Figure 2.3: (a) Variation of graft level (%) as a function of irradiation dose for NVP grafting onto ETFE at different NVP concentrations. Grafting conditions: 25µm ETFE, 50 kGy, 60 °C, in 1,4-dioxane. (b) Effect of solvent on graft level (%) for NVP grafting onto ETFE. Grafting conditions: 25 µm ETFE, 50 kGy, 60 °C, 50% (v/v) NVP.

Hegazy et al. reported on simultaneous radiation grafting of aqueous NVP onto low density polyethylene [41] and poly(tetrafluoroethylene-*co*-perfluoropropyl vinyl ether) [42] previously. They pointed out the significant amount of homopolymer formation during grafting if no inhibitor was used. Graft levels about 20% was obtained with irradiation dose of 58 kGy and 50% (v/v) NVP that in the presence of $CuCl_2$ as inhibitor to prevent homopolymerization in simultaneous grafting in their work. Even though preirradiation gives lower graft levels than that of simultaneous irradiation, we obtained much better graft levels without using an inhibitor as no homopolymerization was observed in our case. In another study, simultaneous-radiation grafting of NVP onto poly(tetrafluoroethylene-hexafluoropropylene- vinylidene fluoride) using different solvents was described [43]. Although a different base polymer was used. Authors found high graft levels in 1,4- dioxane which is in agreement with our study. On the contrary, very high graft levels (up to 200%) were reported previously for simultaneous grafting of NVP onto polypropylene in dimethyl formamide using an inhibitor [44].

Similar to NVP case, nobody reported on radiation- induced grafting of 2VP onto ETFE up to know. From the screening experiments for 2VP grafting onto ETFE, it was observed that 2VP is less reactive compared with 4VP and NVP. Thus, as a first attempt, relatively high irradiation dose was examined. **Figure 2.4a** presents the variation of graft levels with respect to solvents at two different irradiation doses, 10 kGy and 50 kGy, that for 2VP grafting onto ETFE. Although higher graft levels were obtained at 50 kGy, the improvement was not substantial compared with 10 kGy. This may be due to the decomposition of radicals and of recombination or transfer reactions that is expected to occur to some extent by an increasing dose. As a second attempt, the reaction temperature increased to achieve reasonable graft levels since temperature increase is expected to enhance not only the diffusion of monomer toward active sides of base film and the advancement of the grafting front but also the reactivity of radicals [9,56]. **Figure 2.4b** shows the variation of graft level with solvents at two different grafting temperatures (60 °C and 90 °C). It was found that graft levels obtained at different temperatures were not significantly different. In grafting process, grafted zone remains swollen which leads to high mobility of the growing chains within polymer matrix. Therefore, termination of the two growing chains by mutual combination becomes dominant at higher temperatures. At the same time, the primary radical termination may also be accelerated by the time the monomer reaches their vicinity. In addition to that, the increase of the reaction temperature enhances the production of

22

homopolymer in the grafting solution and then the diffusion of the monomer is hindered [56]. All these can be regarded as the reasons of low graft levels. The order of graft levels with respect to solvent for 2VP/ETFE grafting at 50 kGy and 60 °C were determined as follows: benzyl alcohol > methanol > ethanol > 1,4-dioxane > THF > cyclohexanone > isopropanol > n-propanol > n-heptane > water > nitromethane. High graft levels obtained in ethanol, 1,4-dioxane, THF, cyclohexanone, isopropanol, and n-propanol can be ascribed to the closeness of the solubility parameters of these solvents to that of poly(2-vinyl pyridine) [10.4 (cal/cm^3)$^{1/2}$] [57]. The dominance of alcohols in high graft levels for 2VP grafting are probably due to low chain transfer constants of alcohols based on a similar reasoning as earlier. As the nitrogen atom that is situated at the position of pyridine has alone electron pair and shows basic character, its solubility is greater in an alcohol. However, except for alcohols, the order of graft levels with respect to solvent type was found to be significantly different for these isomeric monomers, 2VP and 4VP.

As mentioned at very beginning of this article, there were only two studies on radiation induced grafting of 2VP in literature [46,47]. Authors performed 2VP grafting in the presence of styrene as a second monomer onto isotactic propylene. High graft levels in water and methanol–water were reported. It should be noted though that those earlier results and the present ones are not necessarily directly comparable since the base polymers are different.

Therefore, different radical concentrations produced by the irradiation, different structures of the radical centers, variations in crystallinity and glass transition may result in differences in grafting of 2VP.
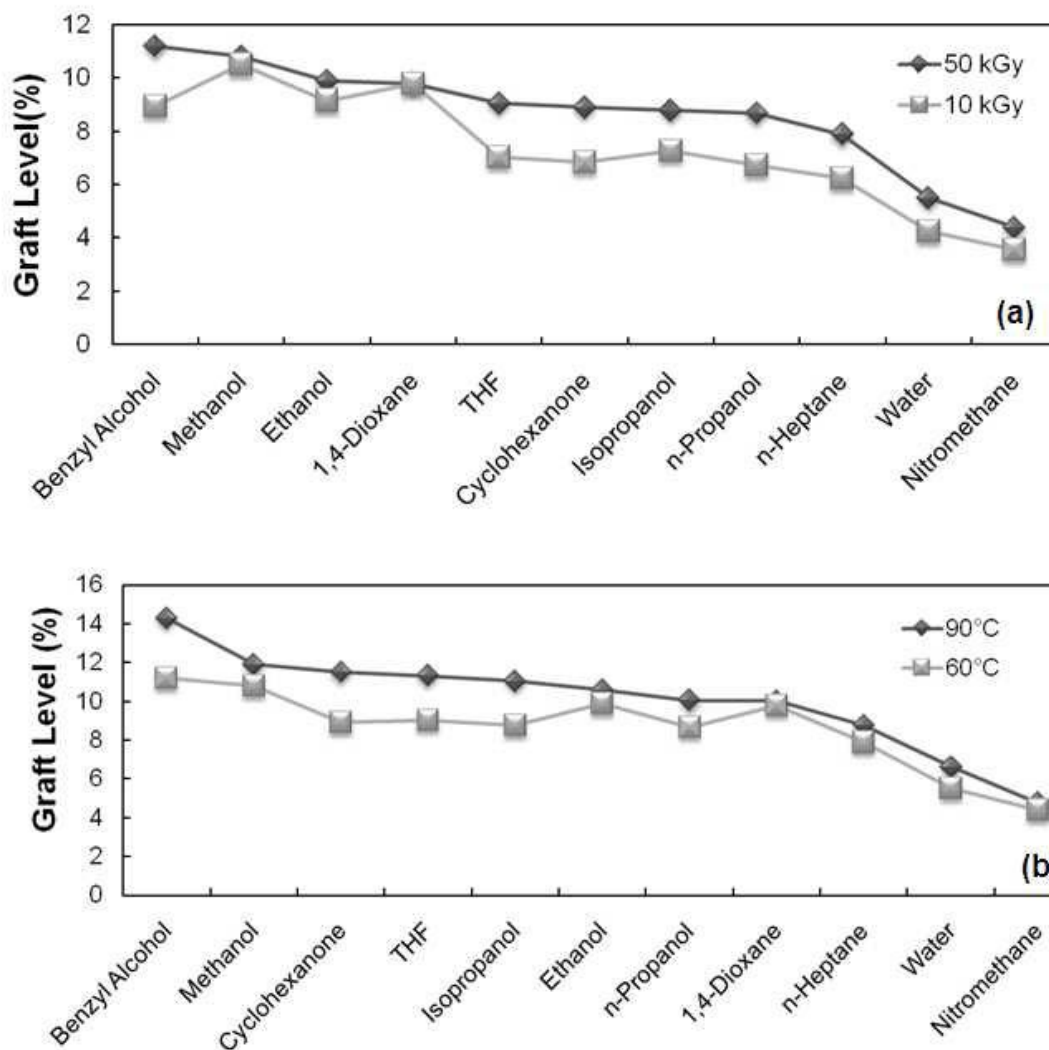
Figure 2.4: (a) Effect of solvent on graft level (%) for 2VP grafting onto ETFE at irradiation doses of 10 kGy and 50 kGy. Grafting conditions: 25 μm ETFE, 60 °C, 50% (v/v) 2VP. (b) Effect of solvent on graft level (%) for 2VP grafting onto ETFE at temperatures of 60 °C and 90 °C. Grafting conditions: 25 μm ETFE, 50 kGy, 50% (v/v) 2VP.

2.3.2 Fourier Transform Infrared Spectroscopy

FTIR spectroscopy was performed for both ETFE base film and graft copolymers to investigate whether the monomer is incorporated with base film or not. Graft copolymers with high graft levels obtained in promising solvents were analyzed for this purpose.

Figure 2.5a shows the FTIR spectra of the ETFE-*g*-P4VP copolymers synthesized in different solvents and ETFE base polymer film. ETFE base film is initially characterized by the presence of strong bands in the range of 1000 to 1400 cm^{-1}

which are characteristics for CF_2 groups. Moreover, symmetric and asymmetric stretching vibrations of CH_2 groups at 2921 cm^{-1} are present in ETFE base film. The peak at 1598 cm^{-1} attributed to C=N bond, and the peak at 1452 cm^{-1} attributed to C=C bonds of 4VP are present in ETFE-g-P4VP [58]. A band at 1248 cm^{-1} due to the C-N vibration of 4VP also exists in ETFE-g- P4VP. The less intense peak at 3730 cm^{-1} belongs to the N-H bonds. Therefore, observed differences between the FTIR spectra of ETFE and those of graft copolymers verified the existence of grafting.

The FTIR spectra of the ETFE-g-PNVP copolymers synthesized using promising solvents and ETFE base film are given in **Figure 2.5b**. Compared with FTIR spectrum of ETFE base polymer, the appearance of new peaks at 1596 cm^{-1}, 1248 cm^{-1}, 1452 cm^{-1} are characteristics to C=O bond, C-N bond, and C=C bond, respectively. In the case of NVP grafting 1590 cm^{-1} that signify the characteristic C=O bond of NVP is distinguished. The peak at 3780 cm^{-1} belongs to the NAH bonds are also observed. As conclusion, grafting of NVP into ETFE film was verified.

FTIR spectra of ETFE-g-P2VP copolymers synthesized in benzyl alcohol and methanol and ETFE base polymer film are depicted in **Figure 2.5c**. The peaks correspond to C=C and C=N of pyridine at 1452 cm^{-1} and 1593 cm^{-1}, respectively, and a band at 1247 cm^{-1} due to the C-N vibration of 2VP are present in ETFE-g-P2VP proved the grafting of 2VP.31 Again, the peak at 3700 cm^{-1} belongs to the N-H bonds.
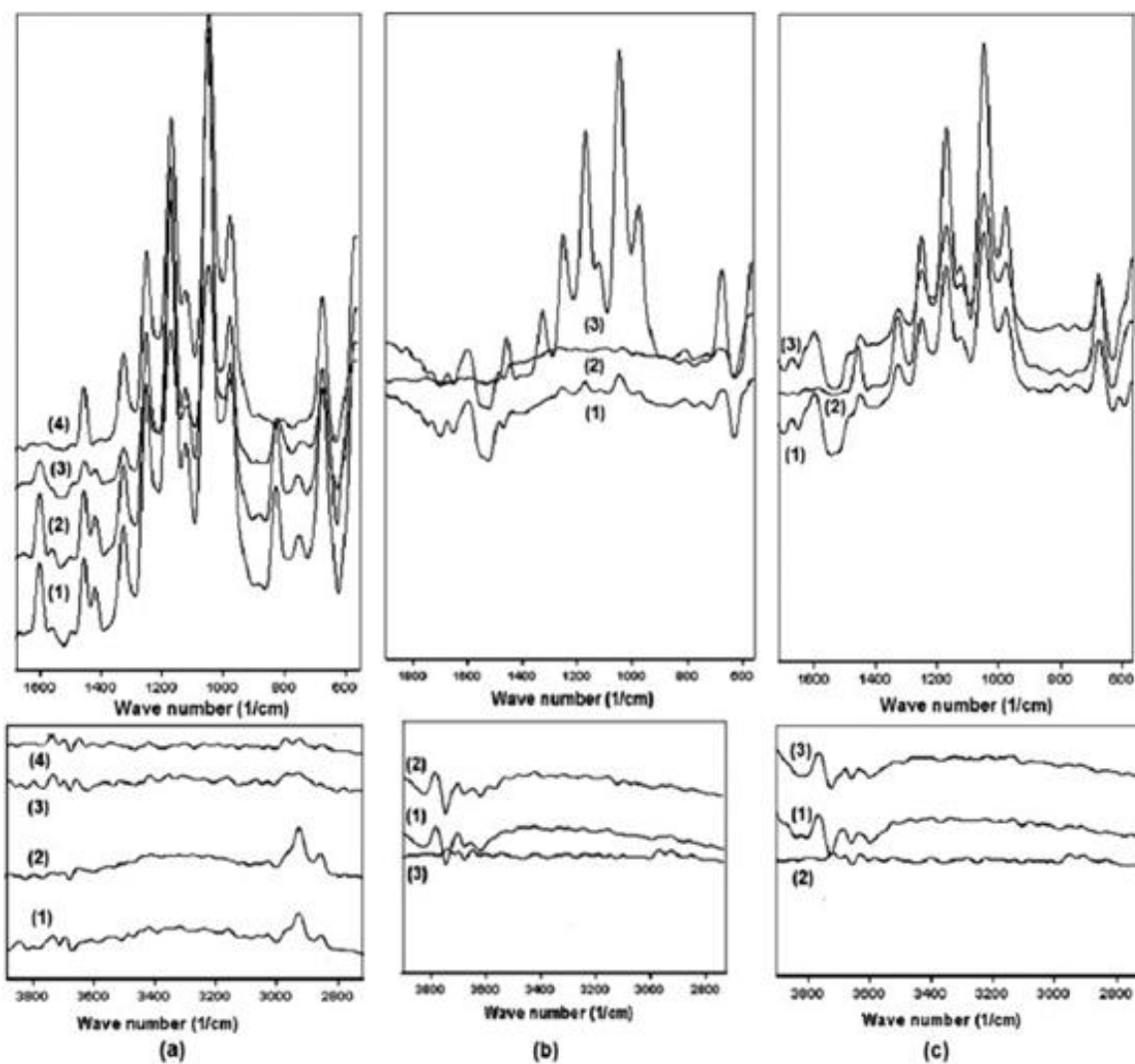
Figure 2.5: (a) Fourier transform infrared (FTIR) spectra of (1) ETFE-*g*-P4VP in synthesized isopropanol, (2) ETFE-g-P4VP synthesized in n-propanol, (3) ETFE-*g*-P4VP synthesized in cyclohexanone, and (4) ETFE base film. (b) FTIR spectra of (1) ETFE-*g*-PNVP synthesized in 1,4-dioxane, (2) ETFE-*g*-PNVP synthesized in THF, and (3) ETFE base film. (c) FTIR spectra of (1) ETFE-*g*-P2VP synthesized in methanol, (2) ETFE base film, and (3) ETFE-*g*-P2VP synthesized in benzyl alcohol.

26

2.3.3 Dynamic Mechanical Analysis

Mechanical behavior of the graft copolymers used for the preparation of fuel cell membranes are important in terms of handling, fabrication of membrane electrode assemblies and to offer a durable material. Moreover, the structural changes and the degradation are usually reflected in the mechanical properties of the copolymers. Thus, it is of interest to investigate the dynamic mechanical properties of graft copolymers synthesized.

The temperature dependence of loss tangent (tan δ) and storage modulus of graft copolymers are represented in **Figure 2.6**, **Figure 2.7**, **Figure 2.8**. Single broad peaks can be observed in tanδ versus temperature plots (**Figure 2.6a, Figure 2.7a and Figure 2.8a**) for each of the copolymers investigated. Single peaks may indicate that there is no phase separation. The maximum of tanδ peaks corresponds to glass transition temperature (T_g) for each case. First of all, as graft level increases, the tanδ maximum shifts to higher temperature which indicates the increase of T_g. For instance, the T_g values for ETFE-g-P4VP copolymers synthesized in isopropanol with graft level of 41%, in n-propanol with graft level of 45%, and in cyclohexanone with graft level of 48% were determined as 130 °C, 140 °C, and 150 °C, respectively, (**Figure 2.6a**). Similarly, T_g values for ETFE-g-PNVP copolymer with graft level of 26% in 1,4-dioxane was 110 °C and the copolymer with graft level of 28% in THF was 150 °C (**Figure 2.7a**). Correlatively, ETFE-g-P2VP copolymers with a graft level of 12% in methanol and 14% in benzyl alcohol exhibit T_g values at 90 °C and 110 °C, respectively, as shown in **Figure 2.8a**. T_g of ETFE base film was reported as 110 to 135 °C in literature [60–62]. The difference in literature values of ETFE base polymer may be resulted from the type of ETFE film (different molecular weight, etc.) and different measurement technique. The increase of T_g with graft level can be attributed to the restrictions in the movements of polymer due to the incorporation of glassy graft chains to the ETFE base film. As expected, the monomer and the solvent employed during grafting influence the T_g of resultant copolymers to different extent.
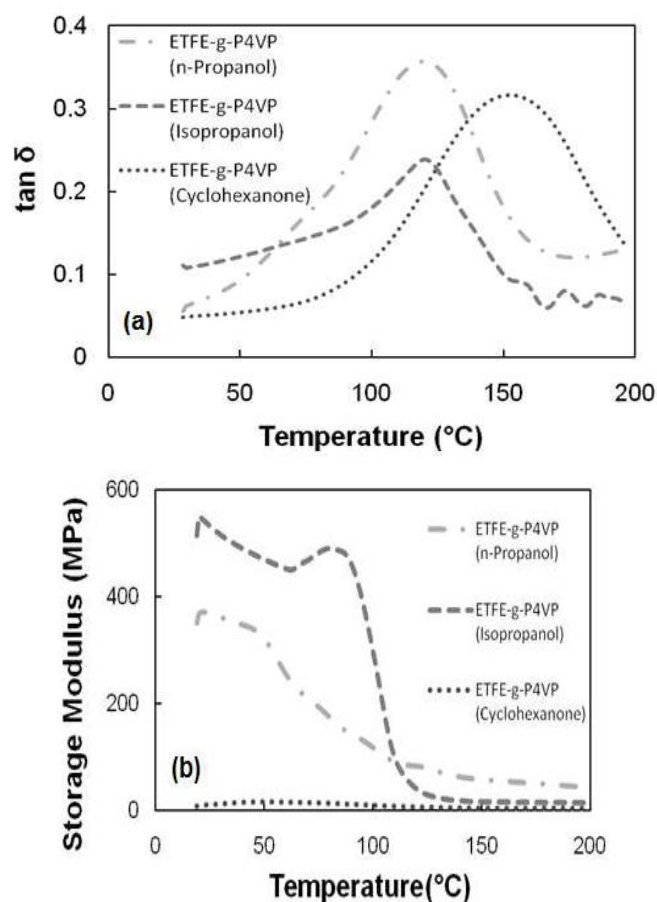
Figure 2.6: (a) The temperature dependence of loss tangent (tan δ) of ETFE-*g*-P4VP (GL: 45%, synthesized in n-propanol), ETFE-*g*-P4VP (GL: 41%, synthesized in isopropanol), ETFE-*g*-P4VP (GL: 48%, synthesized in cyclohexanone) and (b) The temperature dependence of storage modulus of ETFE-*g*-P4VP (GL: 45%, synthesized in n-propanol), ETFE-*g*-P4VP (GL: 41%, synthesized in isopropanol), ETFE-*g*-P4VP (GL: 48%, synthesized in cyclohexanone).

Figure 2.7b shows the variation of storage modulus with respect to temperature for the ETFE-*g*-P4VP copolymers with different graft levels and synthesized in isopropanol, *n*-propanol, and cyclohexanone. In the temperature region investigated, the minimum storage modulus values was obtained for the copolymer obtained in cyclohexanone which was experienced as wrinkled, rough, uneven, and brittle films as well. Copolymer obtained in isopropanol possessed relatively higher storage modulus values compared with the one from *n*-propanol up to 110 °C after which comparable values were obtained.

The graft level is one of the important quantities which has a direct and major influence on different ex-situ and in-situ properties of the grafted films and, subsequently on the membranes. High graft levels of copolymers and resultant membranes are preferred to obtain high ionic conductivity. However, high graft levels

28

may result in the deterioration of some mechanical properties. Therefore, it is necessary to find a compromise between the mechanical robustness of the membrane and its proton conductivity. As a consequence, although cyclohexanone yielded the highest graft level, *n*-propanol and isopropanol were found to be the most promising solvents to obtain both high graft levels and reasonable mechanical properties to synthesize ETFE-*g*- P4VP.
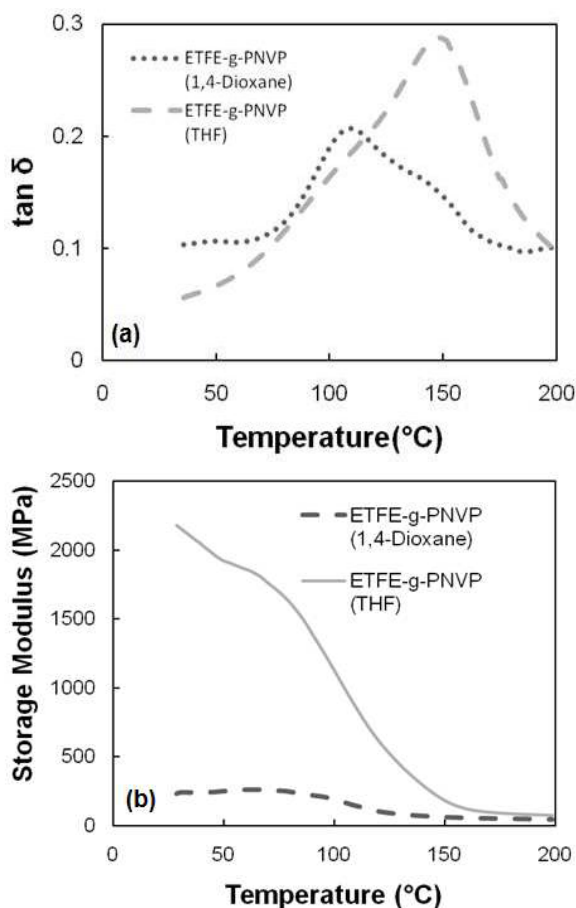
Figure 2.7: (a) The temperature dependence of loss tangent (tan d) of ETFE-*g*-PNVP (GL: 28%, synthesized in THF), ETFE-*g*-PNVP (GL: 26%, synthesized in 1,4-dioxane) and (b) The temperature dependence of storage modulus of ETFE-g-PNVP (GL: 28%, synthesized in THF), ETFE-g-PNVP (GL: 26%, synthesized in 1,4-dioxane).

As far as the storage modulus values of ETFE-*g*-PNVP and ETFE-*g*-P2VP are concerned, both decline sharply as the temperature increases (**Figure 2.7b** and **Figure 2.8b**). It can be seen from **Figure 2.7b** that the storage modulus values of ETFE-*g*-PNVP (in THF) at lower temperature is larger than that of ETFE-*g*-PNVP (in 1,4-dioxane), which indicates ETFE-*g*-PNVP synthesized in THF has higher stiffness. It is found that THF is the most promising solvent for NVP monomer in terms of graft level

and the strength of graft copolymer. Storage modulus values of ETFE-*g*-P2VP copolymer from benzyl alcohol were higher than those from methanol but their difference was not so noticeable at temperatures above 100 °C. Therefore, both benzyl alcohol and methanol can be regarded as the most favorable solvents for 2VP grafting onto ETFE in the sense of graft level and mechanical properties.

As seen in the case of ETFE-*g*-PNVP and ETFE-*g*- P2VP copolymers at low temperatures, the increase of graft level caused to an increase in storage modulus which is an indication of the increased stiffness of copolymers. That may probably be due to the steric hindrance of the pyridine and pyrrolidone groups which results in a stiffer polymer chain.
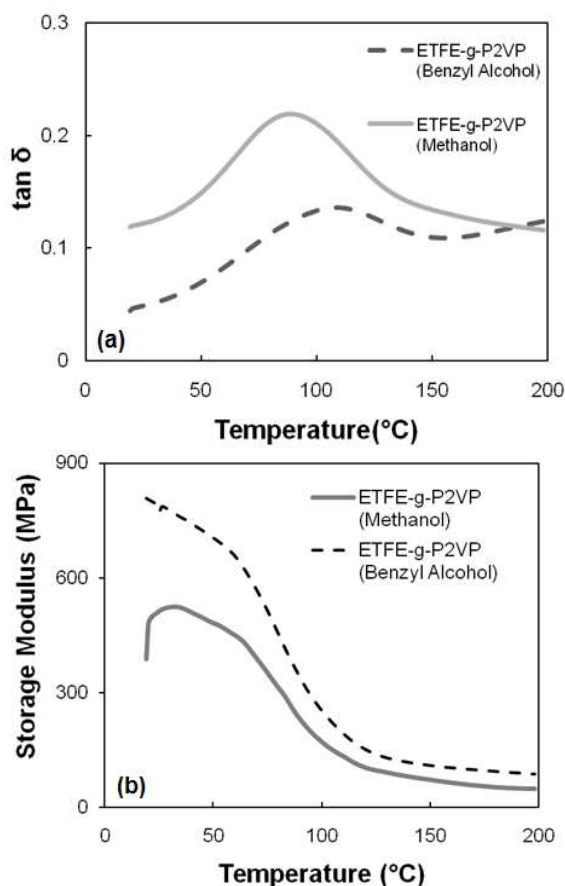
Figure 2.8: (a) The temperature dependence of loss tangent (tan d) of ETFE-g-P2VP (GL; 14%, synthesized in benzyl alcohol), ETFE-*g*-P2VP (GL: 12%, synthesized in methanol) and (b) The temperature dependence of storage modulus of ETFE-*g*-P2VP (GL; 14%, synthesized in benzyl alcohol), ETFE-*g*-P2VP (GL: 12%, synthesized in methanol).

2.3.4 Scanning Electron Microscopy-Energy Dispersive Spectroscopy

The uniform distribution of the grafts is an important factor along with graft level in both copolymers and the resultant membranes to have homogenous ion exchange mechanism. The graft copolymer films synthesized in this study were found to be homogeneous in appearance especially for higher graft levels. However, we know that it is not always possible based on our previous experience. Therefore, we analyzed the surfaces of the graft copolymer films by SEM-EDAX. Since nitrogen is known to be mainly introduced to copolymer structure by grafting of nitrogen containing 4VP, NVP, and 2VP, it can be assumed that the distribution profile of the nitrogen corresponds to that of the P4VP, PNVP, and P2VP grafts.

Figure 2.9 demonstrates the SEM-EDAX images in which white dots are representative of nitrogen of the graft copolymers. It was found that these copolymers were substantially different from each other. In the case of ETFE-*g*-P4VP copolymer, nitrogen was almost uniformly distributed on the surface for the film with having graft level of 48% (in cyclohexanone), whereas less homogenous nitrogen distribution was observed for the film with 5% graft level (in benzyl alcohol) (**Figure 2.9a**). The copolymers of ETFE-*g*-PNVP and ETFE-*g*-P2VP showed relatively uneven and lower nitrogen content at the surface of films compared with ETFE-*g*-P4VP copolymer. This behavior was much more pronounced in the case of copolymers with low graft levels (**Figure 2.9 b, c**). As conclusion, the distribution of nitrogen was strongly influenced by not only the graft levels of the copolymers but also the nature of the grafting medium which takes into account both the monomers and the solvents. The graft level is a bulk property and is averaged over the film thickness and area. At low grafting, the graft distribution was heterogeneous on the surface; however, at high grafting, the surface became more homogenous.
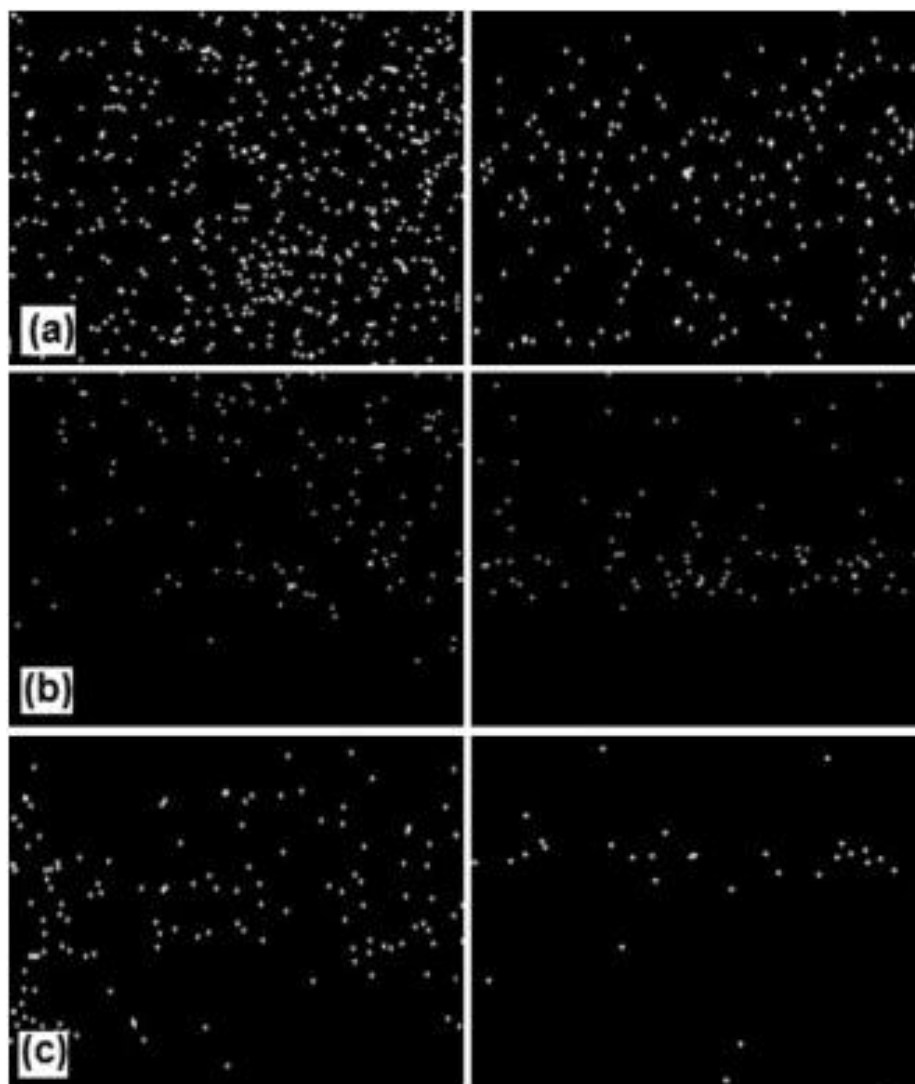
Figure 2.9: (a) Scanning electron microscopy-energy dispersive spectroscopy (SEM-EDAX) micrographs of N mapping for ETFE-*g*-P4VP, GL: 48% synthesized in cyclohexanone (left) and GL: 16% synthesized in benzyl alcohol (right), (b) SEM-EDAX micrographs of N mapping for ETFE-*g*-PNVP, GL: 28% synthesized in THF (left) and GL: 2% synthesized in nitromethane (right), and (c) SEM-EDAX micrographs of N mapping for ETFE-*g*-P2VP, GL: 14% synthesized in benzyl alcohol (left) and GL: 5% synthesized in nitromethane (right).

2.4 CONCLUSION

Graft copolymers using NVP, 4VP, and 2VP are synthesized by radiation-induced grafting. Grafting of 4VP onto pre-irradiated ETFE films has been shown to be possible with high graft levels by employing short reaction time and low irradiation dose (10 kGy) which has the advantage of reduced radiation damage on the base polymer structure due to the high reactivity of 4VP. In the case of both NVP and 2VP grafting onto pre-irradiated ETFE films, relatively higher irradiation doses (30 and 50 kGy) are required.

The application area of the resultant graft copolymers is targeting the high temperature polymer electrolyte membrane fuel cells. Graft copolymer strength plays an important role on the degradation of PEMFC membrane during the operation due that both graft level and mechanical properties of the copolymer should be promising. Graft levels are found to be strongly dependent on the nature of solvents used during grafting. Despite the fact that grafting reactions of 4VP/ETFE performed in cyclohexanone have a highest graft level, DMA indicated that mechanical properties of the resultant copolymers are not favorable. Therefore, *n*-propanol and isopropanol are found to be the most promising solvents to obtain both high graft levels and reasonable mechanical properties to synthesize ETFE-*g*-P4VP copolymers. In the case of NVP grafting, THF is the most promising solvent in terms of both graft level and the strength of graft copolymer. Similarly, both benzyl alcohol and methanol can be regarded as the most favorable solvents for 2VP grafting onto ETFE in the sense of graft level and mechanical properties. DMA results also indicate that grafting resulted in the increase of glass transition temperature and stiffness. SEM-EDAX revealed that copolymers based on 4VP have a much uniform surface depending on graft level. The surface aspects and mechanical properties taken in conjunction, suggest that although grafting in cyclohexanone yields homogeneous copolymer films, their mechanical properties are poor. In the case of NVP and 2VP graft copolymer distribution is not homogenous and graft copolymers tend to gather on one the surface.

CHAPTER 3

WATER FREE PHOSPHORIC ACID DOPED RADIATION-GRAFTED PROTON EXCHANGE MEMBRANE SYNTHESIS AND CHARACTERIZATION

3.1. INTRODUCTION

Most of the shortcomings arises on the PEMFC commercialization due to the operation temperature is limited to below 100 °C (typically 60-80 °C), at atmospheric pressure which is in turn limited by the current state-of-the-art perfluorosulfonic ionomers such as Nafion[®] because of its water assisted conduction mechanism [65].

Nafion[®] membranes have advantages such as high mechanical and chemical stability at temperatures below 100 °C and high proton conductivity in hydrated form as well. However, the water requirement in the membrane limits the operation temperature to below 100 °C in theory. Thus, the synthesis and characterization of proton conducting membranes constitutes a significant step for the development of high temperature PEMFCs.

Efforts have been made to develop proton-exchange membranes for operation at temperatures above 100 °C previously. The developed membranes are classified into three groups: (1) modified perflorosulfonated acid (PFSA) membranes, (2) alternative sulfonated polymers and their composite membranes, and (3) acid-base polymer membranes. Among them, acid-base polymer membranes received attention in the past few years. Phosphoric acid-doped poly(benzimidazole) (PBI) has been presented as a promising thermally and chemically stable material that shows good performance in terms of both proton conduction and fuel cell applications at temperatures up to 180 °C without additional humidification [66]. In spite of that, for further large-scale

applications of this polymer, new methods of synthesis need to be explored. The polymer's shortcomings which are most notably poor mechanical properties, membrane casting, easily washed away unbounded ''free acid'' at high temperatures constitute central issues that require improvement. PBI membranes has better conductivity at higher temperatures (150-200 °C), however the need still arises for membranes that is operating at temperatures between 80-120 °C.

Advantages in manufacturing sulfonic acid doped proton-exchange membranes with radiation-induced grafting method have already been distilled in the literature in much detail [67]. This thesis study proposes water-independent radiation grafted-phosphoric acid based membranes that can operate at temperatures up to 130 °C with stability **(Figure 3.1)**. With respect to phosphoric acid doping, the proton conduction mechanism differs from PFSA membranes, i.e., Nafion[®]. In phosphoric acid doped membranes, four possible proton conduction mechanisms have been proposed in literature: (1) proton hopping from one N site to another (N-N) which is believed to contribute little to conductivity, (2) proton hopping (Grotthuss diffusion mechanism) from the N-H site to a phosphoric acid anion which contributes significantly to conductivity (3) Proton hopping along the $H_2PO_4^-$ anionic chain; especially at high phosphoric acid doping levels, free acid is present and contributes the major part of the conductivity, and (4) Proton hopping via water molecules; the conductivity of phosphoric acid doped membranes is found to improve with increasing atmospheric humidity, though the dependence is smaller than that of Nafion[®] [67].
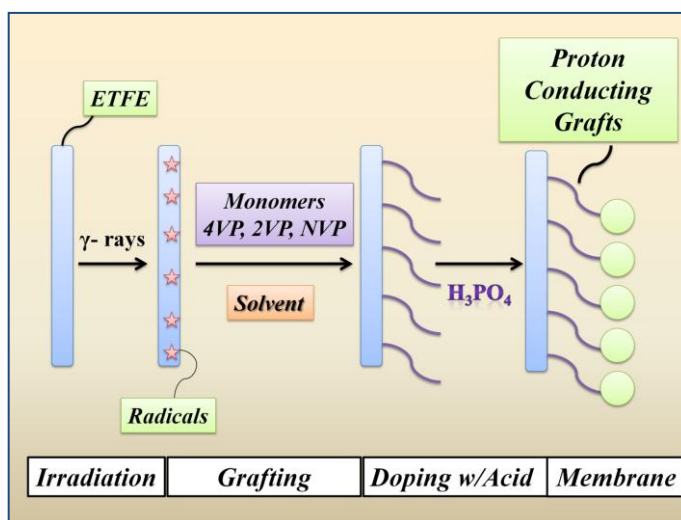
Figure 3.1: Synthesis of radiation grafted phosphoric acid doped proton exchange fuel cell membrane

4-vinyl pyridine (4VP), 2-vinyl pyridine (2VP) and *N*-vinyl-2-pyrrolidone (NVP) monomers were not previously employed in the preparation of proton exchange membranes for fuel cells by radiation-induced grafting except for a study in literature in which 4VP was used. However, this study does not maintain any details in both fuel cell testing and proton conductivity in a wide relative humidity (RH) range [70]. Moreover, recently 4VP monomer has been grafted onto ETFE base film in one more study in literature, however it was not studied   mainly   for high temperature PEMFC applications so that there is no fuel cell testing data presented [71].

Furthermore, phosphoric acid is the most convenient acid due to its conductivity mechanism and thermal stability to manage high temperature conditions in PEMFC [71]. In literature, there are only a few studies for the grafting of 2VP and NVP monomers onto some hydrocarbon base films; however none of them are targeting fuel cell application or doping the copolymers with phosphoric acid [72-73].

This study's main focus is the preparation of radiation grafted phosphoric acid doped proton-exchange membranes based on nitrogen containing 4VP, 2VP and NVP monomers to operate at high temperature (especially above boiling point of water) and water free conditions for PEMFC. Owing to a simple manufacturing process, the procedure that is offered to fabricate high temperature membranes is able to overcome casting (or manufacturing) problems of other high temperature membrane candidates.

In this part of the thesis study, properties of resultant membranes are studied in detail for mainly fuel cell relevant properties including proton conductivity, water uptake, mechanical and thermal properties. The phosphorous distribution is also investigated to obtain information about the homogeneity of the membranes. As a contribution to the literature, the proton conductivity of ETFE-*g*-4VP membranes have been measured in a wide range RH and temperature values to define the temperature and RH dependence of the proton conductivity mechanism.

3.2. EXPERIMENTAL

3.2.1 Materials

The base polymer poly (ethylene-alt-tetrafluoroethylene) ETFE was purchased in the form of a 25 μm thick film (Nowoflon ET-6235) from Nowofol GmbH

(Siegsdorf, Germany). The reagents for membrane preparation, monomers 4-vinyl pyridine (4VP), 2-vinyl pyridine (2VP) and N-vinyl-2-pyrrolidone (NVP) solvents (n-propanol, benzyl alcohol and THF, Sigma Aldrich) and phosphoric acid (H3PO4, Sigma Aldrich), were used without any further purification.

3.2.2 Membrane Preparation

The synthesis of the radiation grafted copolymers has been explained in detail in **Chapter 2** [162]. According to the copolymerization study, grafting solvents were chosen as follows; 4VP: n-propanol, NVP: THF, 2VP: benzyl alcohol. The graft copolymers were obtained at 60 °C and different reaction times as described previously.

For the preparation of proton-conducting membranes, graft copolymer films were doped with H_3PO_4 by simply immersing them in 85 % H_3PO_4 solution at 60 °C for 20 hours. The weight gain from both water and phosphoric acid uptake was determined by comparing the weight change before and after doping. For individual contributions of the doping acid and water uptake, the doped polymer membranes were then dried at 70 °C under vacuum until an unchanged weight was reached. This process lent support to the inference that the weight loss was due to water evaporation which in turn yielded data about the level of acid doping (DL) of proton conducting membranes [74,75].

$$DL = \frac{W_d - W_i}{W_i} x100$$

where w_i and w_d are the weights of the grafted copolymer before and after doping, respectively.

3.2.3 Characterization of Membranes

Proton conductivity of the resultant membranes was measured by Gamry PCI4 Potentiostat with the assistance of BT-1005 Bekktech Scaning DC Software according to in plane four point probe technique with platinum electrodes (**Appendix A**). Samples were cut approximately 2 cm x 2 cm and assembled into the BekkTech Conductivity Cell which was assembled into Greenlight G50 test station to control temperature, flow rate, pressure RH of the dry air. Dry membrane samples have been held in each RH for 30 minutes, and then measurements were obtained.

The mechanical properties of both graft copolymers and proton conducting membranes were investigated by using Zwick/Roell Z100 Universal Testing Machine. For this purpose, samples were prepared in 10 cm x 40 cm; the speed of the jaws was 100 mm min^{-1}. Five samples were tested for each membrane and the average result is reported.

Resultant membranes were weighted after drying at 70 ºC for 12 hours and immersed in deionized water to measure wet weights and obtain water uptake properties. SEM-EDX (Supra 35VP, Leo, Germany) measurement was conducted to investigate the phosphorous distribution on the surface of the membranes. An accelerating voltage of 10 kV was used during the measurements.

TGA measurements were performed on a Shimadzu DTG-60A in nitrogen atmosphere. Indium (T_m=156.6 °C) standards were employed for the temperature and energy calibration. A single heating curve was obtained at a constant heating rate of 5 °C/min over a range 30-600 °C using a constant nitrogen flow.

3.3 RESULTS AND DISCUSSIONS

3.3.1 Preparation of Radiation Grafted Membranes

According to the copolymer study in Chapter 2, *n*-propanol, benzyl alcohol and THF yield maximum graft levels and comparably better mechanical properties in the case of graft copolymers of monomers 4VP, 2VP and NVP, respectively.

Even though increase in the reaction time for radiation grafted sulfonic acid membranes yields more graft level, the present study findings **(Table 3-1)** show that increases in reaction time up to 4 hours for monomers, implicate a decrease in the graft levels for further reaction times [76,77]. More specifically, the graft level increases with increasing reaction time up to 4 hours for 4VP, NVP and 2VP radiation grafted copolymers. This behavior can be attributed to the formation of a grafted copolymer structure which serves as a barrier for grafting front movement of residual monomer. In other words, when reaction time increases graft level rises and growing chains reduce the monomer mobility from the front to the interior of the base film which results in the decreased graft level. Similarly, it was reported previously in the literature that increasing reaction time causes a decrease in graft levels for 4VP due to the mutual

annihilation of the growing polymer chains and barrier effect of the grafted growing polymeric chains [78]. As a result, 4 hours was determined as the optimum reaction time for the synthesis of radiation grafted copolymers based on 4VP, 2VP, NVP with ETFE.

Reaction Time (h)	4VP/ETFE Graft Level (%)	NVP/ETFE Graft Level (%)	2VP/ETFE Graft Level (%)
1/2	15	30	13
1	21	32	20
2	28	34	22
3	34	34	23
4	43	35	24
6	33	26	22
8	28	26	22

Table 3-1: The reaction time required to reach a particular graft level (%) for 4VP, NVP, 2VP grafting onto ETFE

Graft copolymers were treated with H_3PO_4 in order to introduce acidic functionality and therefore to synthesize a proton conducting high temperature PEMFC membrane. Phosphoric acid is of special interest due to its unique proton conductivity at anhydrous conditions, as well as its thermal stability and very low vapor pressure at elevated temperatures.

It is indicated that as the graft level increases, the phosphoric acid doping level for ETFE-*g*-P4VP membrane increases as well due to the interaction of a unit of phosphoric acid and repeating monomer **(Figure 3.2)** [79]. This is in line with findings from the literature that a strong interaction between copolymer and phosphoric acid in membrane may occur when a nitrogen based monomer such as 4VP is immersed in phosphoric acid solution [80].

In the case of ETFE-*g*-PNVP and ETFE-*g*-P2VP membranes, a decrease in weight is observed after doping with phosphoric acid. This decrease implies that during the phosphoric acid doping, due to the para-pyridyl side chain group of 2VP, the strong interaction between protons and nitrogen atoms of imide ring occurs and produces a slightly semicrystalline polymer structure that reduces proton mobility. This salt complex that causes semicrystalline structure might be cleared off by treating the membrane with solvent during washing [81]. As far as the structures of 4VP and 2VP are concerned, although they are very similar, their phosphoric acid doping behaviors

are significantly different. The fact that a robust salt complex seemed to exist between phosphoric acid and matrix-grafted para-pyridyl side-chain groups, but not between the acid and ortho-pyridyl side-chain groups, was justifiable in the sense that the nitrogen atoms of the latter class would, on average, be positioned nearer to the local hydrophobic environment of the polymer backbone. Thus these nitrogen atoms would be expected to experience a more substantial lowering of Brønsted basicity compared to the para pyridyl nitrogen atoms.
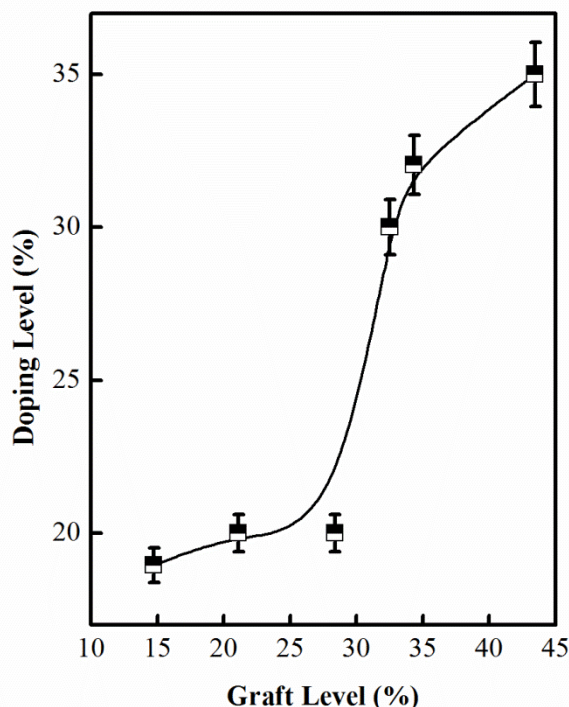
Figure 3.2: Effect of graft level (%) on phosphoric acid doping level (%) for 4VP grafting onto ETFE, (grafting solvent *n*-propanol, irradiation dose 10 kGy)

3.3.2. Proton Conductivity and Water Uptake

In this thesis study, 'water-free' phosphoric acid doped proton conducting membranes able to operate at temperatures up to 120 °C are synthesized. Water as the proton mobility medium in commercially used PEMFC membrane (i.e., Nafion®) is thereby replaced by the acid [82].

Until now various acids have been tried to achieve high proton conductivity for fuel cell membranes. It was found that the conductivity changes in the order of $H_2SO_4 > H_3PO_4 > HClO_4 > HNO_3 > HCl$ mainly for acid-base membranes [83]. It is observed that acid molecules except phosphoric acid, protonate the N atom in the

imidazole ring. Phosphoric acid does not protonate imidazole groups but interacts by hydrogen bonding between the OH and N groups [84-**Error! Reference source not found.**].

Membranes with high phosphoric acid content of 35 % by weight can be obtained by deploying the technique used in here study. From the proton conducting mechanism's point of view, phosphoric acid is interesting since it is amphoteric and has both proton donor (acidic) and proton acceptor (basic) groups to form dynamic hydrogen bond networks which enables protons an easy transfer through hydrogen bond cleavage and formation processes; this process is named as the Grotthuss mechanism [87]. Though, the *N*-heterocycle of the 4VP is involved in the proton transport process, as it provides free electron pairs for proton binding same as PBI ion conduction mechanism.

It is seen that the conductivity increases by increasing graft level which is a direct increase in phosphoric acid doping level for ETFE-*g*-P4VP (**Figure 3.3a**). The literature states that activation energy decreases with increasing doping level and this activation energy is close to that of phosphoric acid (concentrated aqueous solution) [88]. These data indicate that the proton movement becomes easier at higher doping levels since the activation energy closes to the phosphoric acid (concentrated aqueous solution). These findings are expected as there is excess phosphoric acid in the membrane after maximum protonation by acid where the anions are linked to the polymer by rather strong hydrogen bonding. The excess phosphoric acid works similarly to concentrated phosphoric acid solution and contributes to the proton conductivity.

This finding is consistent with the results of the FTIR analysis of resultant membranes since the phosphoric acid doped ETFE-*g*-P4VP membrane did not show the characteristic absorptions of NH^+ groups in the range of 3500-4000 cm^{-1} (**Figure 3.4**). Moreover, FTIR results lend considerable support to Glipa and Bouchet's conclusions [89-90]. Below 2000 cm^{-1}, the spectrum is composed of relatively narrow peaks. In the region 2000-1000 cm^{-1}, cycle vibrations as well as in plane NH and CN deformation modes are expected to occur. In the range 1000-400 cm^{-1}, cycle vibrations and out of plane NH and CN deformation modes are expected to occur. The most relevant region to follow the protonation of the polymer is above 2000 cm^{-1}.
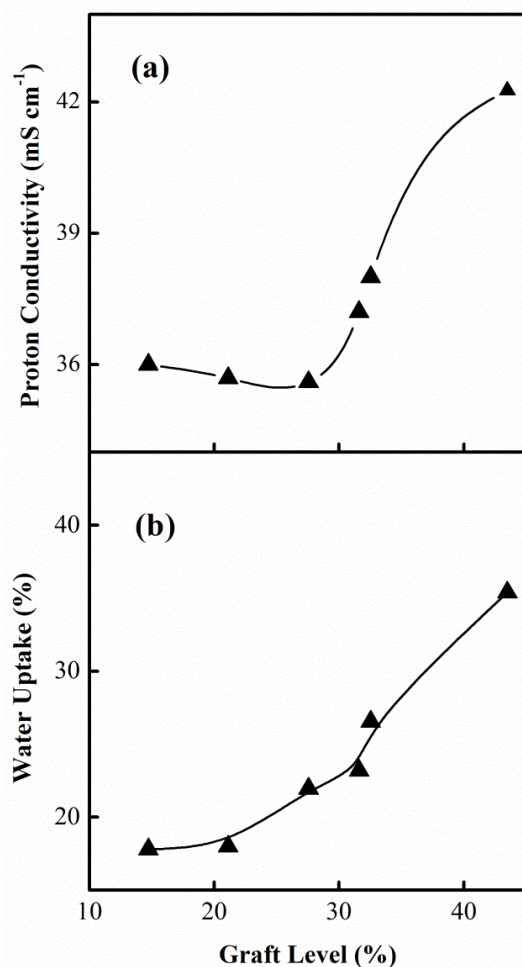
Figure 3.3: Effect of graft level on proton conductivity (mS cm^{-1}) and water uptake (%) for ETFE-*g*-P4VP proton conducting membrane, (grafting solvent *n*-propanol, irradiation dose 10 kGy, grafting time 4 hours)
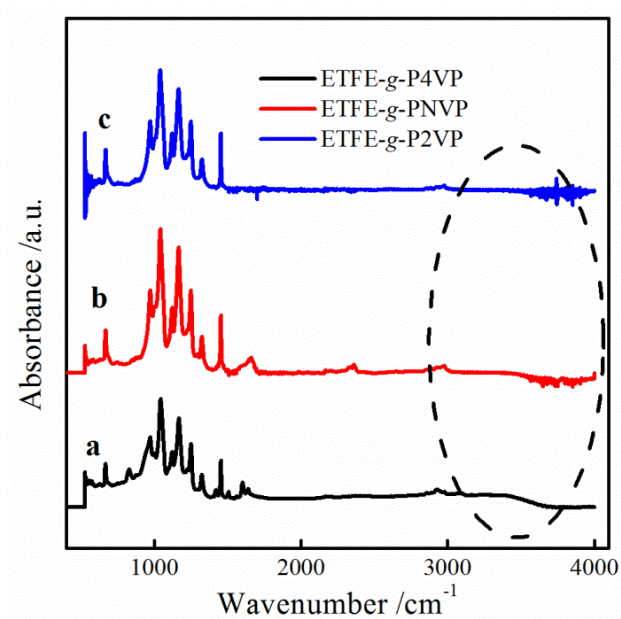
Figure 3.4: FTIR spectra of a) ETFE-*g*-P4VP, b) ETFE-*g*-PNVP, c) ETFE-*g*-P2VP

42

In the proton conductivity manner operating temperatures above boiling point can be achieved since water does not directly contribute to the phosphoric acid proton conductivity mechanism. Although the material is essentially an intrinsic proton conductor, the presence of water and temperature improves conductivity since higher water content in the membrane presumably lowers the viscosity within the membrane, leading to the higher proton mobility and conductivity [91]. Though proton hopping via water molecules contributes to the conductivity, dependence is much smaller than that of Nafion[®] [92]. To understand the water dependence of the presented membranes, the *ex situ* conductivity data at wide range temperature and RH values is provided in our study. It should be mentioned that there is no detailed study on the combined effect of RH (%) and temperature for ETFE-*g*-P4VP membranes in the literature. Thus, **Figure 3.5** strengthens the less water dependence of phosphoric acid doped ETFE-*g*-P4VP membranes. Nafion[®] NR211 and ETFE-*g*-P4VP membranes have been compared according to their proton conductivity at different RH and temperature range. Nafion[®] membranes have high conductivities at higher RH range; however, the conductivity decreases rapidly with reduced RH [93]. For ETFE-*g*-P4VP membrane, high conductivity is extended to 130 °C. The conductivity dependence on the relative humidity becomes significant at high temperatures [8], e.g., an increase in the relative humidity from 1 to 5% resulted in an increase in the conductivity from 55 to 61 mS cm^{-1} in our study. However, by increasing the relative humidity, conductivity slightly increases up to 63 mS cm^{-1}. Compared the previous studies on radiation grafted proton conducting membranes in literature, the proton conductivity values at a lower RH for the membranes obtained in this study are remarkably higher even at moderate graft levels (45%) for ETFE-*g*-P4VP membranes. As an example, in a previous study, the conductivity of radiation grafted trifluorostyrene based membranes at low RH (25%) and 120 °C is in the range of 15–30 mS cm-^{1} for very high graft levels (above 200%) which caused significant deterioration in mechanical properties [94].

Since the proton conductivity of proton-exchange membranes usually increases with an increase in the water absorption, continuous humidification and cooling are essential for commercial polymer electrolyte membrane fuel cells to prevent drying up of Nafion[®] membranes or the flooding over electrodes due to excess water. Such humidification and cooling systems limit the compactness and power density of PEMFCs, and new fuel cell systems, including new catalysts, membranes and other fuels that are expected to achieve highly efficient clean energy without these

humidification and cooling systems [95]. The water absorption behavior and physical state of absorbed water are extremely important in proton conducting membranes, because the proton conductivity is dominated by these factors.
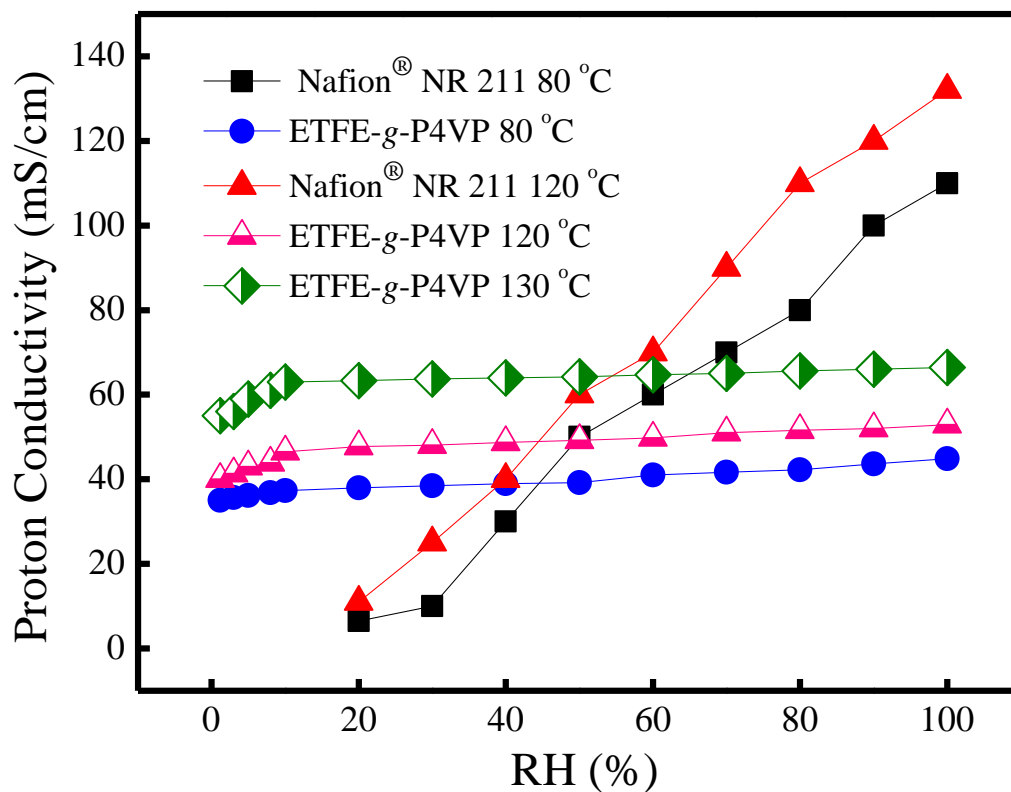
Figure 3.5: Conductivity of Nafion[®] NR 211 and ETFE-*g*-P4VP membranes as a function of relative humidity at different temperatures (GL: 45 %, grafting conditions: solvent *n*-propanol, 10 kGy, 60 °C, 4 hours

The affinity for water is thought to be due to intermolecular hydrogen bonding between water and N of monomer and attraction of water to N-H groups in PBI membrane [96]. Since membranes prepared in this study are expected to have similar proton conduction and water uptake mechanism with acid-base proton conducting membranes such as PBI. Water uptake behavior of ETFE-*g*-P4VP phosphoric acid doped membranes proves that water content inside the membrane increases with increasing graft level which is a direct increase on the N sides (**Figure 3.3b**). This water absorption behavior confirms that the phosphoric acid groups chemically absorb water molecules with the N-H bonding. The highest 30% water uptake is obtained for the highest graft level which is low compared to other polymer electrolyte membranes, i.e., Nafion[®] [97].The low water uptake can therefore be presumed to be due to the high

hydrophobicity and crystallinity as well as conformation of ETFE base polymer units. In the literature Nafion$^{®}$ type polyelectrolyte membranes have excellent processability and sufficient mechanical strength for fuel cell applications but their high expansion under high relative humidity conditions constitutes still a major problem for the fuel cell durability. Even the water in the vapor form can be absorbed easily at the medium operation conditions.

Water uptake and proton conductivity have similar trends with graft level for ETFE-*g*-P4VP membranes (**Figure 3.3**). As the graft level and indirectly acid doping level increase both water uptake and proton conductivity increases. **Figure 3.3** also shows that water uptake is associated with the doping acid. At 20 °C and 100% RH and ionic conductivity over 40 mS/cm was achieved while the conductivity of Nafion$^{®}$ 112 was measured as 80 mS/cm and conductivity of PBI was reported approximately 10 mS/cm at 20 °C [79]. In the literature only one study reported the conductivity (125 °C, RH < 2%) of phosphoric acid doped ETFE-*g*-P4VP membranes as 30 mS/cm [70]. Moreover, in the literature radiation-grafted sulfonic acid based ETFE-*g*-PSSA membranes have the conductivity of 35 mS/cm and promising fuel cell performance for the low temperature PEMFC [98]. The conductivity of radiation grafted ETFE-*g*-P4VP membranes increases with increasing graft level and acid content. At the same time the mechanical strength decreases with acid-doping level as announced in literature. Thus, optimum doping level is thus a compromise between these two effects [99]. The results show that the method that is proposed here offers control of proton conductivity and water uptake by varying the weight content of the graft component or graft level and phosphoric acid group.

On the other hand, this study indicates that there is no significant correlation neither proton conductivity-graft level nor water uptake-graft level for both proton conducting membranes based on NVP and 2VP monomers (**Table 3-2**). The absence of a correlation is attributed to the lost of graft component after phosphoric acid doping. ETFE-*g*-PNVP membranes show relatively low conductivity, i.e., max 12 mS/cm. Nevertheless, ETFE-*g*-P2VP membranes are not proton conductive after phosphoric acid doping.

Monomer	Graft Level (%)	Water Uptake (%)	Conductivity (mS/cm)
2VP	20	9.6	-
2VP	24	10	-
2VP	27	8	-
NVP	20	22	9
NVP	26	20	11
NVP	30	20	12

Table 3-2: Effect of graft level (%) on water uptake and proton conductivity for ETFE-g-PNVP and ETFE-g-P2VP membranes

3.3.3 Mechanical Properties

Acid-doped proton conducting membranes are generally brittle, so ion-exchange capacity must be controlled to maintain their elasticity [100]. As mentioned earlier, proton conductivity increases as the graft level of the resultant membranes rises. However, mechanical properties are the limiting factor while aiming high proton conductivity. It was observed that as the graft level increases to have high proton conductivity, film quality and robustness of the film deteriorate [101].

Therefore, this study examined in detail the variation of the mechanical properties with graft level. The copolymer films and membranes behavior under tensile strength is detected for different graft and doping levels. During mechanical testing, it is assumed that the overall changes during the tensile test follows the Hooke's law and is the superposition of different deformation types (interatomic bond stretching, uncoiling which are recoverable and interchain slippage which is unrecoverable), we can conclude that the branching is increased with graft level and contributes to the mechanical properties [102].

During the tensile test, the ETFE base film possesses about 40 MPa yield strength. This high strength comes from the special position of ETFE as it contains alternating structural units of PE and PTFE that provides it a unique combination of properties conveyed from both fluorocarbon and hydrocarbon polymers [103,104].

The stress-strain curves (**Figure 3.6a**) openly show that the irradiation process causes a slight decrease on the yield strength for low graft levels. On the other hand, the yield strength increases up to 48 MPa for the copolymers with high graft level. For instance, at, yield strength values between 35 to 48 MPa the graft level is 30 to 42%

higher than default. The modulus of elasticity similarly increases by graft level. The rise in strength indicates that by grafting ETFE, graft copolymer matrix contribute to its strength and partly recover the damage of irradiation process. This also shows that a permanent copolymer structure is formed on the base film. It is also observed that lower graft level i.e., 14% creates almost no difference on the base film structure, after 21% graft level there is a significant transform from ETFE to copolymer structure. It is also physically observed that the growing brittleness of copolymers yields a decrease in elongation at break as the graft level increases. Thus there should be higher load and lower elongation before an irreversible deformation occurs on the copolymer films.

In **Figure 3.6b** tensile test results for the ETFE-*g*-P4VP membranes are represented. It is expected that radiation grafted membranes suffer from poor yield strength at high acid doping levels due to deforming effect of acid treatment. The literature reports that a slight loss on tensile strength occurs after acid treatment [106]. On the other hand, in our case, when the phosphoric acid is introduced to the copolymers, the resulting slight increase in tensile strength might be attributed to the new N-H interaction between *N* groups of 4VP and *H* groups of H_3PO_4. However, the most major outcome of this process is an increase in elongation at break at moderate graft levels such as 22, 28 and 37% that might be the reason for the plasticizing effect of acid treatment. The general observation is that the main loss for the elongation at break occurs after the grafting process. Indeed, a decrease of about 50% loss of the elongation at break occur however after acid doping elongation at break value approximates the ETFE base film's behavior.
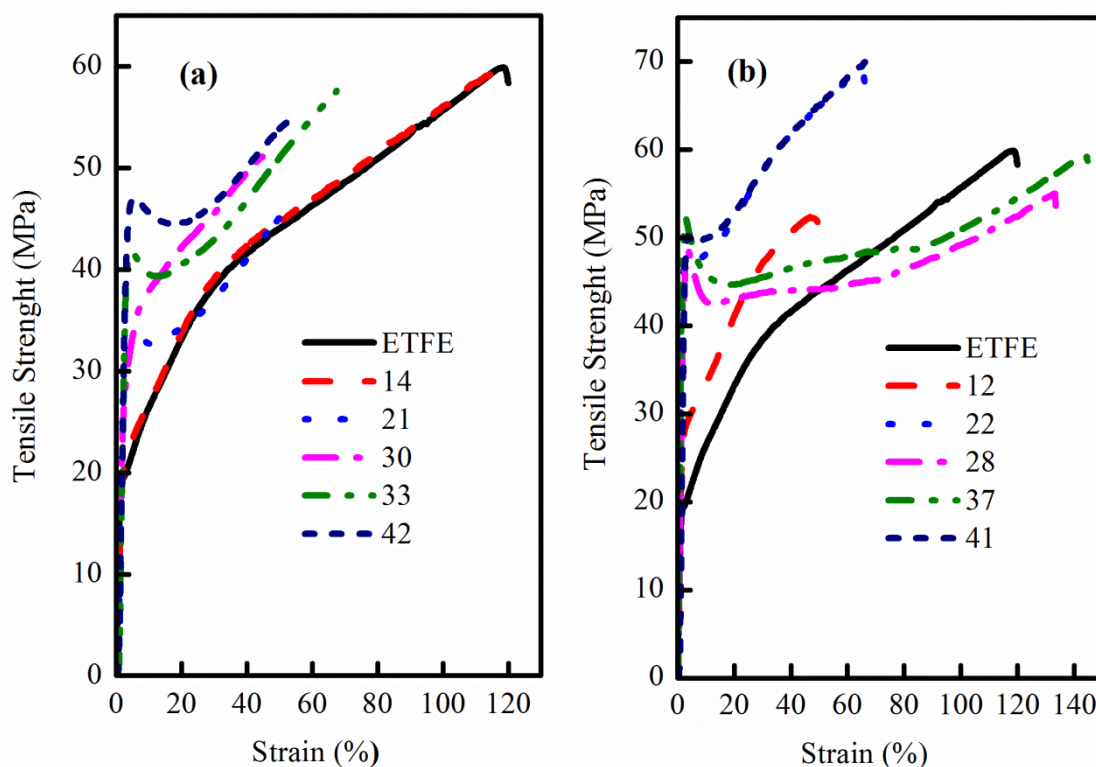
Figure 3.6: Stress-strain curves of ETFE-*g*-P4VP (a) copolymer (b) proton conducting membrane for varying graft levels (grafting conditions: solvent *n*-propanol, 10 kGy, 60 °C, 4 hours)

The radiation grafted ETFE-*g*-P4VP membrane is more rigid and plastic than Nafion® NR 211 since it shows higher tensile modulus (the slope of the initial curve, about 1.7 GPa) and high elongation at break (140%) while Nafion® shows a lower tensile modulus (0.29 GPa) and a higher elongation at break (252%) [107]. However, Nafion® elastic property may be one of the causes of the membrane damage during fuel cell operation [108, 109]. In addition, resultant radiation grafted membrane exhibits higher tensile strength (48 MPa), which is almost two times higher than that of Nafion® membrane (28 MPa). The new ETFE-*g*-P4VP membrane with better tensile property is expected to serve more durably in an operating fuel cell.

In **Figure 3.7**shows the tensile stress-strain curves for ETFE-*g*-PNVP copolymers and membranes at various graft levels. A slight (8% MPa) decrease in the yield strength from ETFE to copolymer, i.e., the maximum yield strength 32 MPa for 35% graft level is observed (**Figure 3.7a**). That might be due to the irradiation process and it is obvious that copolymerization does not contribute to the yield strength for ETFE-*g*-PNVP copolymers. Graft levels for the membranes (**Figure 3.7b**) change between 11-35% and their yield strengths change between 25 to 35 MPa, respectively.

48

Conversely, it should be noted that these yield strength still meet the yield strength of commercial Nafion® NR211 membrane. Elongation at break (%) is lower for the ETFE-*g*-PNVP membranes so that phosphoric acid doping process causes a minor damage on the film structure.
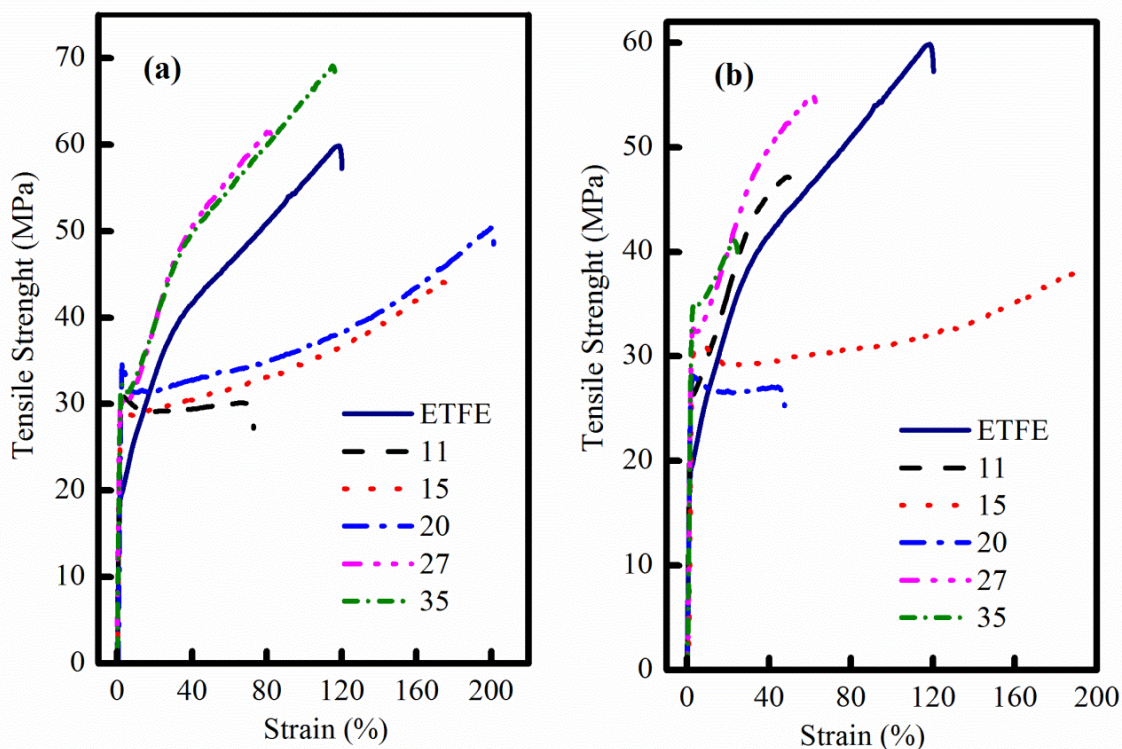
Figure 3.7: Stress- strain curves of ETFE-*g*-PNVP (a) copolymer (b) proton conducting membrane for varying graft levels (grafting conditions: solvent THF, 50 kGy, 60 °C, 4 hours)

The tensile stress-strain curves for ETFE-*g*-P2VP copolymers and membranes are given in **Figure 3.8**. For the copolymers (**Figure 3.8a**) graft level changes from 9 to 18% only a slight increase occurs in tensile strength from low to high graft level. Membrane stress-strain curves prove the fact that during the phosphoric acid doping, phosphoric acid causes considerable damage into the structure that leads weight loss since yield strength of the resultant membranes are lower than ETFE-*g*-P4VP and ETFE-*g*-PNVP membranes, i.e., 20-28 MPa yield strength. It is also considerable that there is an increase in elongation at break for high graft level membranes due to the acid doping and plasticizing effect of phosphoric acid.
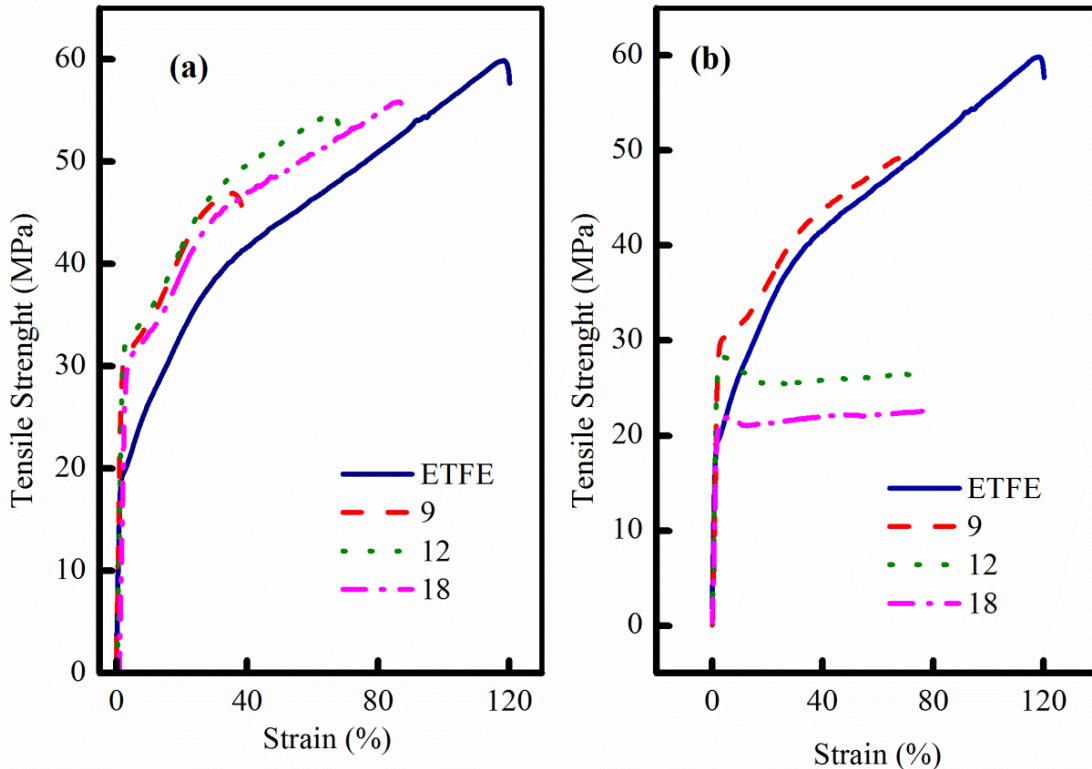
Figure 3.8: Stress- strain curves of ETFE-*g*-P2VP (a) copolymer (b) proton conducting membrane for varying graft levels (grafting conditions: solvent benzyl alcohol, 50 kGy, 60 °C, 4 hours)

3.3.4 Phosphorous Mapping and Elemental Composition of the Membranes

The resultant membranes were investigated for their cross-section morphology, Phosphorous (P) mapping and elemental composition by Scanning Electron Microscopy and Energy Dispersive Analysis (SEM-EDX). Samples which have both high proton conductivity and reasonable mechanical properties are chosen for this purpose.

Figure 3.9a illustrates the surface of the dense, pinhole and crack free radiation grafted fuel cell membrane. Research clarifies that grafting occurs according to grafting front mechanism [105]. In **Figure 3.9b** membrane cross-section is seen as two different layers at different thickness. The reason for two different layers might be the copolymerization starting from the surface of the membrane. This result is extremely essential and confirms the grafting front mechanism. Nevertheless, even grafting occurs according to grafting front mechanism, cross-section morphology and thickness are essential in the case of proton transport in PEMFC. When hydrogen is fed to anode it splits its protons and electrons, protons should go through the membrane without any barrier. To have better proton conductivity during the cell operation, phosphoric acid should be in both cross section and the surface of the resultant proton conducting

membrane. Therefore, the phosphorous (P) distribution is also been examined as seen in **Figure 3.9c**. P distribution also agrees with two layer configuration that is most copolymer positions on the surface and interacts with H_3PO_4, thus P content is much higher than cross-section, although there is still significant P at the cross-section of the membrane. This finding also very well agrees with grafting front theory and might generate a suggestive verification.
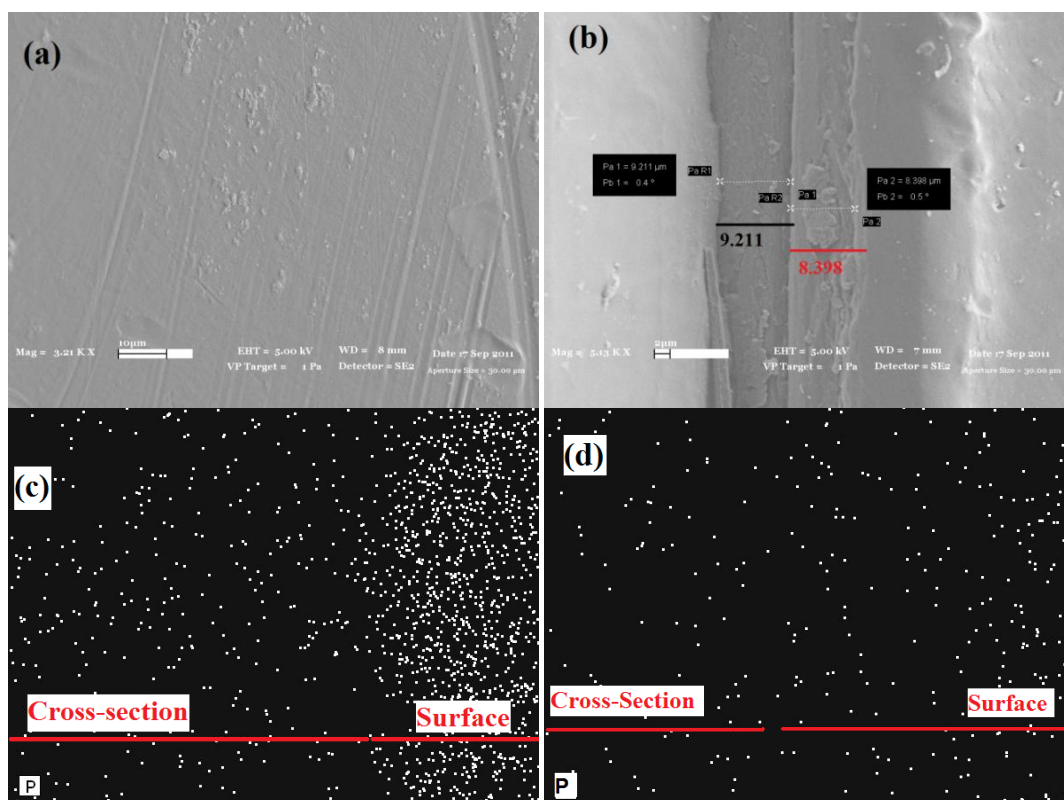
Figure 3.9: Scanning electron microscopy-energy dispersive spectroscopy (SEM-EDX) micrographs of P mapping on cross section of ETFE-*g*-P4VP phosphoric acid doped membranes a) Surface (membrane with graft level of 32%) b) Cross-section (membrane with graft level of 32%) c) P distribution (membrane with graft level of 32%) d) P distribution (membrane with graft level of 21%)

EDX results show that there is no doped P on ETFE-*g*-P2VP copolymers after H_3PO_4 treatment (**Table 3-3**). The P content on ETFE-*g*-PNVP membranes is 10 times lower than ETFE-*g*-P4VP membranes. This result also supports the low proton conductivity of ETFE-*g*-PNVP membranes. It indirectly shows that proton conductivity greatly depends on the interaction between monomer and H_3PO_4 (N-H interaction).

Element	Normalized Weight (%) 4VP/ETFE	Normalized Weight (%) NVP/ETFE	Normalized Weight (%) 2VP/ETFE
Carbon	46	64	50
Nitrogen	7	6	7
Fluorine	31	26	32
Phosphorus	3	0.3	0
Oxygen	13	14	11

Table 3-3: Elemental analysis of the membranes by SEM-EDX

3.3.5 Thermal Stability and Degradation Behavior by TGA

Thermal stability and degradation behavior of radiation grafted copolymer films and membranes were determined by TGA. The thermograms for comparison of the ETFE base polymer, ETFE-*g*-P4VP copolymer film and membrane are shown in **Figure 3.10**. ETFE base polymer demonstrated a single-step degradation pattern with transition at about 380 °C due to the decomposition on molecular chains of partially fluorinated ETFE base polymer, beyond which a smooth decrease in weight is detected. Upon irradiation, due to the degradation on ETFE morphological structure, weight loss (%) slightly increases and degradation starts similarly at about 380°C. Thus irradiation does not affect decomposition temperature of the ETFE base polymer matrix since the radiation doses is low, i.e., 10 kGy. Interestingly, a quite different result was obtained in an earlier work in which it was reported that irradiation may enhance the thermal degradation of ETFE due to the presence of oxygen-based radicals in the films whereas a different irradiation procedure was employed in this earlier work [110].
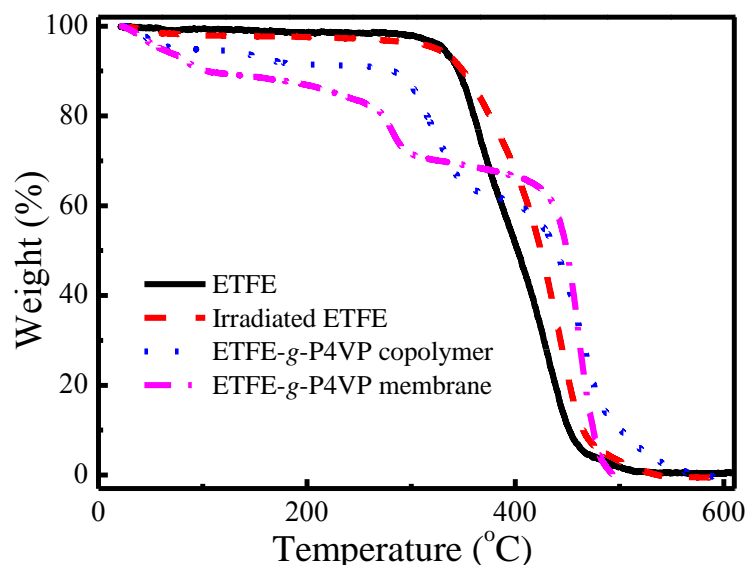
Figure 3.10: TGA thermograms of ETFE base polymer matrix, irradiated (10 kGy) ETFE base polymer matrix, ETFE-*g*-P4VP copolymer films and membranes

After grafting an additional degradation step is introduced starting at about 300 °C due to the degradation of grafted P4VP. The graft component degradation is followed by the degradation of backbone. The presence of P4VP grafts enhances the decomposition temperature of the ETFE base polymer matrix up to 440 °C. It is simply a result of the stronger C-C bonds in matrix, which leads to harder abstraction reactions. The miscibility of P4VP with the amorphous regions (C-H) of ETFE base polymers may be somewhat better than more rigid and stronger (C-F) regions. The ETFE-*g*-P4VP copolymer films behave as a two phase system, where the P4VP grafts forms a separate micro domain in the base polymer matrix [111]. The phosphoric acid doped ETFE-*g*-P4VP membrane showed a multistage degradation pattern as follows; (1) weight loss starts below 100 °C, (2) at 230 °C, (3) at 300 °C, and (4) at 440 °C. These results can be explained by taking the hygroscopic nature of the H_3PO_4 doped membranes into account. The initial weight loss at the first stage can be attributed to the loss of free water that was absorbed from atmospheric humidity. The continuous weight loss in step 2 is caused by the loss of water produced by acid dimerization: $2H_3PO_4 \rightarrow H_4P_2O_7 + H_2O$ [89]. The weight loss in step 3 corresponds to the decomposition of the P4VP grafts of the membrane. The substantial weight loss in step 4 is due to the degradation of ETFE base polymer matrix.

Figure 3.11 shows the influence of the graft level on the weight loss of the membranes. Four step degradation mechanisms are more evident for the membranes

with a high graft level. The hydrophilic structure of the membrane is enhanced by increasing graft level, thus a sharp weight loss has been occurred at around 130 °C for high graft level (40 %).

Moreover, since the increase amount of protonated grafts increases with graft level, the weight loss around 200 °C due to the phosphoric acid treatment has increased. On the other hand, the weight loss due to the ETFE base polymer matrix decreases as the graft level increases. It is another evident that grafting process contributes base polymer matrix stability.
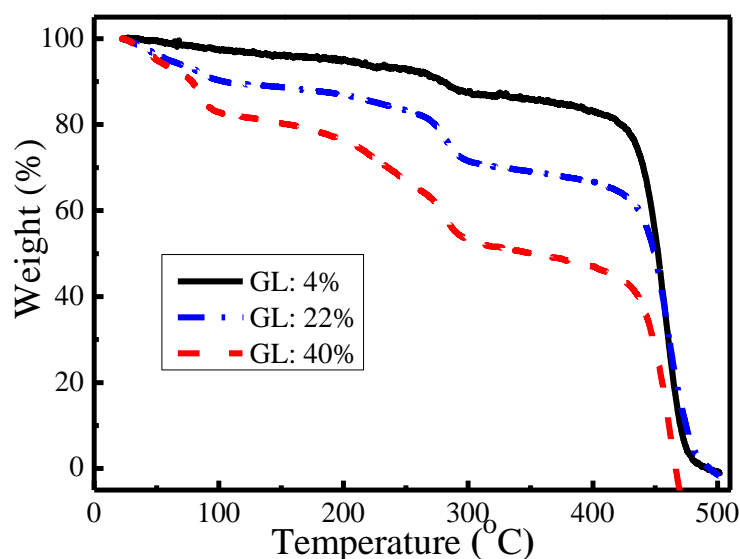
Figure 3.11: Effect of graft level on the thermal stability of ETFE-*g*-P4VP

Figure 3.12 and **Figure 3.13** demonstrate the comparison of copolymer and phosphoric acid doped copolymers with ETFE and irradiated ETFE base polymer matrix for both ETFE-*g*-PNVP and both ETFE-*g*-P2VP. The most vital impact of the resultant thermograms are that it confirms the damage of H_3PO_4 treatment on the PNVP and P2VP grafts. The graft copolymers exhibit two stage degradation mechanisms. In the first stage graft copolymers have been corrupted at about 300 °C. In the second stage, the ETFE base film has been decomposed at about 430 °C. However, ETFE-*g*-PNVP and ETFE-*g*-P2VP membranes have exhibited the same pattern with ETFE irradiated and ETFE base polymer matrix. Moreover, the weight loss mentioned in previous sections is another proof of the lost graft component on the base polymer matrix after H_3PO_4 treatment. On the other hand, decomposition temperature still higher than that of ETFE base polymer matrix, which is another indication of the PNVP grafts present in the membrane. In short ETFE and irradiated ETFE base polymer matrix

decomposition temperature is at about 380 °C, but graft copolymer and membrane decomposition temperature increase up to 430 °C.
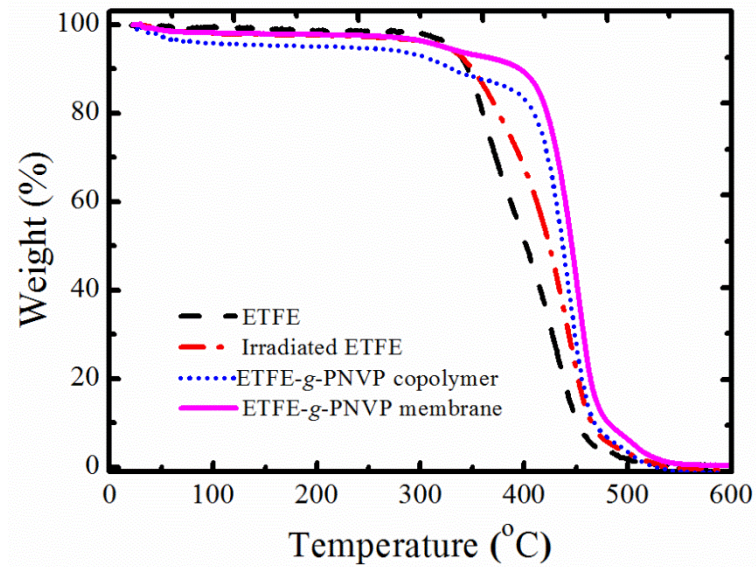
Figure 3.12: TGA thermograms of ETFE base polymer matrix, irradiated (50 kGy) ETFE base polymer matrix, ETFE-*g*-PNVP copolymer films and membranes.
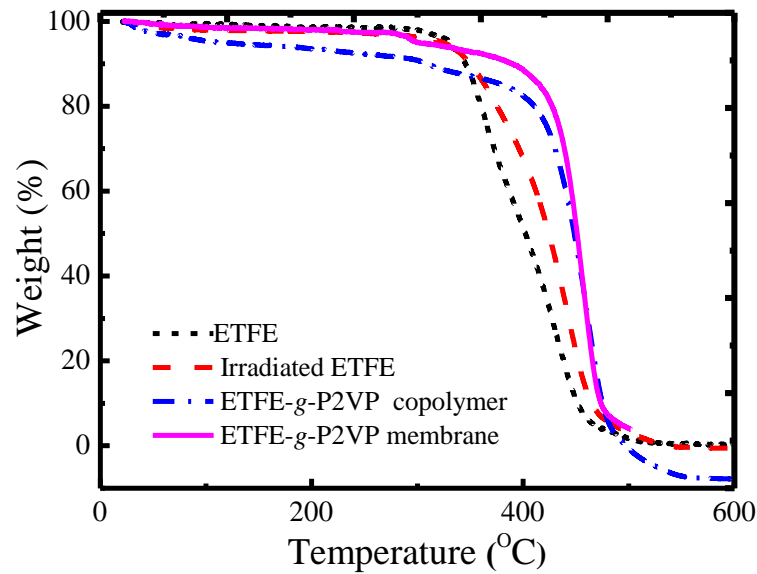
Figure 3.13: TGA thermograms of ETFE base polymer matrix, irradiated (50 kGy) ETFE base polymer matrix, ETFE-*g*-P2VP copolymer films and membranes.

3.4 CONCLUSIONS

In this part of thesis alternative, cost competitive, proton conducting membranes for high temperature PEMFC operations are manufactured. Radiation grafting method is used due to the ease of the polymerization process and convenience for membrane preparation. 4VP, NVP and 2VP monomers are selected since strong interaction with H_3PO_4 to create N-H interaction to operate at high temperature is expected. It is observed that 4VP monomer is a promising candidate to produce proton- exchange membrane since the resulting membranes exhibit promising thermal and mechanical properties, lower water uptake and encouraging proton conductivity. On the other hand, in the case of NVP and 2VP monomers weight lost after phosphoric acid doping and low proton conductivity have been observed. Moreover, both the *ex situ* proton conductivity measurements and fuel cell testing prove that ETFE-*g*-P4VP membranes are very promising to operate at high temperature and dry PEMFC operation conditions. We have observed that the ETFE-*g*-P4VP membrane can contribute PEMFC commercialization for portable and transport applications by reducing the membrane cost, enhancing water management and increasing overall system efficiency by operating at high temperatures (i.e., up to 120 °C). In the following section of this thesis study, FTA and DEA fuel cell test is going to demonstrate for ETFE-*g*-P4VP membranes.

CHAPTER 4

DEAD ENDED ANODE AND FLOW THROUGH ANODE PEM FUEL CELL TESTING OF HIGH TEMPERATURE PROTON EXCHANGE MEMBRANES

4.1 INTRODUCTION

4.1.1 DEA Operational System

The conventional PEMFC system can be organized into three main categories; (i) reactant gas supply (air or oxygen and hydrogen), (ii) thermal management and (iii) water management. In forced air systems which is used mostly in automotive applications, a centrifugal compressor is used to increases the oxygen partial pressure in the gas channels and hence the power density of the system [112]. The actuators control the supply rate and back-pressure of the air to the cathode side of the fuel cell. The excess air is supplied to the cathode to remove the liquid water from the channels [113, 114,115]. Since excess air is supplied, typically 2-3 times the amount required to support the reaction, there is a very high flow rate of gas through the cathode channels and humidification of the incoming air is required to prevent drying the Nafion$^®$ membrane. Bubblers are employed for the inlet fuel and air humidification.

This thesis uses a DEA system fed by pure dry hydrogen, which is regulated to maintain anode pressure and supply exactly the amount of hydrogen needed (SR=1) to support the reaction. DEA operation does not have as strict requirements as the RCA system on hydrogen inlet humidification due to the lower flow velocity in the channels. The water crossing through the membrane (from cathode to anode) could be enough to humidify the hydrogen if the membrane proton conductivity is depending on its water content, i.e., Nafion$^®$. The use of a pressure regulator instead of the outlet water

separator, hydrogen ejectors or blower, and inlet humidification of the RCA yield a system with lower cost and volume in DEA operation mode.

4.1.2 MEA Preparation

Since the synthesized membranes would be tested in PEMFC, the MEA preparation methods were investigated. There are two main ways to deposit the catalyst-carbon powder ink on the membrane; (i) Catalyst Coated Membrane method (CCM): the catalyst ink is directly sprayed onto the membrane (ii) Catalyst Coated Substrate (CCS) the catalyst ink is directly sprayed on GDL. In our study, the CCS is purchased and glued to the membrane with an ionomer solution. However, due to the high temperatures, choice of the ionomer was questionable. Bonville et al. [116] utilised the CCM method in the preparation of their MEA with Nafion$^{®}$ ionomer for phosphotungstic acid (known as PTA) membranes. When tested at a high temperature, they achieved good performance. Alternative ionomers have been used in the MEA fabrication process. Lee et al. [117] were using a PBI based membrane and thus chose to use PBI ionomer along with Teflon in the catalyst layer. From their polarization curve, the 5 wt % loading of PBI ionomer data gives the best results whereas the 10 wt% loadings seem to decrease the power output. This may be due to PBI being only poorly proton conducting by itself, requiring phosphoric acid to improve its proton conductivity thus leading to an overall decrease in the electrochemically active surface area. This was also seen to be the case when Lobato et al. [118] conducted tests on how the amount of PBI in the catalyst layer affected the electrochemical characteristics of it. Further research is required to in find novel ionomer materials, all of which need to be adaptable and be physically strong in both wet and dry conditions. The ionomer should be able to integrate well with the GDL as well as the membrane thus to allow for low interfacial resistance. Once the MEA is prepared, it can be tested inside a fuel cell test stand.

4.1.3. Degradation

The degradation mechanism of high temperature DEA operated ETFE-g-P4VP membranes has three intercepts in the degradation phenomena of PEMFC; (i) the effect of high temperature, (ii) the degradation mechanism of radiation induced grafted proton conducting membrane (iii) the effect of DEA operation

The first two mechanisms have a few examples in the literature and explained in detail in the following sections. On the other hand, there is only one degradation study reported in literature that subjects the degradation of DEA operation of Nafion$^{®}$ membrane. In this study, Matsuura et. al. [119] concludes two major degradation patterns associated with DEA operations. The first one is carbon corrosion in the catalyst layer that is observed at the cathode outlet, whereas the membrane polymer delamination is observed near the inlet. The degradation is much more severe under high current loads, which produces more local water distribution and higher membrane dehydration in the inlet region. The second deformation is the pinhole failure of membrane clearly affect to cell performance in DEA operation because hydrogen crossover from anode to cathode could increase dramatically due to high pressure difference during purging.

4.1.3.1 High Temperature Membrane Degradation

Fuel cell durability is an essential parameter for fuel cell development. The acidic environment of the fuel cell combined with the humidity level and temperature creates a harsh environment for the components of the fuel cell. This environment results in degradation of fuel cell components and to loss of performance in the fuel cell. In high temperature PEMFCs, the increase in temperature and the low humidity enhances the degradation rate. The lifetime of the fuel cell is one of the major challenges for high temperature PEMFCs. To the best of our knowledge, the longest lifetime reported is 18,000 h [120] under steady state conditions for PBI membranes. The main problems reported in the literature are the loss in the catalyst active area due to catalyst agglomeration, and phosphoric acid leaching out from the cell [121,122]. It is the opinion of Yu et al. [124] and Wannek et al. [125] that the main source of performance loss is due to catalyst agglomeration. Moçotéguy et al. [126] reported steady-state long term testing for a single cell and a 500 W stack with pure and

simulated reformate fuel. They achieved 1105 and 658 hours for the single cell and the stack, respectively. Hu et al. [123] ran a PBI membrane fuel cell for 500 h under steady-state conditions at constant current. The test showed that for the first 100 h the cell was operating properly, and then degradation started. They also found that the cathode catalyst particle size grew from 3.8 nm to 6.9 nm. This is confirmed by Zhai et al. [ref 6] who reported a loss in catalyst stability at high temperature resulting in 55% loss in the electrode surface area due to agglomeration. Yu et al. [124] studied phosphoric acid leaching from the membrane under steady-state conditions and reported that the level of leaching of the acid is very low which indicates a capability of operation for over 10,000 h. However, leaching was found to be dependent on temperature and load conditions and it mainly occurs on the cathode side [124]. An increase in the cell resistance due to loss of membrane conductivity was observed in the fuel cell due to the loss of phosphoric acid [97,119]. Also, delamination of MEA components occurs due to the hydrate expansion difference which is reported in [123,127]. Other lifetime related study is Cheng et al. [125] studied hydrogen crossover in HT-PEMFCs, and degradation in the PBI membrane has been reported due to hydrogen peroxide formation [128]. From all of the studies shown, it can be seen that the catalyst sintering and agglomeration is one of the biggest challenges to the long-term durability, especially if an acid-base system is used.

4.3.1.2 Degradation of Grafted Membranes

Micro-Raman spectroscopy revealed that after operation in a fuel cell, poly(vinylidene fluoride)-*graft*-poly(styrene sulfonic acid), (PVDF-*g*-PSSA), showed a significant decrease in all modes of PSSA. This shows that the degradation consisted of the loss of entire sulfonated styrene groups [129,130]. X-ray photoelectron spectroscopy (XPS) analysis showed that the chemical attack on poly(tetrafluoroethylene-*co*-perfluorovinyl ether)-*graft*-polystyrene sulfonic acid (PFA-*g*-PSSA) took place at the hydrocarbon fraction of the membrane (the grafted part portion of the structure) [129].As with other membranes, the hydroxyl radicals attack the tertiary hydrogen of the carbon. The graft fraction was found to decrease. The XPS results showed that after degradation, the polymer returned to a structure corresponding to the original, pre-grafted PFA film [131]. Similar results were seen in degradation studies of poly(fluoroethylene-*co*-hexafluoropropylene)-*graft*-polystyrenesulfonic (FEP-*g*-PSSA)

acid by Büchi et al. [132]. Ion exchange capacity (IEC) and IR spectral data showed that the polystyrene chain degraded and caused a decrease in IEC. Their results also provide a support for a degradation mechanism containing HOO˙ radicals formed at the anode. They analyzed the product water by high performance liquid chromatography (HPLC) and found several benzenesulfonic acids, including 4-hydroxy and 4-carboxybenzene-sulfonic acids. Gubler et. al. [133] observed that using a cross-linking agent (such as divinylbenze) enhances chemical stability.

In the following sections of this chapter, the experimental procedure is explained in a chronological order to explain how to perform high temperature DEA operation of the synthesized high temperature proton exchange membranes.

4.2. EXPERIMENTAL

The experimental fuel cell testing started with FTA operation to calibrate the test station. The FTA and DEA operated single fuel cell experiments were conducted in Greenlight$^®$ FC G50 test station in Sabancı University. The test station was in flow through operation mode, and then it is modified according to dead ended mode that is explained in details in the following sections.

4.2.1 Hardware and Components

The single PEM fuel cell hardware FC Pro1 consist of aluminum endplates, gold coated aluminum current collectors, and graphite flow fields. The flow fields are comprised of machined graphite plates with gas channels that are approximately 1 mm wide and depth, the flow pattern consists of semi-serpentine passages on both anode and cathode (26 channels in parallel that are 7 cm in length with two 180$^°$ turns). A square 60 W resistive heater, with a surface area of 25 cm^2, is attached to each end plate.

The 50 cm^2 MEA with Kapton$^®$ (polyimide based film) framed Nafion$^®$ N 111 IP membrane which is 600 μm thick with anode and cathode catalyst layers are containing 0.3 mg cm^{-2} Pt loading was purchased from Ion Power. SGL 10BC nonwoven carbon paper GDLs, were used, which have an uncompressed thickness of 450 μm and a porosity of $ε = 0.84$. SGL 10BC has a weight as 135 g/m^2, air

permeability as 1.45 cm^3/cm^2 s and electrical resistivity as 16 mΩcm^2. The IP MEA was chosen since it is the most improved commercial MEA. The result would be good comparison in literature.

Figure 4.1 shows experimental Greenlight® FC G50 PEMFC test station. The flow of the reactant gases are controlled by the mass flow controllers (MFC) of the test station (**Figure 4.2**). The temperature control of the supplied hydrogen and oxygen/air were maintained by the flexible hose heaters that covers the gas pathways. The dew pointer temperature, load box loading and end plates heaters temperature were controlled with the test station.
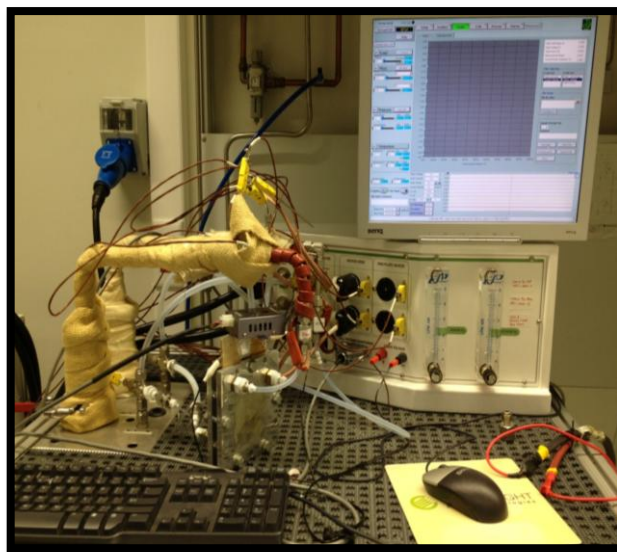
Figure 4.1: The experimental Greenlight® FC G50 fuel cell test station in FTA mode

Load Box control (RS 232)

Anode and Cathode MFCs
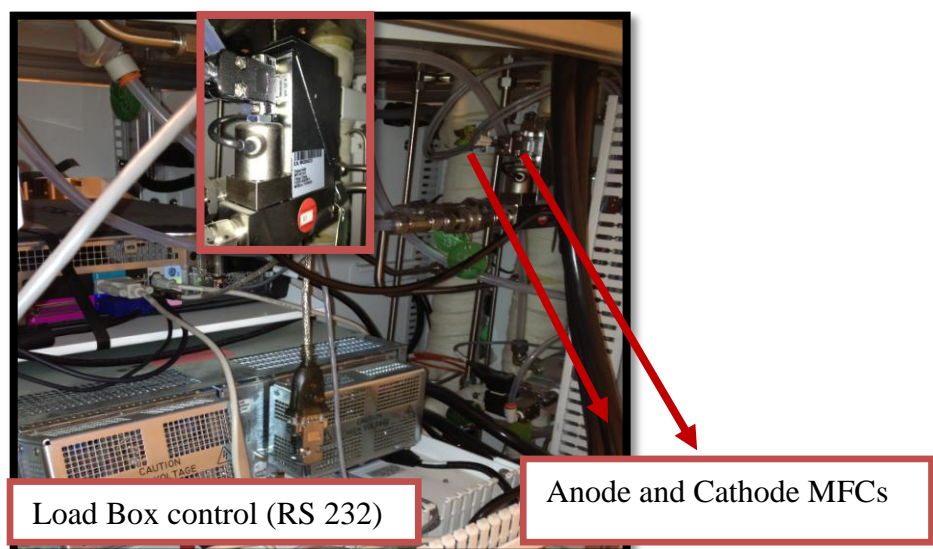
Figure 4.2: Greenlight® FC G50 MFCs and Load box control

After FTA operation fuel cell tests have been completed, the test station has been modified according to DEA operation. **Figure 4.3** shows the modified connections of test station and single cell. Two solenoid valves; one to anode inlet and one to anode exit have been connected to operate the test station in DEA mode. The hydrogen that was fed to anode inlet was also fed to the test station fuel exhaust, hence test station operated without any emergency shut downs. The schematic of the modified connections (Hoses, T-valve and solenoid valves) is presented in **Figure 4.4.** The accumulated species (nitrogen, liquid or vapor water) at the anode exit were removed by 5 seconds purging. The on/off position of the solenoid valves were controlled with NI 6220 card.

In the DEA experiments the anode and cathode were operated at FTA conditions in OCV for 30 minutes. After the load current was applied to the cell, the solenoid valve at anode exit was closed. The solenoid valve at the anode inlet was kept on. The air flow rate was kept at a SR of 3 for all working current densities. During the experiments, the cell voltage was monitored, when the cell voltage decreased to a particular value, the solenoid valve at anode downstream is opened, the cell is purged for 5 seconds and then solenoid is closed. The detailed pictures of the experimental set up of DEA operation can be found in **Appendix B**.
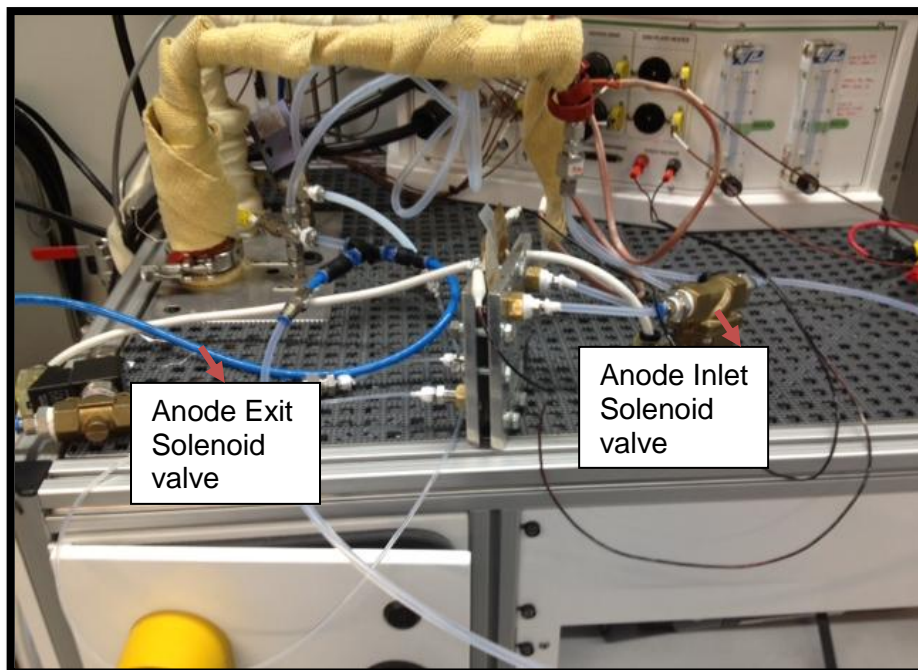
Figure 4.3: Greenlight® FC G50 Test Station according to DEA operation
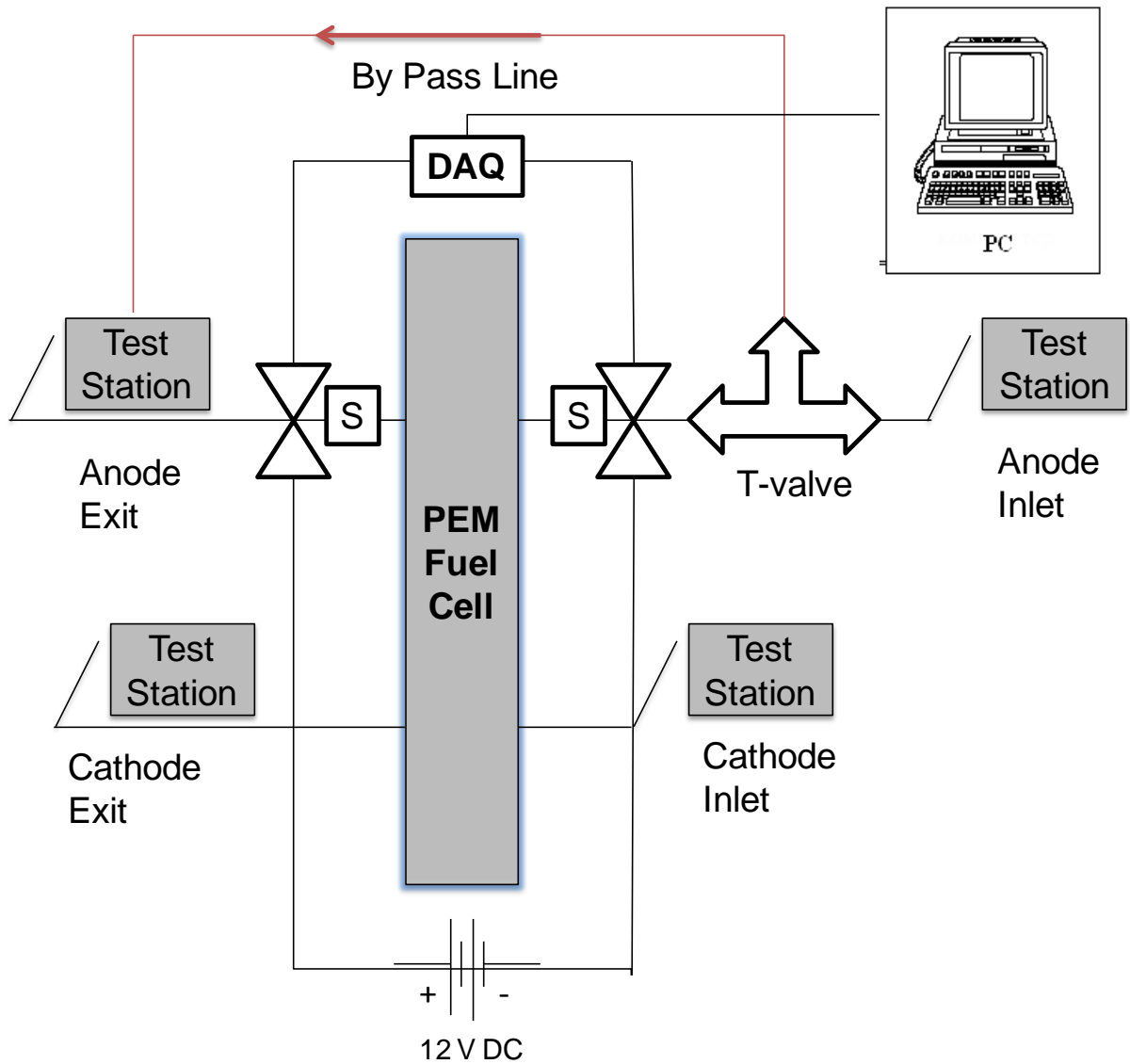
Figure 4.4: Schematic of DEA operation connection of Greenlight® FC G50 test station

4.2.2 Assembly of Single PEM Fuel Cell

The assembly of single PEMFC is constituted from outer to inner; end plate heater, end plate, current collector, graphite gas diffusion channels, and MEA consisting of a membrane and gas diffusion electrodes (**Figure 4.5**). MEA is placed in between anode and cathode.

Another essential component in PEMFC is the gasket that maintains sealing between the anode and the cathode compartments. Gasket is placed between the graphite plate and MEA to prevent gas leakage and its crossover on both anode and cathode sides. Typical gasket materials utilized in PEM fuel cells are EPDM and silicone [134]. The selection of gasket thickness is crucial to prevent gas leakage and depending on the MEA thickness. In our experiments, 150 and 250 μm ETFE base films have been used for the first time in literature as a gasket material. Since the synthesized high temperature proton exchange membrane base and gaskets have same base (ETFE), it is expected that the MEA degradation due to the silicon gasket contamination lessen particularly at high temperatures.
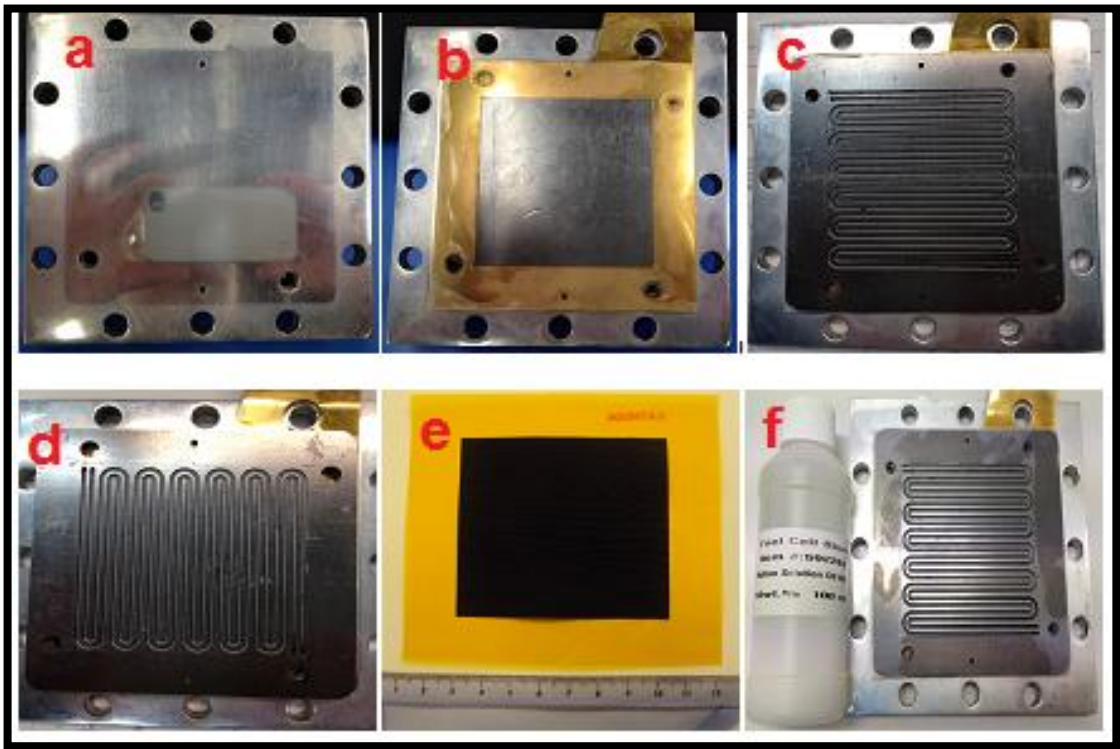
Figure 4.5: a) End Plate b) Current collector on end plate c) Cathode side gas diffusion channel d)Anode side gas diffusion channel e) Kapton® framed MEA f) Placement of sealing on gas diffusion channel

Assembly Torque

After all the layers have been lined up, the cell bolds have been inserted. The torque amount that is applied on the cell bold has been assessed according to the literature and hydrogen leakage has been monitored [135].

The total applied compression is 5 Nm. It is vital that the pressure should be homogenous during compression to reduce the mechanical stresses and degradations on the MEA. This requires the cell bolds to be numbered and the application of torque in order to cross steps (**Figure 4.6**). In every step, 0.5 Nm torque applied. In 10 steps, the cell has been compressed with 5 Nm by a torque meter. This procedure is extremely curial since if the compression is low the internal cell resistance increases, on the other hand if the compression is too much MEA active area reduces. The reduction can cause a reduction on the open circuit cell voltage.

Figure 4.6: The applied torque to assemble the test cell

4.2.3 Membrane Electrode Assembly Preparation

Membrane electrode assembly (MEA) fabrication has been conducted for *in situ* fuel cell performance of selected ETFE-*g*-P4VP membranes. EP4019 type of carbon paper electrodes (Fuel Cell Earth LLC, MA, USA) were impregnated with 10 wt.% Nafion® solution (purchased from FuelCellStore.com) using an airbrush. The membrane was sandwiched between anode and cathode electrodes with hot-pressing. The hot-pressing was conducted at 10 MPa pressure at 90 °C for 90 seconds (**Appendix C**).

4.3 RESULTS AND DISCUSSIONS

4.3.1 FTA Operated PEM Single Fuel Cell Tests

The initial PEM single fuel cell tests have been started with purchased MEAs to control and optimize the cell properties, such as cell compression, pressure, flow rates. **Figure 4.7** shows the initial voltage-current density curve of a purchased MEA with Nafion[®] 112 membrane. Even though the initial single fuel cell tests have been conducted under room temperature (T_{cell}: 23 °C), the results are important to show the performance of contaminated MEA performance since it has been stayed under unsuitable storage conditions. The MEA was un-functionalized due to the contaminations on the Pt catalyst and Nafion[®] membrane.
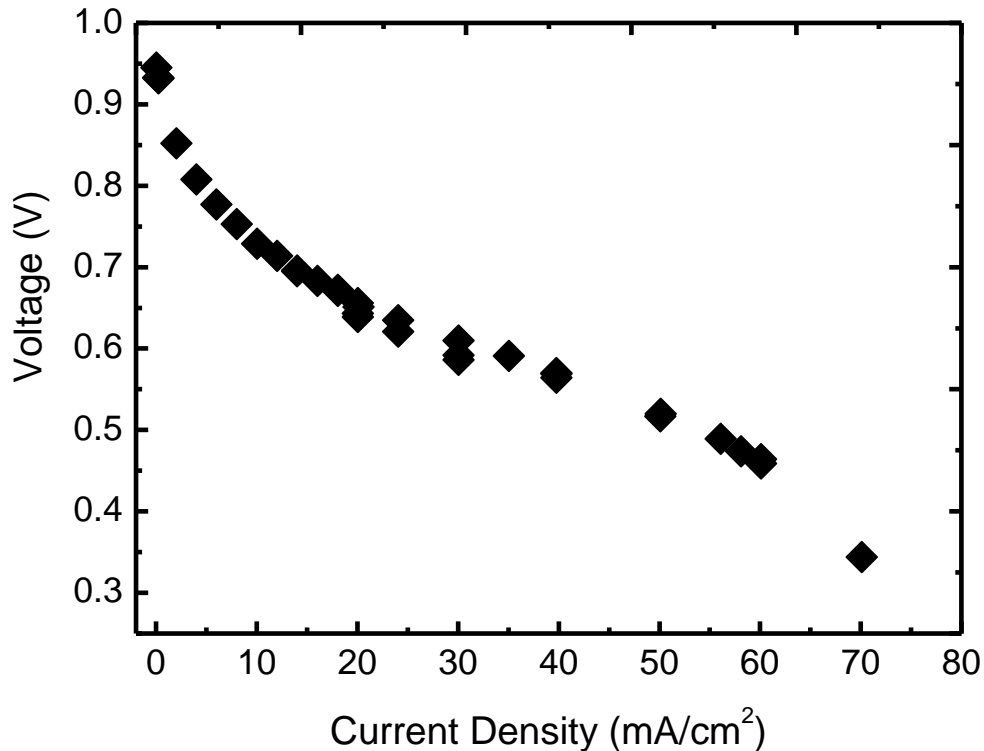
Figure 4.7: Voltage-current density curve of the PEM single cell under constant current, membrane: Nafion[®] 112, T_{cell}: 23 °C, Flow rate$_{an,H2}$: 0.5 nlpm, Flow rate$_{ca,O2}$: 0.8 nlpm, $P_{an,ca}$: 125 kPa

Figure 4.8 demonstrates the same MEA performance after four hours open circuit voltage (OCV). In literature the term conditioning of the PEM fuel cell is used to stabilize the cell initially before a load are conducted. Moreover, during conditioning chemical reaction sides are activates by eliminating the contaminations. Thus, the MEA

conditioning have continued during four hours and driven current density increased to 110 mA/cm^2 due to the activation of reaction sides. After perished MEA has been replaced with new MEA with Nafion® N111 IP membrane, single fuel cell test were continued to perform.
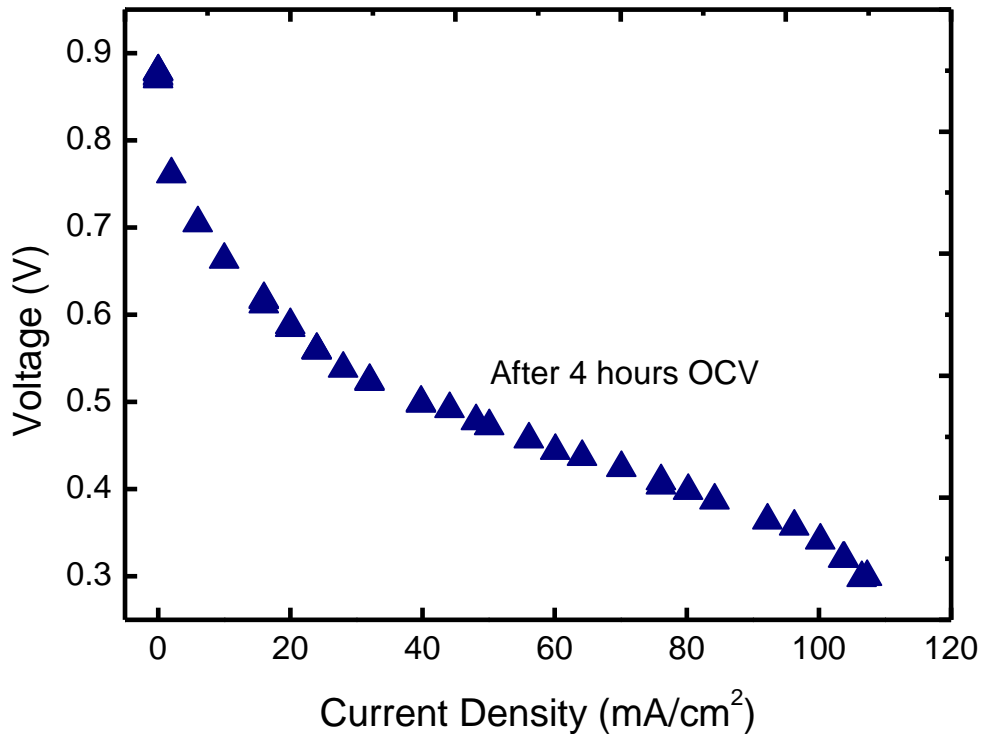
Figure 4.8: Voltage-current density curve of the PEM single cell under constant current, membrane: Nafion® 112, T_{cell}: 23 °C, Flow rate$_{an,H2}$: 0.5 nlpm, Flow rate$_{ca,O2}$: 0.8 nlpm, $P_{an,ca}$: 125 kPa

Figure 4.9 represents the voltage current density curve of MEA with Nafion® N 111 IP membrane at 50 °C for RH 60%. Since the membrane thickness was 25 μm and total MEA thickness was 450 μm, the ETFE gasket was in 250 μm thick is used and, no hydrogen leakage was observed during the single cell testing. However, after fuel cell experiments it has been observed that OCV of the cell drops under 0.7 V, it is most probably due to the hydrogen cross over to the cathode side. Thus, the cell is unassembled and MEA degradation has been detected. It has been observed that half of the MEA active area was worn out and there was a bluish green hydrogen peroxide (H_2O_2) formation on the cathode side (**Figure 4.10**). The hydrogen and oxygen were formed hydrogen peroxide on the cathode due to the hydrogen leakage to the cathode side. The hydrogen peroxide formation reversed the cell voltage, damaged the MEA, and caused power losses. It should be noted that one reason to the hydrogen cross over was the anode/cathode layer design of the experimental single cell. Due to the cell

design, hydrogen and oxygen/air enter the cell from the same side (inlet side is same). While oxygen spreads out on the inlet gas channels and forms cathode, hydrogen should cross over to the exit and spread out on the anode gas channels (inlet is cathode/exit is anode side according to the testing fuel cell design). To prevent hydrogen crossover, the sealing especially at the inlet holes had to be modified. High viscosity silicone oil (10 Pa. s) has been used for extra sealing at the anode and cathode inlet holes where the reactant gases enter the cell. Additionally, the total torque on one bold is increased to 5.5 Nm and anode/cathode has been operated at different pressure where the back pressure difference was at least 25 kPa ($P_{an} > P_{ca}$)
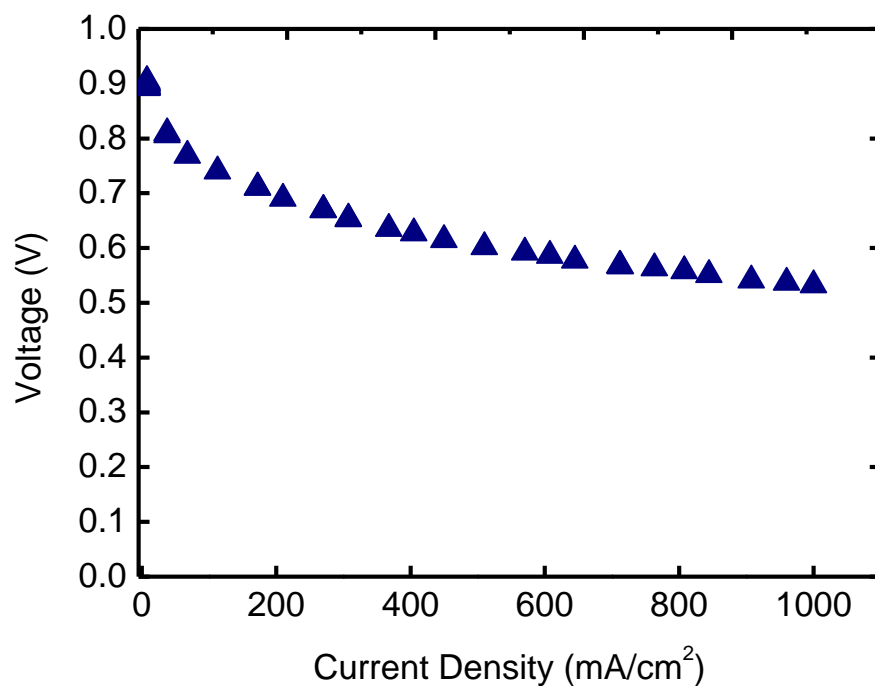
Figure 4.9: Membrane Nafion[®] N 111 IP, T_{cell}: 60 °C, T_{dp}: 50 °C, RH: 60 %, SR_{an}: 1.5, SR_{ca}: 2, P_{cell}: 125 kPa
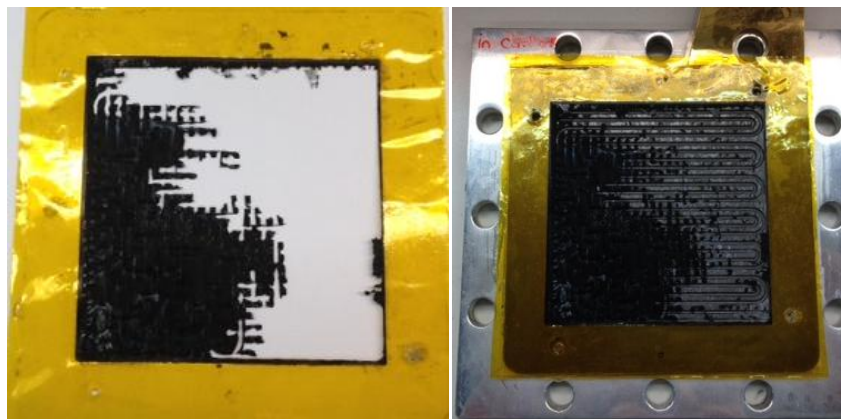
Figure 4.10: The deformed MEA with Nafion[®] N 111 IP due to the hydrogen leakage to the cathode

After hydrogen leakage was prevented, fuel cell tests were performed at different temperatures to see the effect of increased temperature in the case of Nafion[®] N 111 IP membrane. **Figure 4.11** shows the voltage-current density performance of the MEA with Nafion[®] N 111 IP membrane The increased temperature results in increased potential. Even though the activation losses (increased Tafel slope) increase, the increased temperature reasults in exponentially higher exchange current density and improved mass transport properties. Thus, cell voltage slightly increases with increased temperature. Since Nafion[®] membrane's proton conductivity depends on its water content, as the temperature increases the voltage losses at ohmic region increases. The mass transport loss region in the polarization curve improves as seen in **Figure 4.11**.
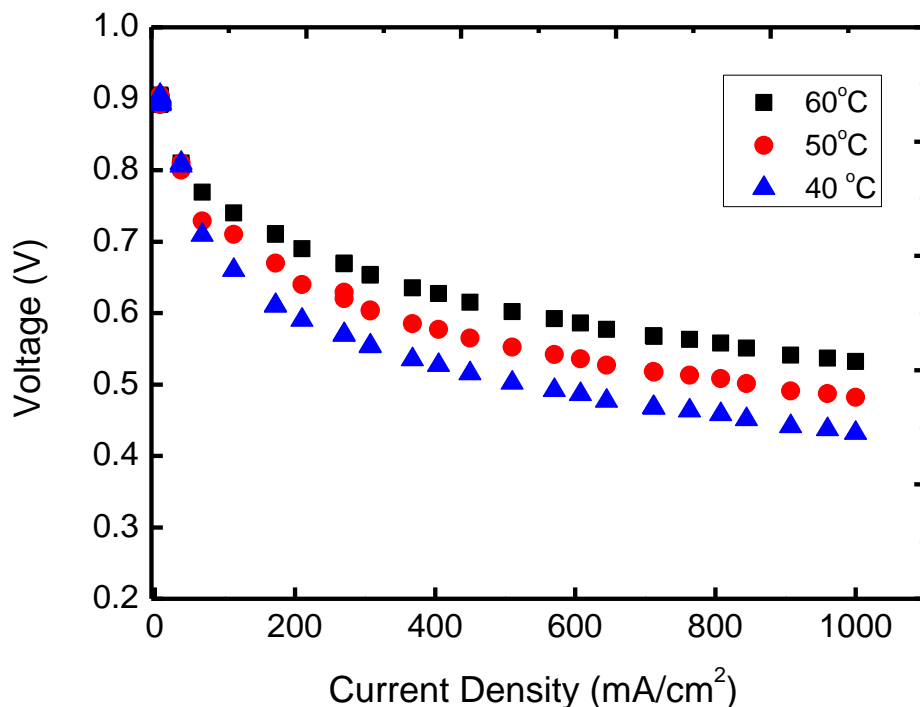
Figure 4.11: Voltage-current density curve of PEM single cell under constant current load, Membrane Nafion[®] N 111 IP, P_{ca}: 150 kPa, P_{an}: 125 kPa, $RH_{an,H2}$: 70%, $RH_{an,O2}$: 70%, SR_{an}: 1.5, SR_{ca}: 2

Typically the DEA operated PEMFCs for automotive applications are using dry hydrogen as a fuel ambient air as the oxidant, the further single fuel cell test was performed with dry anode and full humidified cathode air for Nafion[®] membrane. **Figure 4.12** shows the voltage-current density performance of the MEA with Nafion[®] N 111 IP membrane. The initial OCV of the cell is low, because oxygen concentration in air is only 21%. The operation with pure oxygen results in a gain

similar to elevating the air by a factor of 1/0.21. The performances of the MEAs are similar to the literature findings so that our test station and single cell assembled very well.
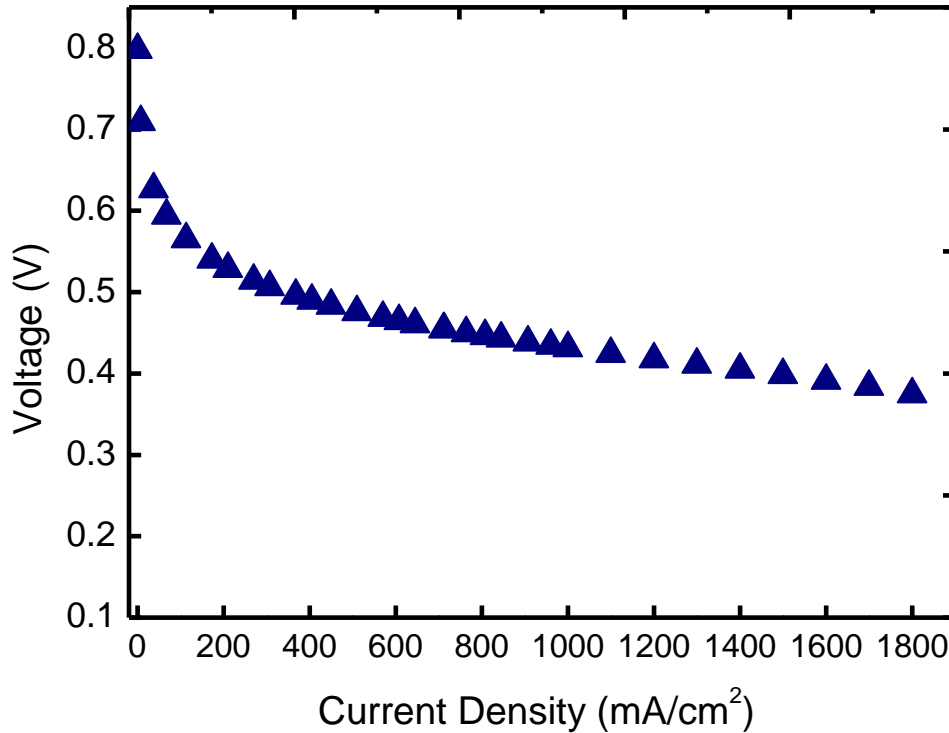
Figure 4.12: Voltage-current density curve of PEM single cell under constant current load, Membrane: Nafion[®] 111 IP, P_{ca}: 150 kPa, P_{an}: 125 kPa, $RH_{an,H2} < 2\%$ (dry),$RH_{ca, air}$:100 %, T_{cell}: 60 °C, SR_{an}: 1.5, SR_{ca}: 3

Furthermore, the single fuel cell tests were continued with synthesized ETFE-*g*-P4VP high temperature proton exchange membranes in this thesis study. **Figure 4.13** shows the single cell performance of the membranes using H_2 and O_2 as reactants at cell temperatures 80 °C and 120 °C. Both H_2 and O_2 feed stream were dry (RH < 2 %). Since these membranes are new in literature there is no well defined MEA preparation procedure. The initial single fuel cell tests were conducted without hot pressing the MEA. The ETFE-*g*-P4VP membrane is placed between purchased EP4019 type of carbon papers gas diffusion electrodes with using Nafion[®] ionomer solution as a binder. However, the interfacial contact losses were higher in the MEAs that are produced without hot pressing. Thus, initial single fuel cell performance should be improved.
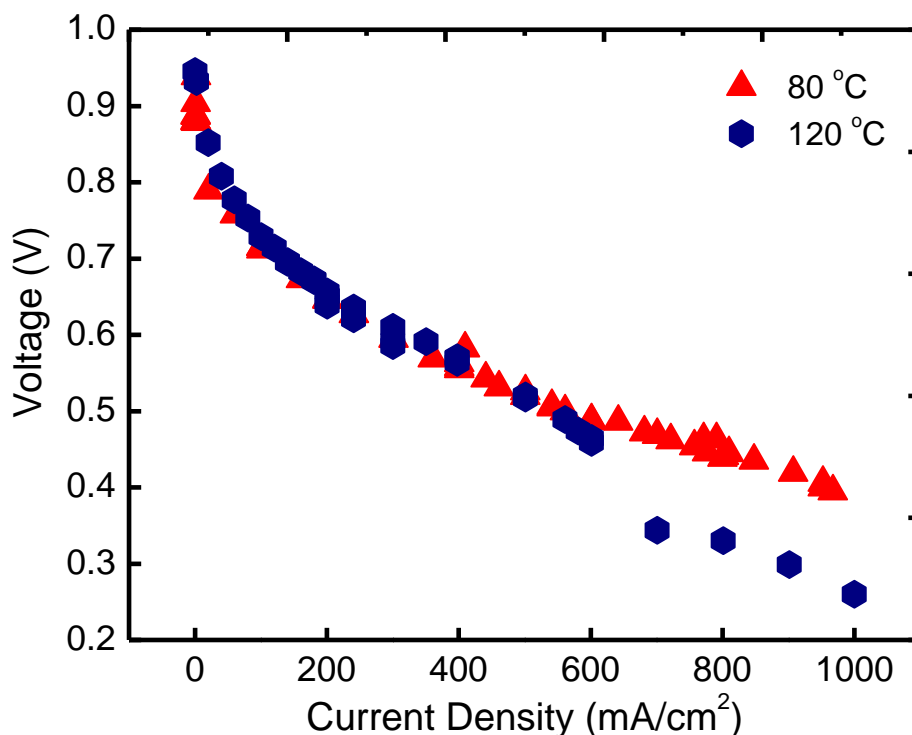
Figure 4.13: Voltage-current density curve of ETFE-*g*-P4VP membranes, MEA is fabricated without hotpressing, P_{ca}: 150 kPa, P_{an}: 125 kPa, $RH_{an,ka} < 3\%$, SR_{an}: 1.5, SR_{ca}: 2

Figure 4.14 shows polarization curves of the MEAs that are prepared with hot pressing of ETFE-*g*-P4VP membranes with electrode layers, at temperatures 80 °C, 100 °C and 120 °C. When **Figure 4.13** and **Figure 4.14** are compared, it is concluded that the hot pressing MEAs containing grafted membranes lead to superior performance.

Moreover, as seen from **Figure 4.14**, the increase in the operational temperature from 100 to 120 °C significantly improves the fuel cell performance of the membrane that indicates the benefit of high-temperature operation. **Figure 4.14** also shows the calculated power output as a function of current density, the highest power output around 0.55 W/cm^2 is obtained at current density of 1100 mA cm^{-2} at 120 °C. It can be observed from **Figure 4.14** that the gaps between polarization curves increase with an increase in temperature. For example, at the current density of 800 mA cm^{-2}, the voltage difference between 800 and 100 °C is 200 mV, while the voltage differences between 100 and 120 °C are 100 mV. This may indicate that the temperature effect on fuel cell performance is more pronounced at lower temperatures than at higher temperatures that is also agrees well with the conductivity results (**Figure 3.5**).
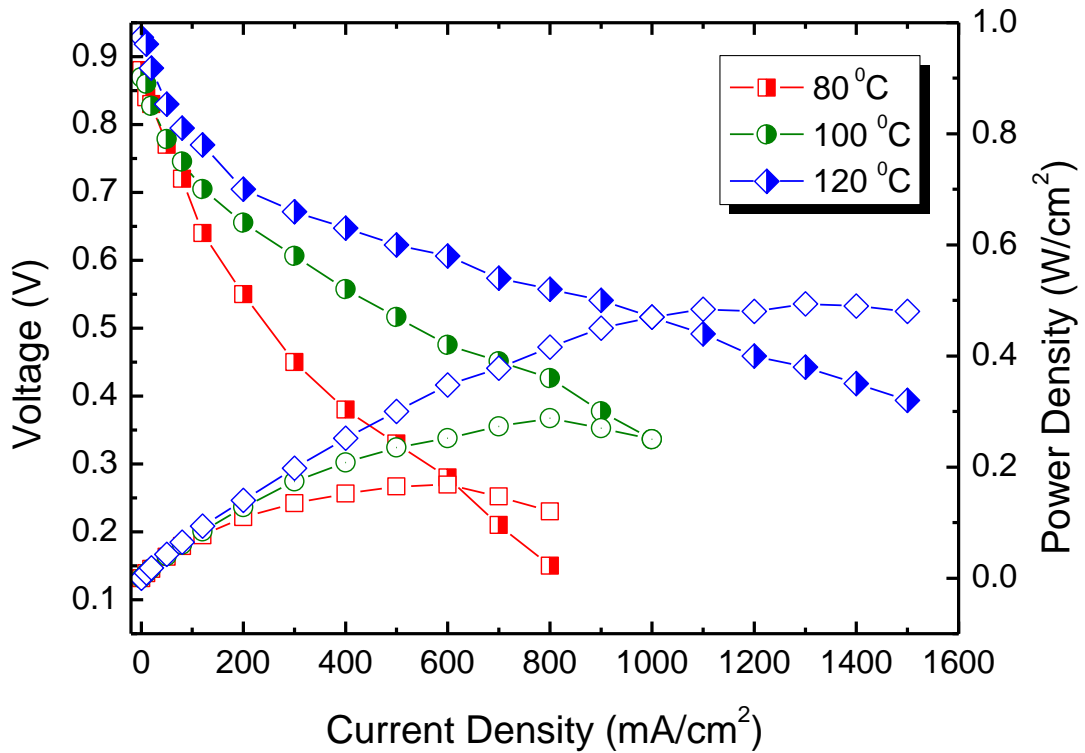
Figure 4.14: Voltage-current density curve of ETFE-*g*-P4VP membranes, MEA is fabricated without hot pressing, P_{ca}: 150 kPa, P_{an}: 125 kPa, $RH_{O2,H2} < 2\%$, SR_{an}: 1.5, SR_{ca}: 2, Tcell:60 °C

4.3.2 DEA operated PEM Single Cell Tests

Figure 4.15 demonstrates the cell voltage in a DEA operated PEM fuel cell under moderate constant current density (400 mA cm^{-2}). The MEA with Nafion$^®$ N111 IP is used, during the operation the RHs of hydrogen and air were <2%. The DEA cell was operated under constant 400 mA cm^{-2} (20 A) current density. The initial 0.58 V cell voltage was kept during 350 seconds. Due to the nitrogen and water accumulation on the anode the cell voltage starts to ramp down and reaches to 0.15 V after 650 seconds.
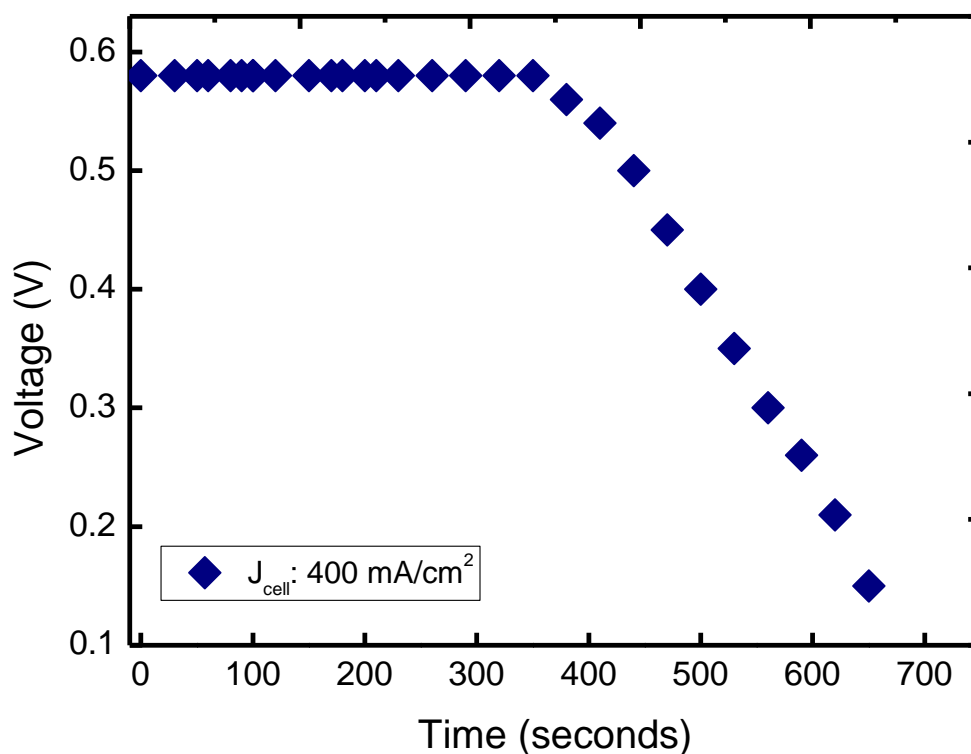
Figure 4.15: Cell voltage of the single cell with dead-ended mode operated at 400 mA/cm^{-2} constant current density. MEA with Nafion$^®$ N 111 IP. $RH_{an, H2} < 3\%$, $RH_{ca, air}$: 100% ,T_{cell}: 60 °C, P_{an}:125 kPa, P_{ca}:150 kPa, SR_{ca}: 3

e hydrophobic backbone and hydrophilic graft components, the backbone provides important properties including durability, mechanical strength, wetting properties, gas permeability, and surface energy. On the other hand irradiation, grafting and acid treatment caused defect on the membrane backbone. The earlier investigations of this type of membranes are shown that both oxygen and nitrogen diffusion and permeability increase with increasing graft level [115,135]. This concludes that in the radiation grafting membranes diffusion mainly occurs in the hydrophilic region. Moreover, in the case of PBI membranes it is observed that as the fuel cell operation temperature and acid doping level increases the gas permeability of the membrane increases [80]. The acid (H_3PO_4) increases the distance between backbone of polymer and contributes to the membrane expansion so that the gas permeation of the membrane.
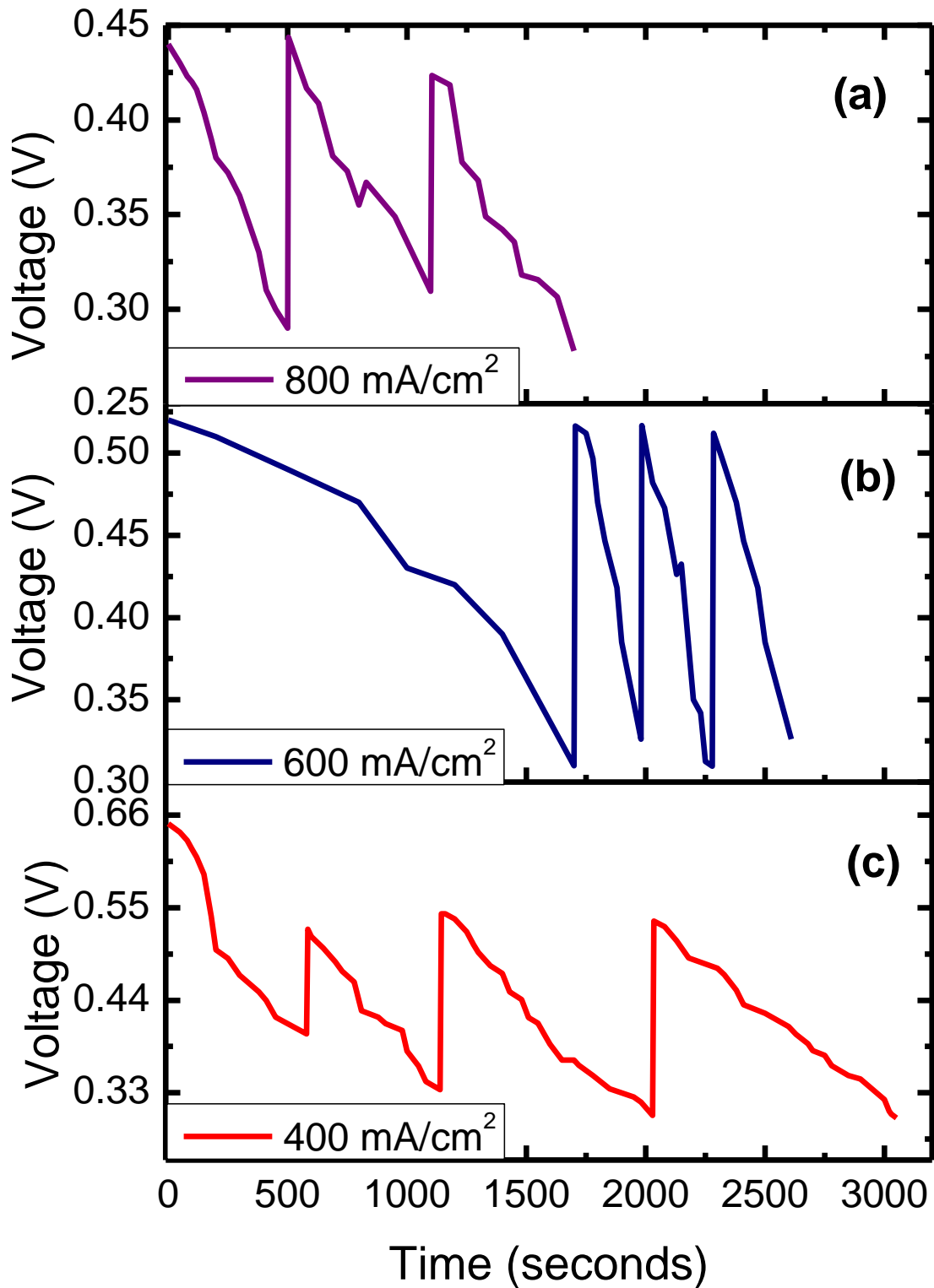
Figure 4.16: Cell voltage of the single cell with dead-ended mode operated at different constant current densities. (a) 400 mA cm^{-2} (b)600 mA cm^{-2} (c) 800 mA cm^{-2} MEA with ETFE-*g*-P4VP membrane, RH$_{an, H2}$: < 3%, RH$_{ca, air}$: <3% ,T$_{hücre}$: 110 °C, P$_{an}$:125 kPa, P$_{ca}$:150 kPa, SR$_{ca}$: 3

4.3.3 MEA Degradation

Figure 4.17 presents SEM images locations No.1 to No.3 after DEA operation of the MEA with Nafion$^®$ N 111 IP membrane. It was noted that the MEA degradation was very similar with the hydrogen crossover to the anode side (**Figure 4.10**); however there was no pronounced hydrogen peroxide formation was on the MEA's cathode (No blue peroxide color was observed). On the other hand, the DEA operation time is very short to degrade the MEA while comparing with the literature [119]. Hence, it is concluded that there should be a coupled effect of DEA operation and radical formation that degrades the graft component of the membrane on the degradation mechanism.

The SEM micrographs are shown in **Figure 4.18.** The membrane degradation is more pronounced at location No.1 where close to the dry hydrogen inlet than other locations. The hole formation on the membrane (**Figure 14.8a**) is observed that indicates the deformation on the repeated unit of the membrane backbone ($-CF_2$) due to the radical formation ($^·OOH$, $^·OH$). The deformation on the polymer repeat units causes hole formations inside the membrane structure that also lead to pin hole formation on the membrane surface. The pinhole formation causes severe irreversible voltage degradation due to the gas crossovers.

In literature, it is observed that the membrane is deformed by thinning according to its distance to dry anode inlet in DEA operation [119]. Similarly in our study, Nafion$^®$ membrane becomes thinner (i.e., from 30 μm to 20-15 μm). From **Figure 4.18a** to **Figure 4.18c,** SEM migrographs of membrane crossover present the effect of local membrane decomposition. It has been reported that the Nafion$^®$ membrane decomposition proceeds more rapidly under low RH [2]. The finding is in agreement with our observations. Since the membrane is much drier at the inlet and liquid water accumulates at the outlet of the cell in DEA operations, membrane become thinner in the dry regions.
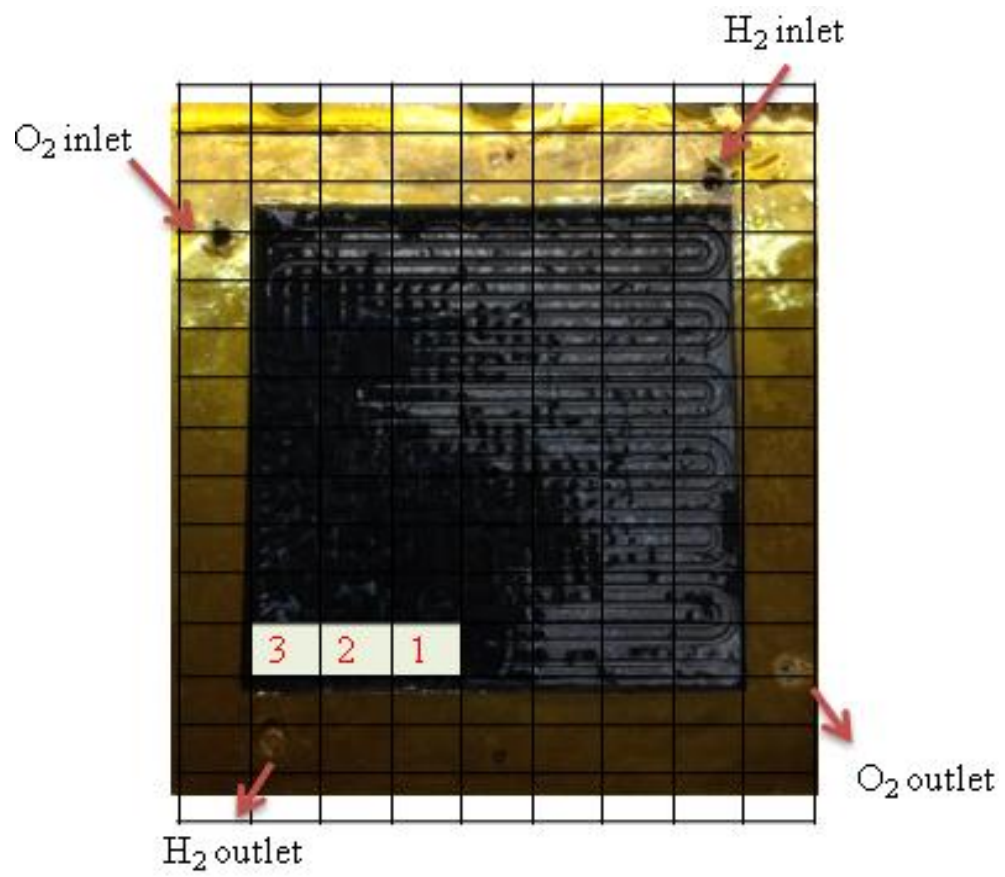
Figure 4.17: Schematic of locations of SEM samples
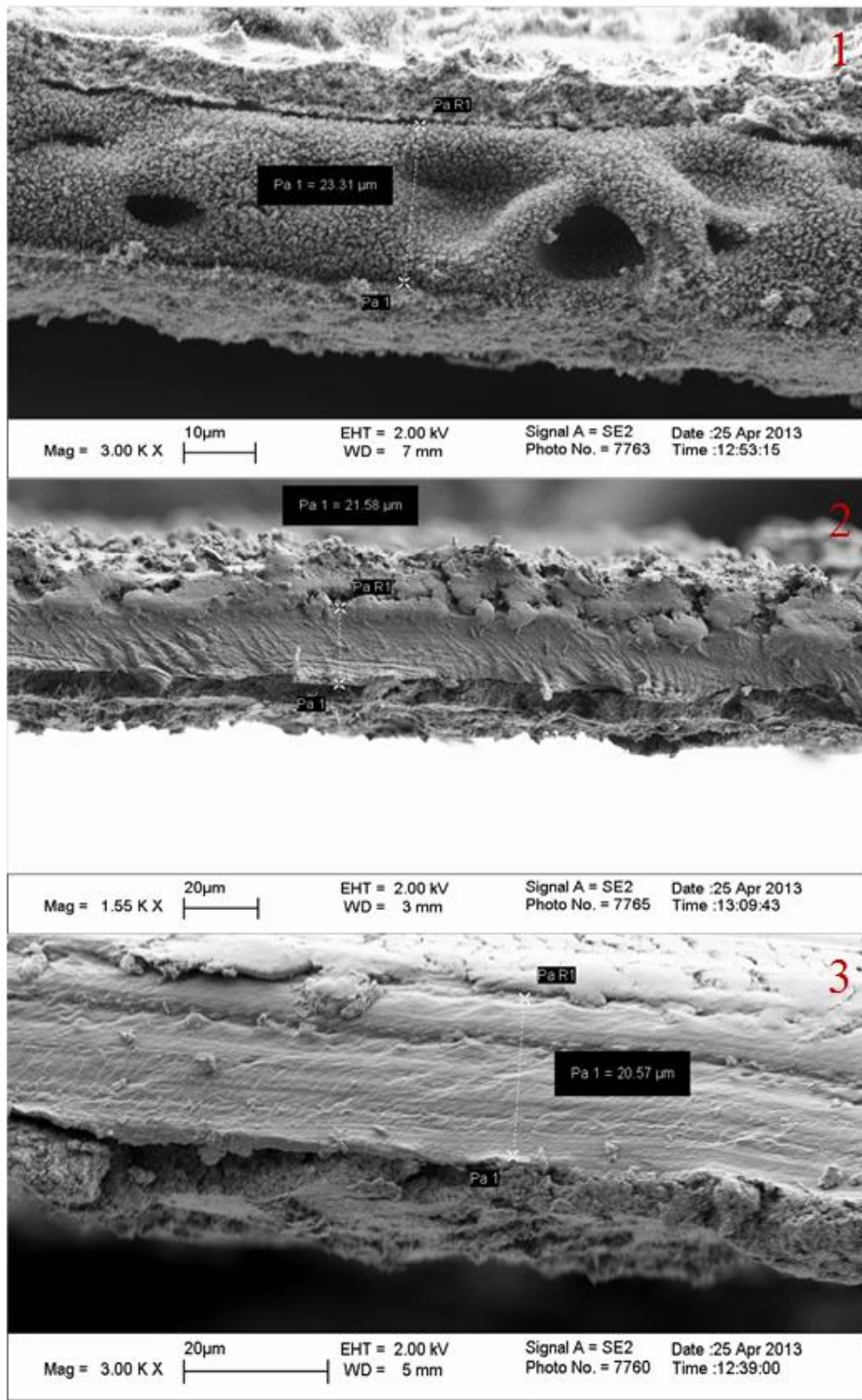
Figure 4.18: SEM micrographs of MEA with Nafion® 111 IP membrane after DEA operation

Figure 4.19 illustrates the SEM micrographs of the high temperature ETFE-*g*-P4VP membranes after DEA operation. The degradation of high temperature of high temperature ETFE-*g*-P4VP membranes is different than that of Nafion[®] membrane in DEA operation [119]. Since the high temperature DEA operation has the advantage of absence of water, membrane thickness difference between inlet and outlet due to the dry spots is not pronounced. On the other hand, by a simple averaging the thickness of unused ETFE-*g*-P4VP membrane is 48 μm which is thicker than un-doped copolymer owing to the swelling of the copolymer film after acid doping. The thickness of the ETFE-*g*-P4VP film is 40 μm which is thinner that its original thickness. In literature it is known that the attack of $\cdot$OH and HO_2 radicals produced by the incomplete reduction of oxygen on the cathode side is the main factor for the oxidative degradation of the radiation grafted membranes.

Moreover, there is no pinhole formation have been observed on the membranes. In literature, the failure mechanism for radiation grafting membranes is not well defined since the grafting component, base film and polymerization conditions are changing according to the study. On the other hand, the rough estimations based on IEC (ion exchange capacity), FTIR and XPS (X-ray photoelectron spectroscopy) analysis are in harmony with a degradation mechanism based on the formation of $\cdot$OH radicals at the anode [132]. This mechanism assumes the diffusion of oxygen through the membrane onto the anode side and formation of $\cdot$OH at the platinum catalyst which may attack the tertiary hydrogen at the α-carbon of the graft component. Especially, the IEC and FTIR results evidence that break down of graft component is responsible for the loss of ionic conductivity; therefore the ionic resistance of the membrane increases and failure begins on the cell voltage. It should be noted the base film is not degraded after the fuel cell test.

As conclusion, ETFE-*g*-P4VP membrane failure differs from Nafion[®] membrane failure in both FTA and DEA operated PEMFC. Since, gas crossovers that causes radical formation are dominant in ETFE-*g*-P4VP membranes, the graft component that maintains ionic conductivity degrades and nonionic base film remain after fuel cell operation. Hence, unlike the Nafion[®] membrane, no pinhole formation is observed. On the other hand FTA operated membrane resist longer than DEA operated membrane.
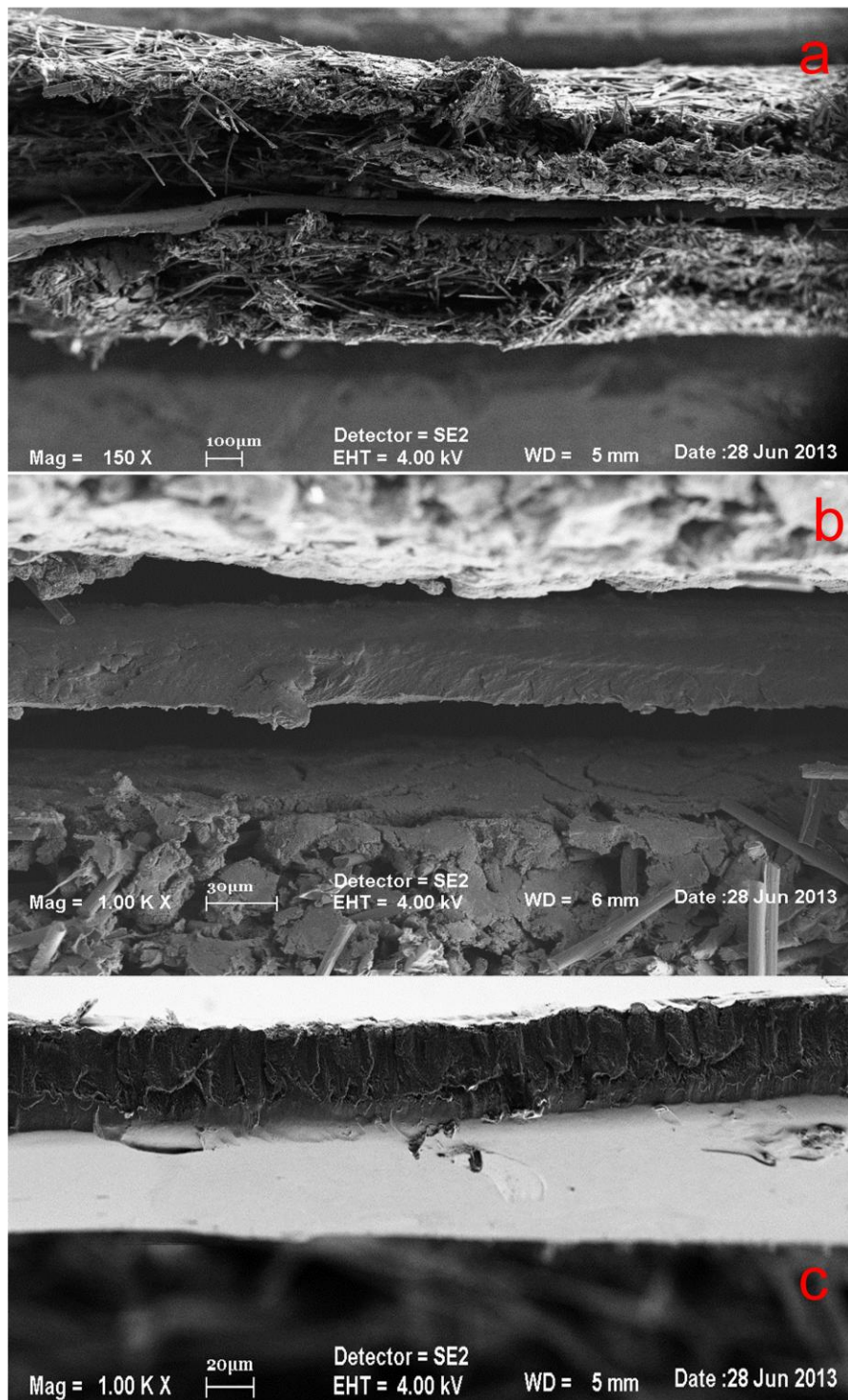
Figure 4.19: SEM micrographs of MEA with ETFE-*g*-P4VP membrane after DEA operation

4.4 CONCLUSIONS

In this part of the thesis, the FTA and DEA operated PEM fuel cell test of the Nafion$^®$ and ETFE-g-P4VP membranes are presented. The test station is prepared for the DEA operation with starting the FTA operation of the commercial Nafion$^®$ membranes. The fuel cell performance at different temperature and oxidant conditions were conducted and compared with the literature findings. It is concluded that the experimental fuel cell test station and single fuel cell is ready. Then, the DEA operated PEMFC tests were continued.

If the FTA operations of Nafion$^®$ and ETFE-g-P4VP membranes are compared, it can be concluded that the synthesized high temperature ETFE-g-P4VP membranes have promising fuel cell performance. Even though, the operation temperature range is not comparable since the Nafion$^®$ membrane cannot be operated at temperatures over 80 °C, but the Nafion$^®$ 60 C and ETFE-g-P4VP membrane 120 °C voltage values are similar. Hence, the synthesized high temperature membranes can be good alternative to use the water free PEMFC operations.

Moreover, if the DEA operations of Nafion$^®$ and ETFE-g-P4VP membranes are compared, it is seen that ETFE-g-P4VP membrane DEA transient time is slightly lower than that of Nafion$^®$ membrane. Moreover, it is observed that the DEA transient frequency increases with increased current density in the high temperature DEA operation Even though, a direct measurement for the gas permeation of ETFE-g-P4VP membrane was not performed, high gas permeation results can be detected during the fuel cell operation in the case of ETFE-g-P4VP membrane. The nitrogen crossover rate from cathode to anode in DEA operation caused shorter DEA transient time. Since the nitrogen accumulation and blanketing on the anode active area increased, the purge cycle must be increased to recover the voltage. The increased purge cycle may also contribute to the mechanical deformation of the MEA.

Additionally, from the SEM results of ETFE-g-P4VP, we have examined that the degradation mechanism is different from that of Nafion$^®$ that is well defined in literature. The gradual reduction in membrane thickness according to membrane local distance to the anode inlet, and pinhole formation on the membrane are the mechanisms that cause degradation in the DEA operation of Nafion$^®$. On the other hand, in the ETFE-g-P4VP membrane degradation, due to the oxygen crossover and radical

formation, the graft component that maintains the proton conductivity is worn out. As result the proton conductivity reduces and irreversible voltage decline takes place. But, the base film remains as gas barrier, thus pinhole formation is not pronounced for radiation grafted membrane. Moreover, due to the loss of graft component and high temperature operation, the membrane becomes thinner after fuel cell operations.

CHAPTER 5

TWO PHASE TRANSPORT MODELING OF THE DEAD ENDED OPERATON OF POLYMER ELECTROLYTE MEMBRANE FUEL CELL

In this chapter of the thesis study, the two-phase water transport of the DEA operated Nafion[®] membranes at temperature below 80 °C are modeled. The model is validated with a study in literature that measures the water amount in anode/cathode GDL and gas channels of a DEA operated PEMFC by neutron imaging technique. The validated numerical model will be used to model the high temperature ETFE-*g*-P4VP membrane DEA performance; however it will be the subject of our future study.

5.1. INTRODUCTION

To date, there are numbers of numerical studies focused on flow-through conditions on PEMFC [137,138]. However, there is less numerical study focused on understanding of DEA operation. In literature, Mocoteguy et al. [139] modeled one dimensional, single phase, DEA operated PEMFC based on semi-empirical relations; however, they neglected the influence of anode side on its transient behavior. Dumercy et al. [140] simulated pseudo-two-dimensional fluid characteristics along the channel on the anode side with dead-end mode to optimize the stack properties. Kocha et al. [141] developed a model which predicts nitrogen crossover from cathode to anode. Ahluwalia et al. also studied the effect of nitrogen crossover and derived the membrane-water content dependent permeability of nitrogen [142]. In two studies, it is concluded that at high cell current density and high humidification rates (i.e. > 75%) in the cathode, accumulated nitrogen that diffused to anode leads to voltage losses. McKay et al. modeled a semi-empirical one dimensional isothermal two-phase model for DEA

PEMFC, they concluded that the voltage degradation is mainly caused by accumulation of liquid water in the anode channel which blocking the fuel cell active area [143].

In the previous study, one dimensional, single phase, along the channel model DEA operation of PEMFC was developed. The model concludes that the voltage degradation is caused by nitrogen accumulation, however on the study the effect of two phase water transport is not taken into account [144]. In the present chapter, the model is further extended to include the two phase water transport considering both convection and diffusion effects. It is intended to develop a fundamental understanding of the two phase phenomena occurring in DEA operated PEMFC. Water accumulation on the cathode and back diffusion to the anode effects were considered in our time-dependent transient analysis of one dimensional, two-phase along the channel numerical model.

Figure 5.1 represents two phase water and nitrogen transfer mechanism between anode and cathode during the DEA transient. The nitrogen permeation of the Nafion$^{®}$ membrane increases with its water content. On the upper portion of the cell, water vapor diffuses through the membrane from cathode to anode. Additionally, nitrogen permeates through the membrane to anode due to its increased partial pressure in the cathode. Towards the end of anode channel (where the exit is closed) water starts to accumulate and causes H_2 starvation together with diffused nitrogen.

Since, the anode local electrochemical reaction rate that depends on the hydrogen concentration due to the regulated anode pressure, determines the local water generation rate which affects directly the Nafion$^{®}$ membrane water content. Even though nitrogen accumulation dominates on the cell voltage losses, since membrane nitrogen permeation depends on membrane's water content, there is a coupled effect of water and nitrogen accumulation on the cell voltage performance in DEA operation.

As continued mechanism, the accumulated nitrogen on the anode exit diffuses to the cathode (positive x-direction) due to increased partial pressure on the anode side. Moreover, increased saturation of liquid water at the anode exit positively contributes to the diffusion of nitrogen back to the cathode side.
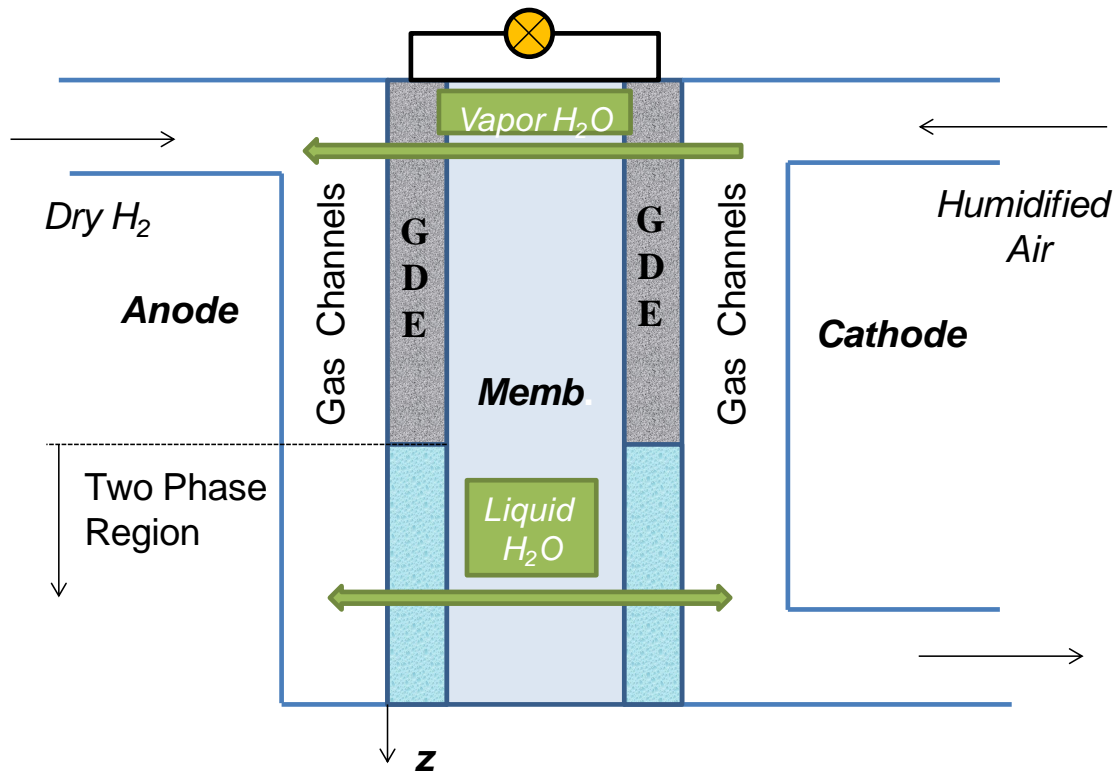
Figure 5.1: The two phase liquid-vapor water and nitrogen transport mechanism in DEA

The experimental DEA operated PEMFC used in our model validation is explained in detail by Siegel et al. [8]. In their experiments, the liquid water amount during a DEA transient is measured by neutron imaging inside anode/cathode channels and GDLs. Our model results were compared with the neutron imaging results and can be used to predict the accumulated liquid water amount.

5.2 MATHEMATICAL MODEL

Time-depended, one-dimensional, two phase, along the channel model of DEA operated PEMFC between purge cycles is presented in our numerical model. The model is validated with Siegel et al. [8] experimental set up that consists of a membrane placed between anode and cathode gas diffusion electrodes (containing micro porous layer) and gas diffusion channels. The computational domain is demonstrated in **Figure 5.2**.
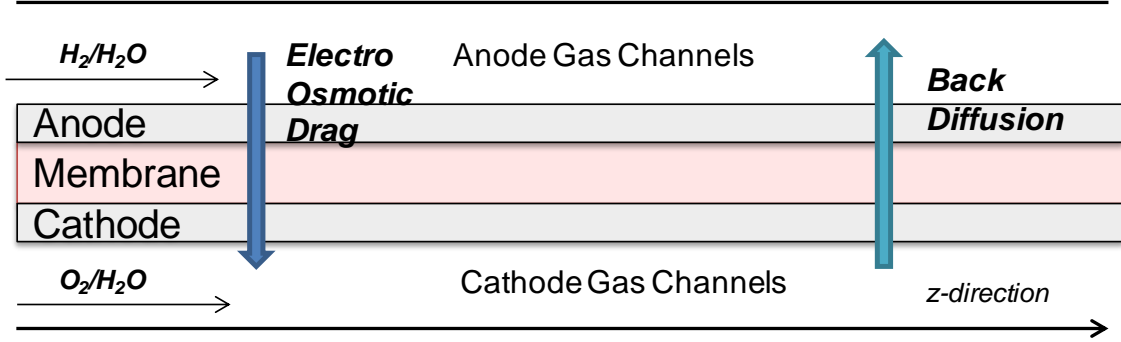
Figure 5.2: One dimensional modeling domain

Our numerical model consists of by three sub-models: (i) Maxwell-Stefan transport equations were used for conservation of mass (ii) Then, Maxwell-Stefan equations were coupled with a voltage model to obtain the kinetics of reactions (iii) two-phase transport of the liquid water. The mass conservation equations were coupled with electrochemical process through the source terms.

In the modeling, it is assumed that the anode and the cathode volumes contain a mixture of hydrogen/oxygen, nitrogen and water vapor. The species' concentrations in the channel are calculated based on the conservation of mass assuming the channel is homogeneous and isothermal. Water vapor from reactions and supplied with the cathode gas stream is exchanged between the anode and the cathode through the hydrophilic membrane. Water exchange takes place according to the back diffusion due to concentration gradient from the cathode to the anode and electro-osmotic drag from anode to cathode. Although, the thin polymeric membrane permits the crossover of molecules when there is a concentration gradient across the membrane, oxygen and hydrogen crossover were negligible. Thus, only water and nitrogen crossover across the membrane were considered for the sake of model simplicity. The details on the mathematical model are explained on the following sections

5.2.1. Mass Transfer

The Maxwell-Stefan diffusion and convection equations are used to model the time-dependent transport of species along the anode and cathode channels:

$$\frac{\partial}{\partial t}\rho w_i + \frac{\partial}{\partial z}\left(-\rho w_i \sum_j D_{ij}\frac{\partial x_j}{\partial z} + \rho w_i U\right) = r_i \qquad (5.1)$$

where w is the mass fraction, x is the mole fraction, ρ is the density, D_{ij} binary diffusion coefficient of species i and j, z is the coordinate in the direction of the flow, t is time, U

is the convective velocity and r is the reaction rate: species in the anode channel are H_2, H_2O vapor and N_2, and in the cathode are O_2, H_2O vapor and N_2. The Maxwell-Stefan equations are solved for two species at the anode and cathode; the mole fraction (or the mass fraction) of the third component is determined from the conservation of total mass:

$$x_3 = 1 - x_1 - x_2 \qquad (5.2)$$

In (5.1), binary diffusion coefficients which characterize the interactions between a pair of species are obtained for multi-component mixtures [145]:

$$D_{ij} = 3.16 \times 10^{-8} \left(\frac{T^{1.75}}{p \left(v_i^3 + v_j^3 \right)^2} \right) \left(\frac{1}{M_i} + \frac{1}{M_j} \right)^{1/2} \qquad (5.3)$$

where P is the pressure, v_i is the molar volume of species i, T is temperature, and M_i is the molecular weight of species, i. In Maxwell-Stefan equation (5.1), the density of the mixture, ρ, is given by densities of mixtures in the anode and cathode is obtained from the Dalton's Law:

$$\frac{1}{\rho} = \frac{\sum_i \dfrac{w_i}{M_i}}{p / (RT)} \qquad (5.4)$$

where R is the universal gas constant.

The convective velocity, U, in (5.1) is the average velocity of the flow. The convective velocity, U is the sum of the velocity that corresponds to the exit stoichiometric ratio of the flow and the velocity obtained from total flux of the species reacting at the catalyst layer and exchanged at the membrane:

$$U = U_{exit} + U_{flux} \qquad (5.5)$$

Convective velocities at the anode and cathode are verified from different factors. In the cathode, the convective velocity is determined from the stoichiometric ratio of the flow, which is usually set to a value sufficiently larger than one. In the anode, the flow of hydrogen, especially near the inlet, is the major part of the convective velocity, since all the hydrogen consumed in the reaction flows through the inlet. The convective velocity due to fluxes of species reacting and crossing over the membrane at a given position is the integral of the mass fluxes downstream, i.e.:

$$U_{flux}^{an}\left(z \right) = -\frac{1}{\rho_{an}} \int_z^L N_{H_2}^{an}\left(z' \right) + N_{N_2}^{an}\left(z' \right) + N_{H_2O}^{an}\left(z' \right) \, dz' \qquad (5.6)$$

Here, L is the length of the channels, $N_{i,an}$ are the inward mass fluxes at the membrane interface.

The inward mass flux of hydrogen that reacts at the catalyst layer is obtained from:

$$N_{H_2}^{an} = -\frac{M_{H_2}}{2F} J_{cell} + J_{loss} \tag{5.7}$$

where F is the Faraday's constant, J_{cell} is the local current density and J_{loss} is the parasitic current density due to the loss of hydrogen that might crossover the membrane to the cathode side. It is assumed that the parasitic loss is proportional to the mole fraction of hydrogen:

$$J_{loss} = J_{loss,0} x_{H_2} \tag{5.8}$$

where $J_{loss,0}$ is an estimated constant based on the permeance of hydrogen through the Nafion® membrane [3].

The local flux of nitrogen through the membrane is calculated from the difference between the partial pressures of nitrogen in the cathode and the anode:

$$N_{N_2}^{an} = M_{N_2} \psi_{N_2} \frac{p \; x_{N_2}^{ca} - x_{N_2}^{an}}{\delta_m} \tag{5.9}$$

Here, δ_m is the thickness of the membrane, and ψ_{N_2} is the membrane water-content dependent permeance of nitrogen as the water content increases nitrogen permeability of the membrane increases. The correlation is given by [142]:

$$\psi_{N_2} = \psi_{N_2}^0 \; \left(0.0295 + 1.21 f_V - 1.93 f_V^2 \right) \exp\left[\frac{E_{N_2}}{R} \frac{T - T_0}{T T_0} \right] \tag{5.10}$$

where $\psi_{N_2}^0$ is 1×10^{-14} mole/m^2, E_{N_2} is 24 kJ/mole and f_V is the volumetric ratio of the liquid water in the membrane, and given by:

$$f_V = \frac{\lambda V_{H_2O}}{V_m + V_{H_2O}} \tag{5.11}$$

Here, λ is the molar ratio of water molecules per sulfonic group in the membrane, V_m and V_{H2O} are the molar volumes of the dry membrane and liquid water.

In Eq. (5.6), the flux of water vapor across the membrane is given by:

$$N_{H_2O}^{an} = M_{H_2O} \left[\frac{c_{SO_3}^0 \; \lambda_{eq}^{ca} - \lambda_{eq}^{an}}{R_m} - n_d \frac{J_{cell}}{F} \right] \tag{5.12}$$

where $\lambda_{eq}^{an,ca}$ is the water content of the membrane at the local equilibrium conditions at the anode and cathode; $c_{SO_3}^0$ is the molar concentration of sulfonic groups in the dry membrane; and n_d is the electro-osmotic drag coefficient that gives the number of water molecules dragged by each proton; and R_m is the membrane's resistance to water flux and given by:

$$R_m = \frac{1}{k_{ads}} + \frac{1}{k_{des}} + \frac{\delta_m}{D_\lambda} \tag{5.13}$$

In Eq. (5.13), k_{des} and k_{ads} are desorption and adsorption coefficients and D_λ is the diffusion coefficient of water; k_{des}, k_{ads} and D_λ are experimentally measured by Ge et al. [146] and given by:

$$k_{des} = 4.59 \times 10^{-5} f_V \exp\left[2416\left(\frac{1}{T} - \frac{1}{T_0}\right)\right] \tag{5.14}$$

$$k_{ads} = 1.14 \times 10^{-5} f_V \exp\left[2416\left(\frac{1}{T} - \frac{1}{T_0}\right)\right] \tag{5.15}$$

$$D_\lambda = 2.72 \times 10^{-9} f_\lambda \exp\left[2416\left(\frac{1}{T} - \frac{1}{T_0}\right)\right] \tag{5.16}$$

where f_λ is temperature dependent coefficient and specified as:

$$f_\lambda = \begin{cases} .0543 + .00336\lambda, T = 323\text{K} \\ .0771 + .00259\lambda, T = 353\text{K} \end{cases} \tag{5.17}$$

On the cathode, the local inward oxygen flux due to the reaction at the catalyst layer is given:

$$N_{O_2}^{ca} = -\frac{1}{4F} M_{O_2} \ J_{cell} + J_{loss} \tag{5.18}$$

The local inward flux of water vapor on the cathode is the sum of the opposite of the flux going into the anode and the water coming out from the reaction at the catalyst layer:

$$N_{H_2O}^{ca} = M_{H_2O}\left[-c_{SO_3}^0 \frac{\lambda_{eq}^{ca} - \lambda_{eq}^{an}}{R_m} + \left(\frac{1}{2} + n_d\right)\frac{J_{cell}}{F}\right] \tag{5.19}$$

The nitrogen flux into the cathode is the opposite of the flux going into the anode, which is given by (5.9).

In the Maxwell-Stefan equations given by (5.1), reaction rates are determined from the mass flux of each species given by (5.7), (5.9) and (5.12),

$$r_i = \frac{N_i}{d_{eff}} \tag{5.20}$$

where d_{eff} is the effective depth of the anode and cathode channels and defined as the ratio of the total volume available to species, V_{Total}, and the active area of the fuel cell, A_{cell}, i.e.:

$$d_{eff}^{an,ca} = \frac{V_{Total}^{an,ca}}{A_{cell}} \tag{5.21}$$

5.2.2. The Voltage Model

The cell potential can be calculated from the membrane resistance and electrode polarizations. In the voltage model, cathode electrode potential is expressed as the loss from the reversible cell potential, V_{rev}, due to potential drop in the membrane, ΔV_m, and anode activation, ΔV_{an}, and cathode activation, ΔV_{ca} by assuming that the anode electrode is kept at ground.

$$V_e = V_{rev} - \Delta V_{an} - \Delta V_{ca} - \Delta V_m \tag{5.23}$$

The reversible cell potential is given by:

$$V_{rev} = V_0 + \frac{RT}{2F}\left[\frac{1}{2}\log\left(\frac{c_{O_2}}{c_{O_2}^{ref}}\right) + \log\left(\frac{c_{H_2}}{c_{H_2}^{ref}}\right)\right] \tag{5.24}$$

Here, c_i^{ref} refers to reference concentration of species i, V_0 is the open-circuit potential and given by [3]:

$$V_0 = 1.23 - 0.00083 \times T - 298 \tag{5.25}$$

The anode and cathode activation over potentials in (5.23) are given by [147]:

$$\Delta V_{an} = \frac{RT}{F\beta_{an}}\operatorname{asinh}\left[\frac{J_{cell}}{i_{0,ref}^{an}}\left(\frac{c_{H_2}^{ref}}{c_{H_2}^{CL}}\right)^{\gamma_{H_2}}\right] \tag{5.26}$$

$$\Delta V_{ca} = \frac{RT}{F\beta_{ca}}\operatorname{asinh}\left[\frac{J_{cell}}{i_{0,ref}^{ca}}\left(\frac{c_{O_2}^{ref}}{c_{O_2}^{CL}}\right)^{\gamma_{O_2}}\left(\frac{c_{H^+}^{ref}}{c_{H^+}^{CL}}\right)^{\gamma_{H^+}}\right] \tag{5.27}$$

In (5.26) and (5.27), β is the transfer coefficient, γ is the concentration parameter and $i_{0,ref}$ is the reference current density, c_i^{CL} is the concentration of species i in the catalyst layer, and calculated from the resistance model in the GDL:

$$c_i^{CL} = c_i - \frac{\delta_{GDL}}{D_{i,N_2}} N_i \qquad (5.28)$$

where δ is the thickness of the GDL, $D_{i,N2}$ is the binary diffusion coefficient of species i and nitrogen, and N_i is the mass flux.

The last term in the parentheses in (5.27) represents the overpotential due to proton shortage in the cathode catalyst layer. In the dead-ended operation there is a severe fuel starvation in parts of the cell, and, hence, the cell current diminishes and the oxygen reaction in the cathode stops as well. We assume that the proton concentration in the cathode remains at equilibrium and does not add to the activation loss. The potential drop in the membrane is due to Ohmic loss:

$$DV_m = \frac{\delta_m}{\sigma_m} J_{cell} \qquad (5.29)$$

where σ_m is the membrane's ionic conductivity and experimentally measured, correlated the temperature and membrane water content (λ) [148];

$$\sigma_m = -0.326 + 0.514 \lambda \ \exp\left[1268\left(\frac{1}{303} - \frac{1}{T}\right)\right] \qquad (5.30)$$

The cell potential, V_{cell}, at the cathode current collector must be constant, due to the high conductivity of the plate, and can be determined from the current density and the total electric resistance of the solid components including contacts, R_{solid}; the electric resistance can be estimated from the slope of the polarization curve of the cell. The cell potential is obtained from:

$$V_{cell} = V_e - R_{solid} J_{cell} \qquad (5.31)$$

The integral of the current density, J_{cell}, must be equal to the total load current, I_{load}, which is specified as an input in the model, as follows:

$$\int_{A_{cell}} J_{cell} dA = A_{cell} J_{load} = I_{load} \qquad (5.32)$$

The unknowns, which are total of six molar fractions (interchangeably mass fractions) of species, x_i (or w_i), current density, J_{cell}, and the cell potential, V_{cell} are obtained from the solution of the Maxwell-Stefan equations for conservation of mass of

individual species, conservation of total mass, coupled with the cell potential and current density equations given by, (5.31) and (5.32) respectively.

5.2.3. Two-Phase Liquid Water Transport Model

The measurement of both vapor and liquid water in operating PEMFCs is one of the greatest challenges for controlling PEMFC operation due to the lack of availability, and cost, of sensors. Therefore, models which can predict accurately amount of water inside the PEMFC are essential. Due to low operating temperatures (60-80°C) at high humidity and current density, two-phase gas liquid formation is unavoidable inside the PEMFC. When GDL and catalyst layer (together gas diffusion electrode) become saturated with water vapor, the product water starts to condense and blocks open pores reducing available paths for oxygen transport at the cathode side (cathode flooding).

PEMFC operates mostly under flow through or re-circulated anode conditions in which anode liquid water formation is very low compared to the cathode so that there are few studies referring to the anode water accumulation in literature. On the other hand in DEA operation, product water which diffuses through the membrane (negative x-direction) back to the anode condenses and accumulates in the anode GDL and channels in the anode (y-direction), reducing the hydrogen concentration on the anode. The prevention of hydrogen from reaching the catalyst stops the production of electricity from the blocked region of the cell. Hydrogen starvation causes reverse cell potential and degradation on the electrodes. Observation of water accumulation in the DEA operation and the voltage drop between purge cycles motivate the development of a model to predict the water accumulation in the GDLs and channels and to determine its impact on hydrogen starvation [8,143].

In our study, one dimensional modeling approach is considered for two-phase flow of water through the membrane and the porous media. In the hydrophobic GDL, two-phase flow and transport is governed largely by capillary forces as the gravitational and viscous forces are relatively small due to the small pore size and thickness of the GDL. As the liquid water fills the pores of the GDL, the capillary pressure increases and the liquid is forced to flow to adjacent pores with less water. This process creates a flow of liquid water through the GDL, resulting in an injection of liquid into the channel. The resistance to this injection is related with the amount of water inside the GDL. More recent numerical analysis and *in situ* investigation of the liquid water evolution and

transport in MEAs suggest that in PEMFCs, water management is strongly influenced by the transport phenomena at the macroscopic interface between the cathode GDL and channel [158]. The saturation at this interface is paramount in controlling the amount of liquid water existence in the fuel cell components during operation and the spatiotemporal behavior of water in the MEA. Thus, at the GDL-channel interface water accumulates in pendant droplets which detach when gravity and shear forces generated by the two-phase drag exceed the maximum force available to support them [156-157].

The flow of liquid water through the GDL is a function of the capillary pressure gradient as the gas pressure, P_G, inside a porous media is related with the pore size and the capillary pressure, P_C, between the gas phase and water;

$$p_l = p_g - p_c \tag{5.33}$$

In Eq. (5.34) the liquid-phase pressure is expressed by Darcy's law using the relative permeability of individual species. And the liquid velocity is given as a continuity equation:

$$\mathbf{u}_l = -\frac{\kappa}{\mu}\nabla p_l \tag{5.34}$$

where κ represents the relative permeability of the anode and cathode GDL and μ is the viscosity of the liquid.

The capillary pressure, formally defined as the difference between gas and liquid phase pressures resulting from the curved meniscus interface, plays a fundamental role in two-phase flow and phase distribution in porous media. In literature there are some assumptions to calculate the capillary pressure, such as Leverett function ($J(s)$) that describes the relationship between capillary pressure and water saturation, s. In neutron imaging experiments [8], SGL10BB (SGL GROUP, 2010), micro porous layer has been used on top of the GDL. For GDLs with MPLs, Gostick et. al. studied the relation between liquid phase saturation and capillary pressure so that, capillary pressure change according to the saturation is tabulated from this study and written as an equation (5.35) in our numerical model [149].

$$\nabla p_c = \frac{\partial p_c}{\partial s}\nabla s \tag{5.35}$$

The governing convection-diffusion equation that gives the water saturation is as Eq. (5.36)

$$\varepsilon\frac{\partial \rho_l}{\partial t} + \nabla \cdot \gamma_d \rho_l \mathbf{u}_l = S_l \tag{5.36}$$

$\rho_L = s\rho_{liq,H_2O}$ is the density of the liquid water that is blocking the porous GDL, t is time and S_l is a volumetric source term for the liquid water that represents the net water production by condensation and evaporation. Eq. (5.34) is inserted into Eq. (5.36), Eq. (5.37) is obtained.

$$\varepsilon \frac{\partial s}{\partial t} + \nabla \cdot \left(-s\frac{\kappa}{\mu} \nabla \ p_g - p_c \right) = \frac{S_l}{\rho_{liq,H_2O}} \tag{5.37}$$

The term, $-\kappa/\mu \ \nabla p_g$, represents the convective velocity of the gas phase, $\mathbf{u_g}$, in Eq. (5.37). Comparing the capillary pressure, pc, with the change in water vapor pressure, p_g, inside the porous medium (GDL with micro porous layer), p_g can be negligible due to capillary pressure change relatively higher than that of water vapor inside the small pores of GDL[150].

Inserting Eq. (5.35), Eq. (5.37) is written as below

$$\varepsilon \frac{\partial s}{\partial t} + \nabla \cdot \left(\underbrace{-s\frac{\kappa}{\mu}\frac{\partial p_c}{\partial s}\nabla s}_{\text{Diffusive Term}} + \underbrace{\gamma_d \mathbf{u}_g s}_{\text{Convecitve Term}} \right) = \frac{\overbrace{S_l}^{\text{Source Term}}}{\rho_{liq,H_2O}} \tag{5.38}$$

In Eq. (5.38), the first term inside the parenthesis can be thought as the diffusion of the liquid water according to water vapor saturation. The second term inside the parenthesis is the advection of liquid due to the flow of gaseous phase. Eq. (5.39) is the governing convection-diffusion equation according to the water saturation [149]

$$\varepsilon \frac{\partial s}{\partial t} + \nabla \cdot \left(-\underset{s\frac{\kappa}{\mu}\frac{\partial p_c}{\partial s}}{D_s} \frac{\partial s}{\partial x} + \gamma_d \mathbf{u}_g s \right) = \frac{S_l}{\rho_{liq,H_2O}} \tag{5.39}$$

The liquid and vapor water transport is modeled based on two mechanisms in the model ; i) the transport between anode and cathode through membrane ii) the transport between GDL and gas flow channels on anode and cathode. Thus, in the one dimensional model, the water transfer is according to mechanisms discussed above and taken as source or sink terms on the right side of the equation.

The Eq. (5.40) expresses the transport of liquid phase saturation for anode GDL. The water that crosses the membrane and accumulates in GDL layer is the source term (first flux term), and liquid mass transfer from GDL to channel is the sink term (second flux term) in Eq.(5.40).

$$\varepsilon \frac{\partial s_{an}^{GDL}}{\partial t} + \nabla \cdot \left(-D_s \frac{\partial s_{an}^{GDL}}{\partial x} + \underbrace{\mathbf{u}_{g,an} \, s_{an}^{GDL}}_{\cong 0} \right) = \frac{S_l}{\rho_{liq,\mathrm{H_2O}}} + \frac{\overbrace{N_{\mathrm{H_2O}}^{l-l} - N_{\mathrm{H_2O}}^{ch-gdl}}^{\text{Flux Terms}}}{h_{GDL}} \tag{5.40}$$

where h_{GDL}, is the thickness of the GDL, $\mathbf{u}_{g,an}$, is the velocity of the gases (hydrogen) of the gases in the GDL. Since the velocity of the gas phase is relatively small due to the dead ended operation, it is assumed as zero.

The mass flux of liquid water that back diffuses to the anode side through the membrane has been depended on capillary pressures on the GDL since it has a porous SGL 10BB [151]. This term is added to the S_L, as a source term in Eq. (5.44) and written as;

$$N_{\mathrm{H_2O}}^{l-l} = \alpha_{l-l}^m \ p_{l,ca} - p_{l,an} \tag{5.44}$$

The term, $p_{l,ca}$ is pressure of liquid phase on cathode side, $p_{l,an}$ is pressure of liquid phase on anode side in Eq. (5.44) and can be calculated from Eq. (5.33). α_{l-l}^m, liquid-liquid permeation coefficient has been calculated from the experimental study of Adachi et. al. [152]. In the study transient rates of water ingress to or egress from the membrane was measured and validated with the literature.

The equation defines the saturation of the liquid phase water where builds up on the anode gas channels is as Eq. (5.45)

$$\varepsilon \frac{\partial s_{an}^{ch}}{\partial t} + \nabla \cdot \left(-D_s^{ch} \frac{\partial s_{an}^{ch}}{\partial x} + \gamma_{d_{an,ch}} \mathbf{u}_{ch} s_{an}^{ch} \right) = \frac{S_l}{\rho_{liq,\mathrm{H_2O}}} + \frac{N_l^{ch-gdl}}{h_{ch,eff,an}} \tag{5.45}$$

where D_s^{ch} is the diffusion coefficient that gives water droplets diffusion inside the gas diffusion channels and it depends channel surface roughness. $h_{ch,eff}$ is the channel effective height that is defined as total channel area over channel cross section area. $\gamma_{d_{an,ch}}$, is the mass transport coefficient for liquid water drag inside the anode channel since anode gas channels are straight the coefficient is set to 250. $\gamma_{d_{ca,ch}}$, is the mass transport coefficient for liquid water drift inside the cathode channel, since the cathode channels are parallel the drag should be lower than that of anode and it is set to 1/250. These constants are defined according to the two phase flow behavior inside the PEMFC parallel channels in the very low saturations rates in the channels [153]

The term $\mathbf{u}_{ch}$, is the convective velocity of droplets inside the gas channels. ℓ is the length of one gas diffusion channel and $u_{ch,0}$ is the coefficient is set according to the gravity constant due to the position of the experimental fuel cell.

$$\mathbf{u}_{ch} = u_{ch,0} \ \ell - x \ s_{an}^{CH}$$

(5.46)

In Eq. (5.40) and (5.45) the water transport from GDL to gas channels is defined as the difference of water saturation and written as a linear mass transport equation as in Eq. (5.47). The neutron imaging experiments show the presence of the liquid water inside the gas channels on DEA operation, the liquid water transport from GDL to the gas channels is modeled with mass transfer coefficients in our model.

$$N_l^{ch-gdl} = h_l^{ch-gdl} \ s_{an}^{GDL} - s_{an}^{CH}$$

(5.47)

In Eq. (5.47), h_l^{ch-gdl} is the defined as the mass transfer coefficient that identifies the liquid water transport from GDL to the gas flow channel. If the flow inside the gas channels is laminar, Sherwood number which is a dimensionless concentration gradient can be assumed as 2.35 [154]. $D_s^{ch} 2$ is 10^{-7} and $h_{ch,eff,an}$ is approximately 10^{-4}, so that h_L^{ch-gdl} can be calculated as 10^{-3} if the saturation difference between GDL and gas channel high, i.e., there is higher amount of liquid water inside the GDLs . On the other hand, if the saturation of GDL and that of gas channel are close another mass transport mechanism is take place such as siphoning (i.e., **Figure 5.2**) [155]. If the there is enough liquid water formation both on GDL and gas channel, then the mass transfer coefficient can be set a higher value than 10^{-3}, i.e. 1 in our model. The resistance to liquid water flow from GDL to gas channel is lower since the liquid water is transported across the GDL through the largest pores and once the water penetrates the largest pores the liquid can freely drain to the gas channel [155].

The equilibrium liquid water density in membrane and anode/cathode side interfaces are calculated according to liquid phase saturation, i.e Eq. (5.48)

$$\lambda^{eq} = s\lambda_{liq} + 1 - s \ \lambda_v^{eq}$$

(5.48)

where s is the liquid pahse saturation between membrane and gas diffusion layer, λ_{liq} is the lequilibrium membrane water content in contact with liquid water which is 22 for

Nafion® membrane [3]. λ_v^{eq} equilibrium water content in contact with vapor and a is the vapor activation in equation (5.49) [146]:

$$\lambda_v^{eq} = \begin{cases} 0.043 + 17.81\,a - 39.85\,a^2 + 36\,a^3, \ T = 303\text{K} \\ 0.3 + 10.8\,a - 16\,a^2 + 14.1\,a^3, \quad T = 353\text{ K} \end{cases}$$

(5.49)

The boundary conditions of the Maxwell-Stefan equations in (5.1) are specified at inlets and outlets of the anode and cathode channels. At the anode inlet, it is assumed that dry hydrogen is supplied during purges as well as dead-ended conditions, i.e.:

$$\text{At } z = 0: \quad x_{\text{H}_2} = 1, \quad x_{\text{N}_2,\text{H}_2\text{O}} = 0 \quad \frac{\partial x_{\text{N}_2,\text{H}_2\text{O}}}{\partial N} = 0$$

(5.50)

Similarly to the anode boundary conditions, at the cathode inlet, mass fractions of the species are specified based on the inlet relative humidity and the pressure. At the anode and cathode exits, fluxes of species are set to the convective-flux-only conditions: i.e. the diffusive fluxes are zero:

$$-\rho_i \sum_{j \neq i} D_{ij} \frac{\partial x_j}{\partial z} = 0$$

(5.51)

The convective flux at the exit, $\rho w_i U$, is only from the stoichiometric flow of the species at the exit, U_{exit}, as expressed in (5.5).

5.3. RESULTS AND DISCUSSIONS

5.3.1 Model Validation

Two-phase model results have been compared with resulting neutron imaging experiments [8]. **Figure 5.3** shows the comparison of experiments and model for cathode stochiometry (SRc) is regulated in 2, relative humidity (RH) 75 % and cell temperature (T_{cell}) 50 °C. The cell was under galvanostatic conditions and current density is 3760 A/m^2 for 53 cm^2 active area in the DEA transient. **Figure 5.3a** states that the voltage change according to time in the model is convenient with the experimental data. Voltage starts to ramp-down particularly after 400 seconds according to both model and data. In the previous study it was reported that nitrogen crossover from cathode to anode that decreases the active area in the anode originated voltage

decrease [143]. Additionally, in this study, the effect of liquid water crossover from cathode to anode and its accumulation near the anode exit is also studied. **Figure 5.3b** and **3d** demonstrate the liquid water content inside anode and cathode gas channels respectively. **Figure 5.3b** shows that there is 0.04 g water content inside the anode channels and it does not significantly change even after purging, this is most likely due to the liquid water sticking to the channel walls. The liquid water amount in both cathode channels and GDL are presented in **Figure 5.3c** and **Figure 5.3d**. The measured 1 g liquid water during neutron imaging inside the GDL agrees well with the model findings especially in **Figure 5.3c**. Since water diffuses to the anode and also being dragged with the constant flow from the cathode channels, cathode channels have the lowest liquid water amount, i.e., 0.01 g. Amount of liquid water is constant through the DEA transients in both the GDL and the cathode channels and not affected by the purges.
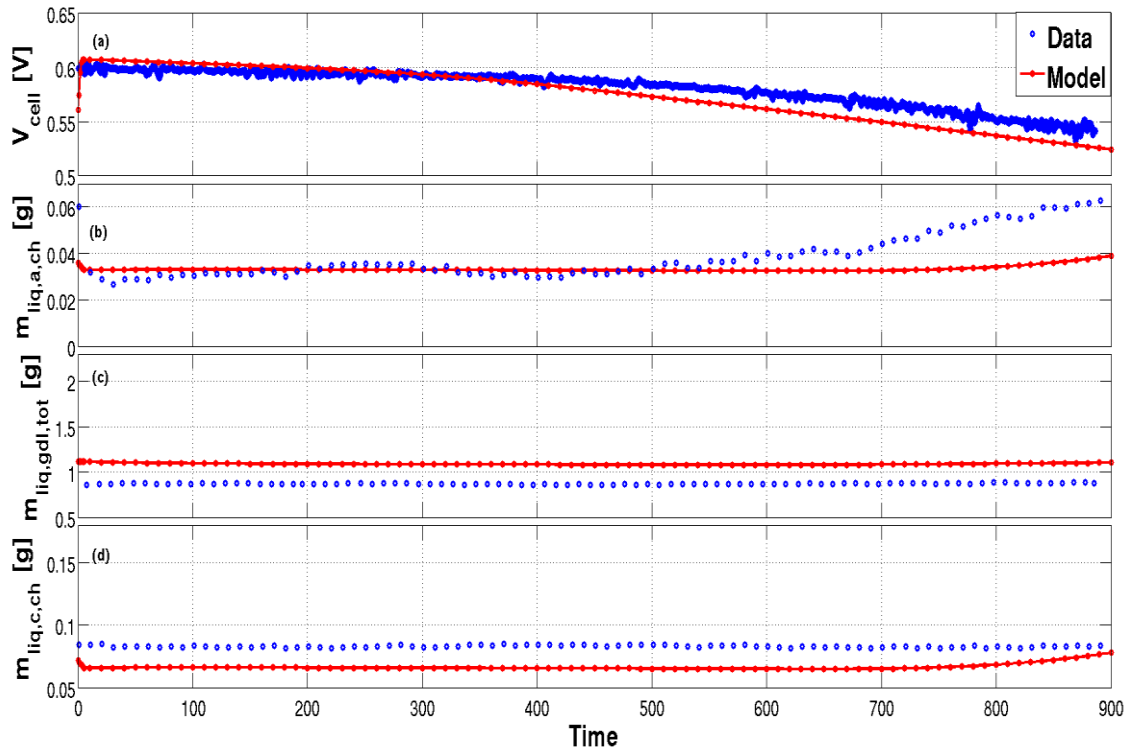
Figure 5.3: According to DEA operation (a) Cell voltage, (b) water accumulation in anode gas channel (c) water accumulation anode cathode gas channel; Current density (J_{load}) : 3760 A m^{-2}, T_{cell}=50 °C, RHc=75%, SRc=3

In **Figure 5.4** for J_{load}=5660 A m^{-2}, RH$_c$ =115 % and T_{cell}=60 °C, model results is compared with experimental results. The model and the experimentally observed voltages agree very well and are demonstrated in **Figure 5.4a**. The voltage starts with 0.58 V and ramps down to 0.51 V, 70 mV voltage drops is observed throughout the

DEA transient. Liquid water in anode gas channels is illustrated in **Figure 5.4b**. Since the driven current increased from 20 A to 30 A, the formed and accumulated liquid water on the anode channel is increased (**Figure 5.3**). There is still water inside the gas channels, (0.02 g for experimental data and 0.06 g for model)   inside the anode channels at the beginning of the transient even after purging due to the liquid water at the exit of cell sticking to the channel walls. However, in both model and experiment the liquid water decreases for a while, since the formed water by reactions humidifies the membrane. Water starts to accumulate inside the anode channels due to the diffusion of water from cathode. At the end of the transient, 0.16 g water accumulated inside the anode channels agrees for both model and experimental findings. **Figure 5.4c** shows 0.5 g liquid water inside the GDL according to experiment and 0.4 g according to the model which is lower than the previous case (**Figure 5.3c**). The finding indicates that infinitely water is transferred from GDL to channels since there is higher amount of water than the initial DEA conditions (**Figure 5.3**). Once the liquid water penetrates to gas channels, it can freely drain from GDL [154].
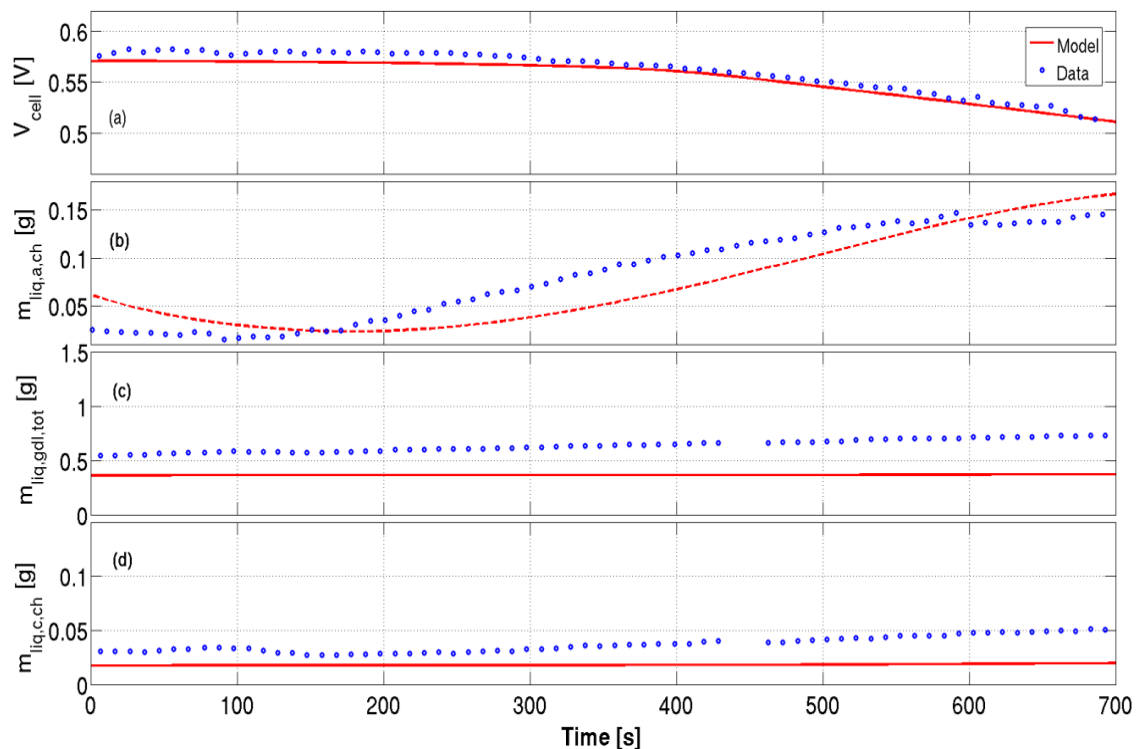
Figure 5.4: DEA operation (a) Cell voltage, (b) water accumulation in anode gas channel (c) water accumulation anode cathode gas channel; Current density (J_{load}) : 5560 A m^{-2}, T_{cell}= 60 °C, RHc=115%,SRc=3

Figure 5.5 shows the water saturation inside anode GDL (circled line) and the gas channel (solid line) at different times of transient from anode inlet to exit. After 5 seconds of purging (t_{purge}=5seconds), there is still liquid water inside the channels and GDL. The liquid saturation increases towards anode exit since back diffused water starts to condensate at the anode exit (**Figure 5.1**). After t >400 seconds, liquid water from cathode initiates the liquid water accumulation on the anode exit, at the end of the transient (t=700 seconds) its amount attains its maxima. The liquid water amount is increasing simultaneously in both the GDL and the gas channels. It indicates that there is no resistance to water transfer from the GDL to the gas channels since both channel and GDL is filled with water. The siphoning from gas channels drains the liquid water from GDL. Zang et al. shown liquid water in both GDL and gas channels after 30 minutes operation at 1000 mA m^{-2}current density and concluded that due to the hydrophilic capillary forces, liquid water easily transferred from GDL to the channels [155].
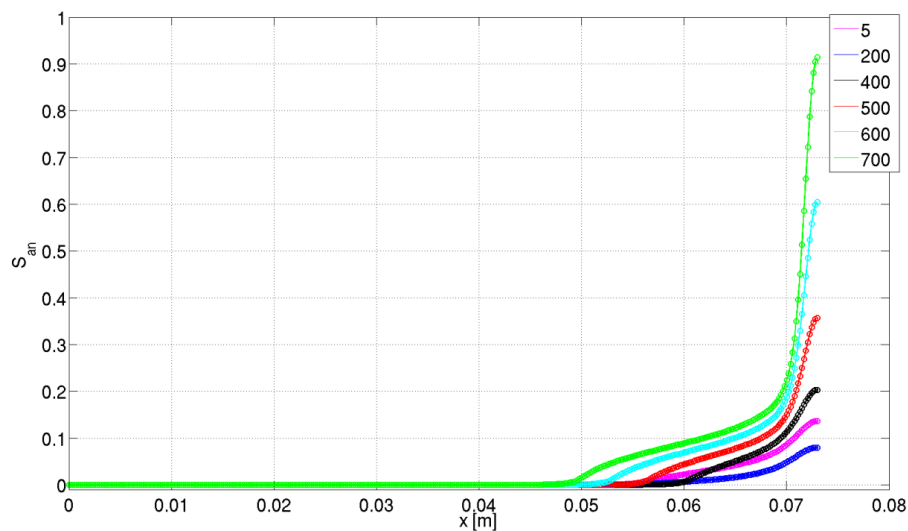
Figure 5.5: Water concentration from anode inlet to exit, in the channels (solid line) and GDL (cirles) at t= 5,200,400,500,600,700 seconds

Figure 5.6 demonstrates the liquid water saturation inside cathode GDL (circled line) and channel (solid line) at different times from inlet to outlet. At the inlet of cathode, x >0, high water saturation decreases and start an increase after x >0.01 m. The rise in saturation occurs in 0.01 m< x < 0.05 due to increased water formation due to the cathode electrochemical reactions. For x >0.05m, t >400 seconds, the water saturation decreases because of back diffusion of water to the anode.
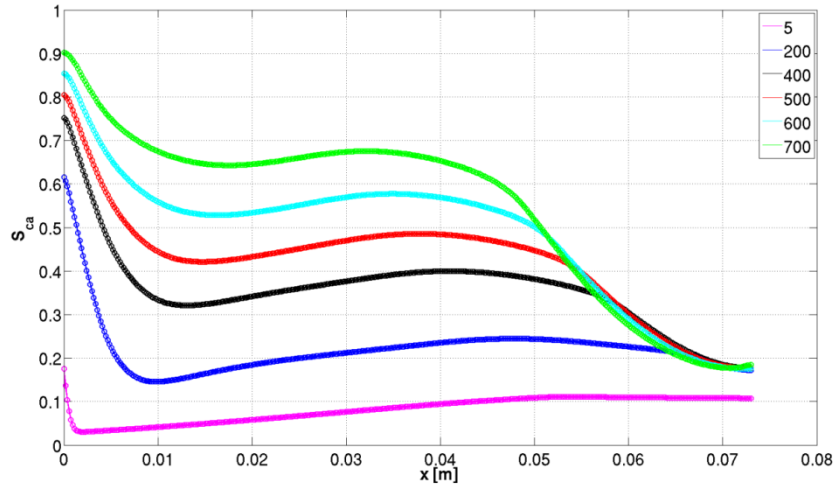
Figure 5.6: Water concentration from cathode inlet to exit, inside the channels (solid line) and GDL (cirles) at t= 5,200,400,500,600,700 seconds

Figure 5.7 represents current density distribution over anode channel for 5, 200, 400, 500 and 700 seconds. After 5 seconds of purging current density is relatively uniform. For 0< t <180 liquid water amount is lower (**Figure 5.4b**), and after 200 seconds the liquid water amount starts to increased, J_{cell} starts to ramp down that indicates that the reactions can occurs on active area from inlet to outlet of anode. After t> 400 seconds due to the nitrogen accumulation active cell area is blocked and current density decreases towards the exit [8].
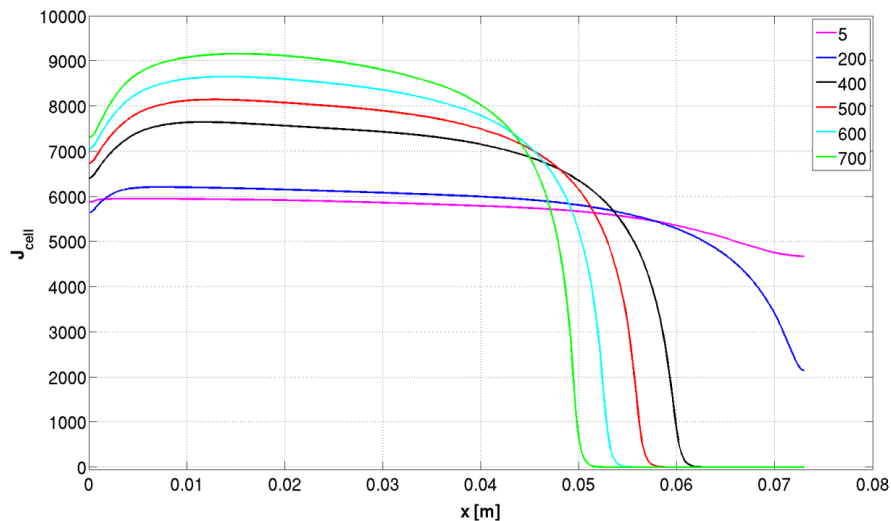
Figure 5.7: Current density of DEA-PEMFC at different time from anode inlet to cathode exit

5.3.2. Effect of Channel Length and Depth on the DEA Performance

Commercial cells (200–800 cm^2) have pronounced effects due to pressure drop, flooding distribution, and non-uniformity in temperature and current distributions due to manifolding constraints. These effects cause stability, durability, and performance problems in general for PEMFC. In the part of our study, a number of transient simulations are carried out to study the effect of the gas channel length and depth on the cell voltage during the dead-ended transient of the cell. These results may be used to develop universal heuristics and dimensionless number correlations in the design of gas flow-fields.

Transient simulations are carried out with a number of gas channel lengths and depths in order to demonstrate the effect of cell geometry on the DEA operation. **Figure 5.8a** and **Figure 5.8b** demonstrate the voltage performance of the cell during a DEA transient for channel lengths 0.090 m, 0.060 m, 0.050 m, 0.030 m, and 0.020 m for J_{load}= 3760 A m^{-2} and J_{load}= 5660 A m^{-2} . According to simulation results in **Figure 5.8a** and **b**, the initial response of the cell voltage remains almost identical for all geometries due to the constant current load. As the gas channel length decreases, the accumulated nitrogen and water on the anode is discharged easily since the convective velocity increases and the rate of cell voltage decline decreases for both current densities (3760 A m^{-2} and 5660 A m^{-2}). The voltage value for 0.020 m gas channel length stays linear for t< 800 seconds and reaches 5 mV decrease at the end of the transient for J_{load} 3760 A m^{-2} and 10 mV decrease for J_{load} 5660 A m^{-2} at the end of the DEA transient. On the other hand longer channel lengths i.e., 0.090 m causes 66 mV voltage lost for J_{load} 3760 A m^{-2}, and 142 mV for J_{load} 5660 A m^{-2}. Due to the reduction on the diffusion from anode inlet to exit in DEA operation, longer channel length causes higher reduction on voltage and reduces the transient time. Moreover, for shorter channel lengths the accumulation of nitrogen is more homogenous over the channel ($L_{cell} \cong l$) thus diffusion is more dominated mechanism to discharge accumulated species.
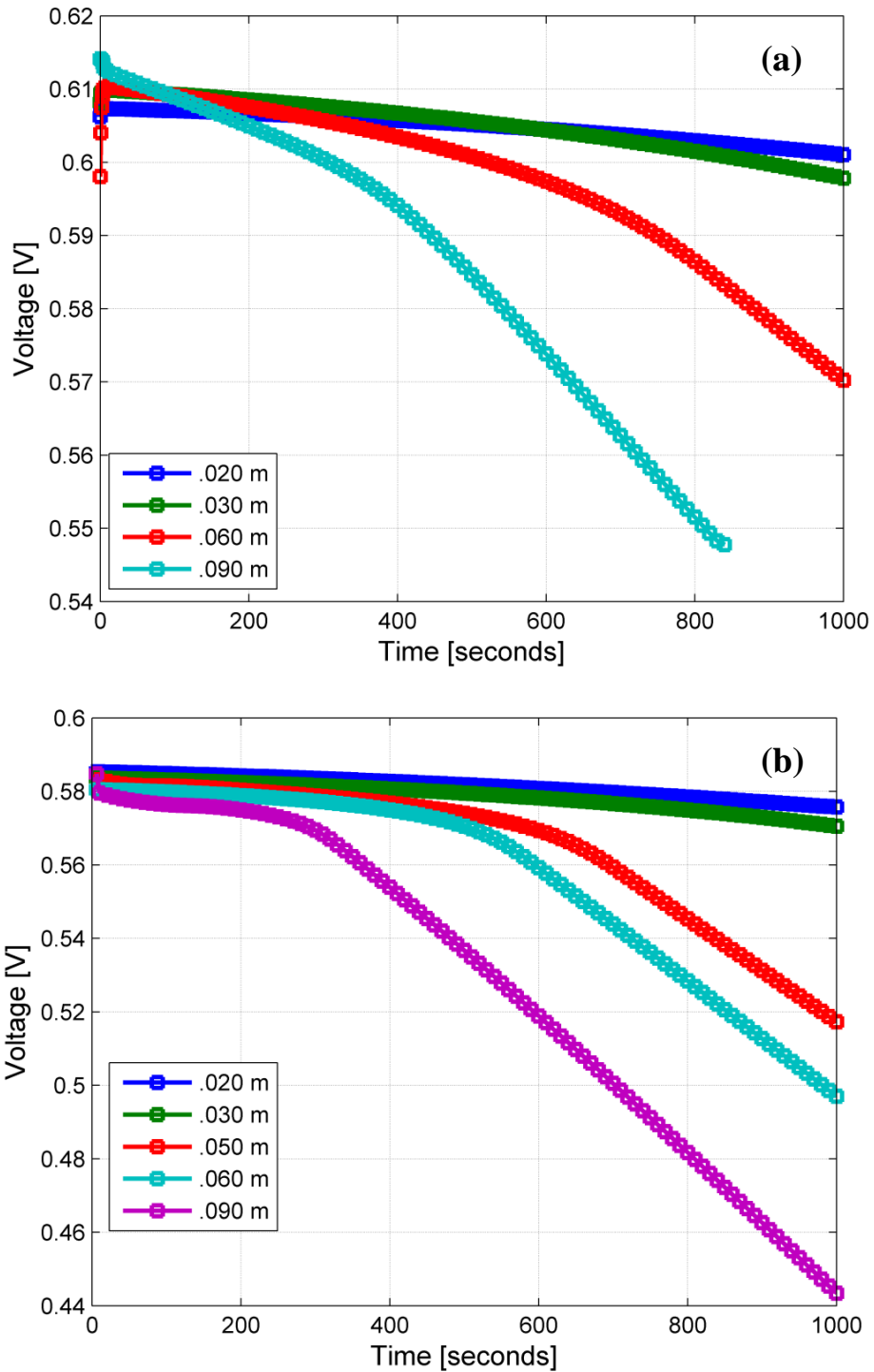
Figure 5.8: Effect of channel length on the voltage performance during DEA-PEMFC transient; a) J_{load} = 3760 A m^{-2} H$_{cell}$= 1.78 mm, b) J_{load} = 5660 A m^{-2}, H$_{cell}$= 1.78 mm

Figure 5.9a and **Figure 5.9b** show the voltage performance of the cell during a DEA transient for channel depths 1.2 mm, 1.5 mm, 2 mm and 3 mm, for J_{load}= 3760 A m^{-2}and J_{load}= 5660 A m^{-2}. Opposite to gas channel length effect, as the gas channel depth increases, the ramp down on the cell voltage reduces. Since the reservoir enlarges on the y direction and diffusion dominates on accumulated species on the anode gas

channels, thus less active area is blocked on the electrode. Therefore, it is better to use deeper and shorter channel configuration while operating in DEA PEMFC to increase the transient time.
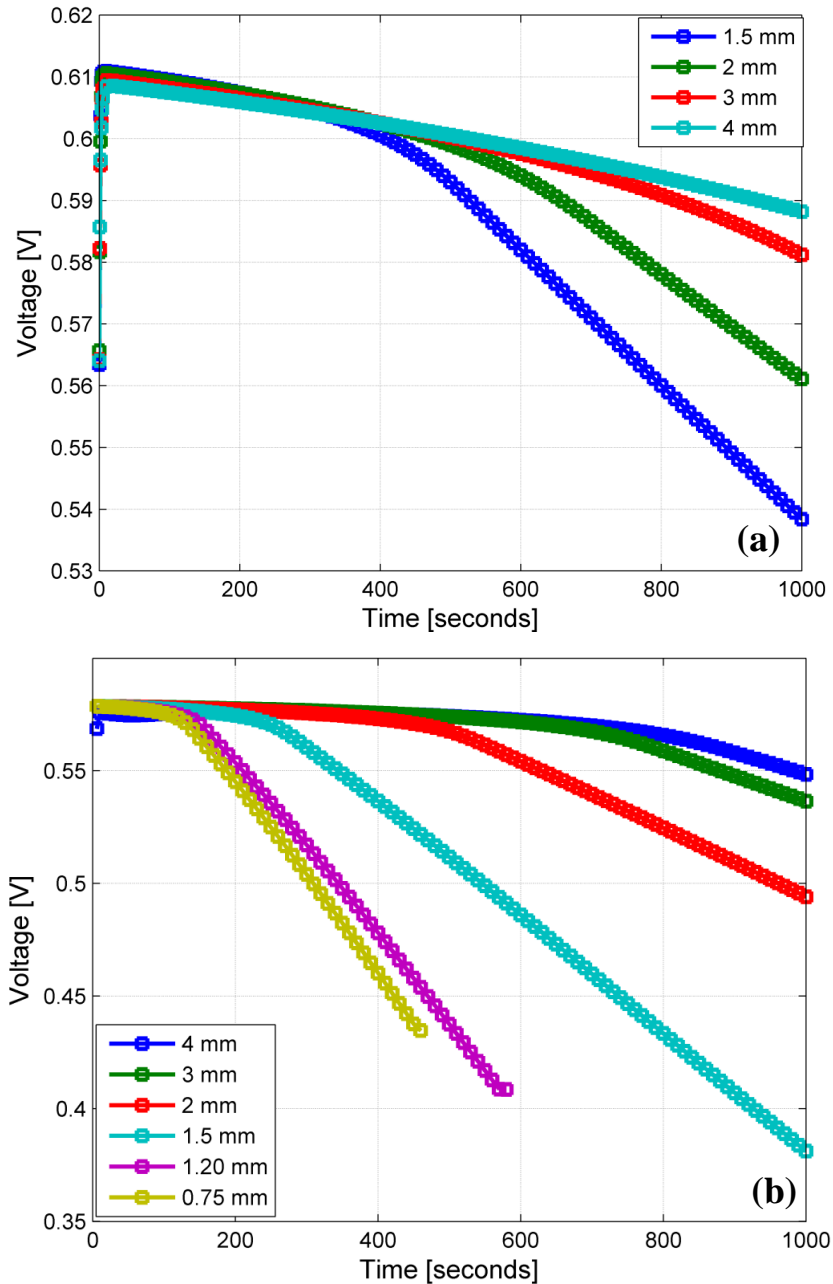
Figure 5.9: Effect of channel depth on the voltage performance during DEA-PEMFC transient, $L_{cell}= 7.3$ cm, a) $J_{load} = 3760$ A m^{-2}, $L_{cell}= 7.3$ cm b) $J_{load} = 5660$ A m^{-2}

In our numerical model, the time that the molar concentration of hydrogen $X_{H2} <0.001$ mole m^{-3} has been taken into account as the onset of hydrogen starvation (**Figure 5. 10**).
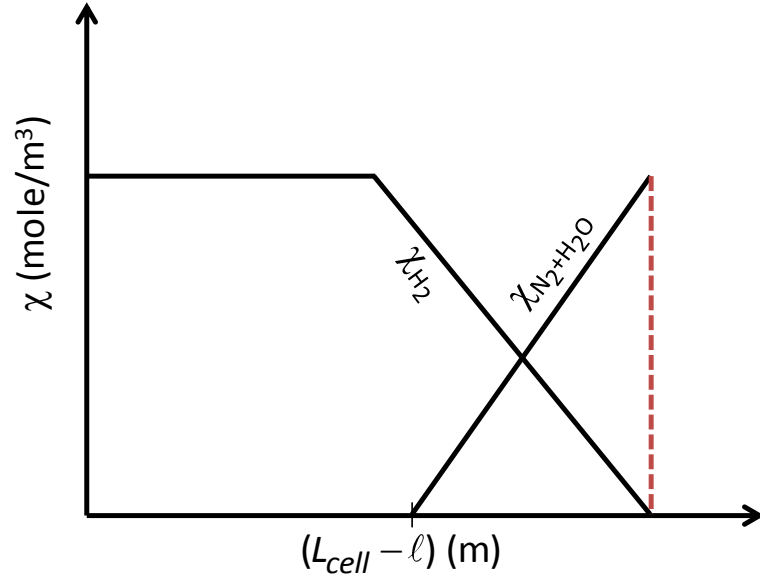
Figure 5.10: Schematic of hydrogen and nitrogen concentration distribution along the anode channel

This time, $t_{x_{H_2 \to 0}}$, that can be defined as fill-up time according to the voltage profile can be shown as in Eq. 52

$$t_{x_{H_2 \to 0}} = \frac{\ell}{2}\left(\frac{\rho_{N_2}}{N^{an}_{N_2}}\right)\frac{H_{cell}}{L_{cell}} \tag{5.52}$$

ℓ, is a simple constant that comes from nitrogen crossover, $N^{an}_{N_2}$ is the nitrogen flux in the anode, L_{cell} is the length of the gas channel and H_{cell} is the height of the gas channel in Eq. (5.52).

The balance between diffusion and convection fluxes of nitrogen concentration in the channel is written as in Eq. (5.53); u is the convective velocity of the nitrogen flux in anode gas channel and D_{i,N_2} is the constant binary diffusion coefficient of the nitrogen.

$$\rho\omega_{H_2}U \cong \rho\omega_{H_2}\frac{D_{H_2N_2}}{\ell}\underbrace{\frac{\partial X_{N_2}}{\partial z}}_{\cong 1} \to \ell \cong \frac{D_{H_2N_2}}{u} \tag{5.53}$$

The relation between ℓ and H_{cell} can be correlated by using the convective velocity of hydrogen in the anode gas channel as shown in Eq. (5.54).

$$u_{H_2} = \frac{Jcell}{2F} \cdot \frac{RT}{\rho_{N_2}} \cdot \frac{\ell}{h} \rightarrow \ell \propto H_{cell}^{1/2} \tag{5.54}$$

where F denotes Faraday constant (96 487 C mol^{-1}), ρ_{N_2} the nitrogen density , R universal gas constant and T is the operation temperature.

If Eq. (5.54) is inserted in Eq. (5.52), the time, $t_{x_{H_2} \rightarrow 0}$, is expressed as below Eq. (5.55)

$$t_{x_{H_2} \rightarrow 0} = \text{Constant} \left[\frac{H_{cell}^{3/2}}{Lcell} \right] \tag{5.55}$$

Note that Eq. (5.55) shows the combined effect of diffusion with the term $H_{cell}^{3/2}$ and convection with the term L_{cell} during the transient of DEA operation. The domination of convection or diffusion on the accumulated species can be estimated approximately from the $H_{cell}^{3/2} / L_{cell}$ mass transfer coefficient. The mass transfer coefficient $H_{cell}^{3/2} / L_{cell}$ is used to estimate the time when the voltage starts the ramp down.

Figure 5.12a and **Figure 5.11b** show the numerical results of time onset of H$_2$ starvation according to the cell channel length and height for J$_{load}$= 3760 A m^{-2} and J$_{load}$=5660 A m^{-2} respectively. The results agree very well as the channel height increases the diffusion (on the y direction) increases and onset of hydrogen starvation time enhances.
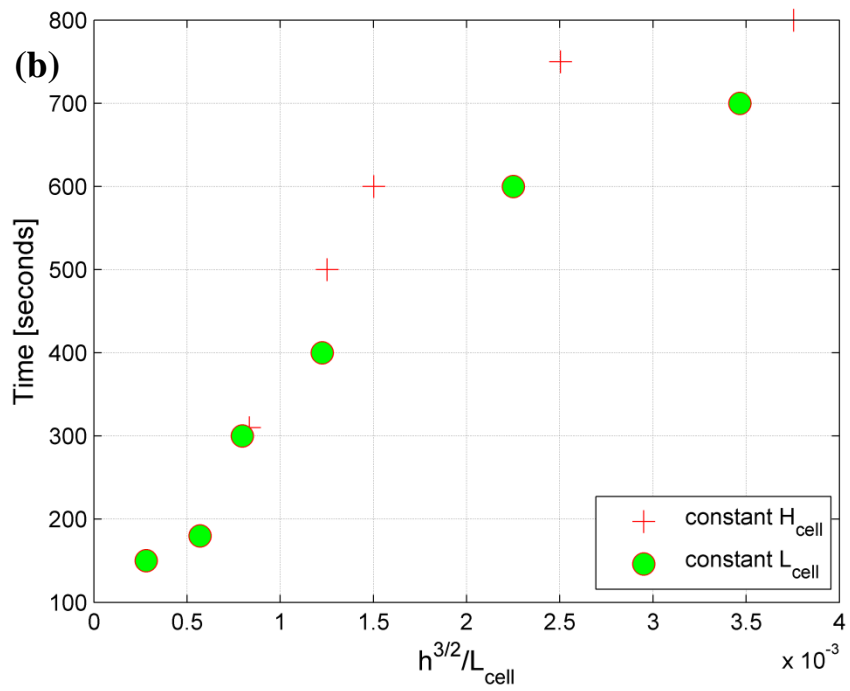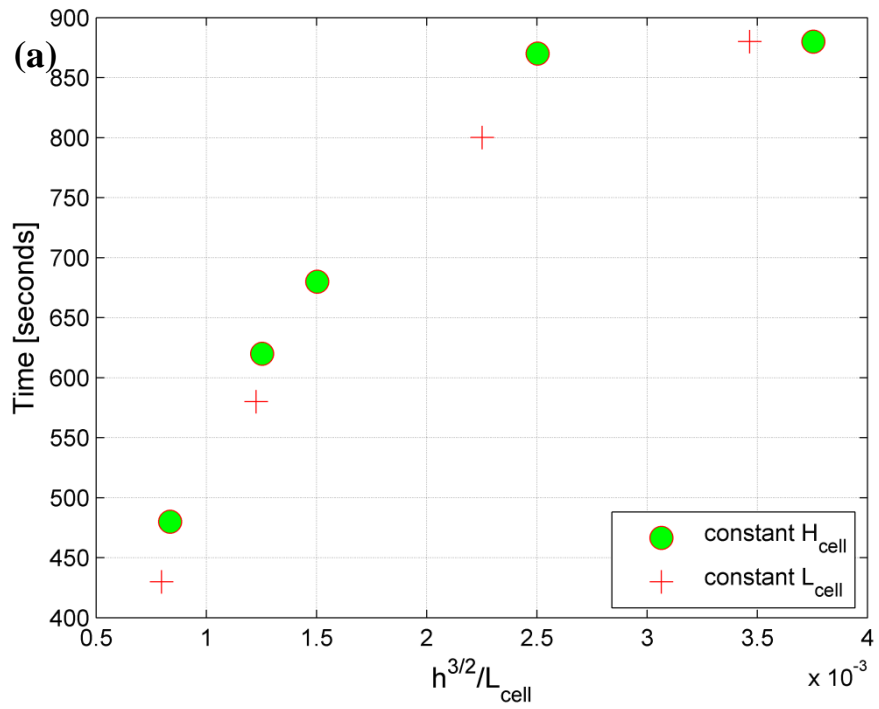
Figure 5.11: Onset of H_2 starvation time as a function of gas channel height and length, (+) constant L_{cell}= 7.3 cm, (o) constant H_{cell}= 0.178 mm a) J_{load}= 3760 A m^{-2} b) J_{load}= 5660 A m^{-2}

5.4. CONCLUSIONS

Two phase flow and transport of liquid water in DEA-PEMFC operation at low temperatures is important since accumulated water has limiting effect on the cell voltage and material life such as carbon corrosion on the electrodes. In our study, we have developed a numerical two phase water transport model to investigate the diffusion and the convection related mechanisms. In order to validate our numerical model, simulations of liquid water accumulation inside the anode/cathode gas channels and GDL are compared with neutron imaging of water in a DEA PEMFC for two load current densities, 3760 and 5660 A m^{-2}. The liquid water accumulation inside anode/cathode gas channels, GDL and voltage transients of the DEA operation agree very well with experimental results in literature [8].

Based on model results; it can be concluded that two phase water transport take place as vapor water back diffuses from cathode to anode and saturates at the exit of anode and dragged from anode to cathode such as an equilibrium phenomena. Moreover, the accumulated liquid water at the anode exit contributes to the nitrogen back diffusion from anode to cathode and decreases the nitrogen blanketing effect.

By using our model; the liquid water amount that is accumulated at anode/cathode GDL and gas channels can be estimated at different load conditions. Since accumulated liquid water has corrosive result on the expensive electrodes by oxidation of carbon support, it is vital to estimate the liquid water amount inside the gas diffusion electrodes.

In our study, it is observed that especially at high current density (i.e. 5660 A cm^{-2}) there is no resistance to the transfer of liquid water from GDL to gas channel. Since there is high amount of liquid water inside the GDL, once the water starts to be drained from GDL to gas channel, a siphoning mechanism from GDL occurs and increases the water transport towards gas channels.

On the other hand, at relatively low current density (i.e. 3760 A cm^{-2}) since the amount of liquid water is low due to less electrochemical production, the resistance to liquid water transport from GDL to gas channel is higher. Moreover, both our numerical model and neutron imaging results show that in DEA operation even purging does not drift the accumulated water inside the GDL; due to the MPL content of the GDL.

Lastly, in our model it is found that onset of hydrogen starvation time is related with gas channel dimensions, i.e., channel length and channel depth. An empirical correlation is estimated as $t_{onset} \propto H_{cell}^{3/2} / L_{cell}$. It is revealed that as the channel length increases the convection also enhances since convective velocity is dominated by channel length however the length that the nitrogen accumulated (l) increases as well. Thus, because of the increased nitrogen blanketing effect the DEA transient time reduces.

CHAPTER 6

CONCLUSIONS

The total cost of the PEMFC system was 275 $/kW in 2002, the achieved goal of today is 60 $/kW and the goal is 30$/kW in 2015. The two main cost factors (50% of the total cost) are the electrolyte and the system components (which reduce the energy density of the total system) in PEMFC. Thus, in this thesis, low cost membrane synthesis which can boost up the operation temperature over 100 °C without sacrificing membrane proton conductivity was one of our targets. Moreover, the dead-ended anode operation of a PEMFC have been used in the previous research studies, however it is not very well adopted by industry. Even though, it has several attractive qualities, such as reduced weight, cost, and system complexity it has problem in anode purge period and duration, and water management at low operating temperatures. Moreover, the DEA operation is a challenging mode of operation to assess durability and degradation issues as well. Hence, the high temperature DEA operation of PEMFC is the subject of this thesis to obtain good system performance. High temperature DEA operation has not been studied before in literature. Since it eliminates liquid related problems, DEA could be more viable with high temperature membranes than Nafion[®].

In the membrane synthesis, this thesis is achieved a patentable high temperature PEMFC membrane. Radiation induced graft copolymerization method has been used to synthesize the high temperature proton exchange membrane out of 4VP, 2VP and NVP monomers onto ETFE base film in a solvent environment at low radiation doses. The membrane synthesis was in two continued studies as the copolymer and the membrane synthesis. The evidence of grafting by FTIR and EDX has been proved. After copolymerization conditions have been defined, the copolymers were doped with phosphoric acid to give the membrane water free proton conductivity mechanism. It is

found that out of three monomers 4VP achieved the best proton conductivity results. Moreover, it was observed that after phosphoric acid doping of ETFE-*g*-P2VP and ETFE-*g*-PNVP copolymers lost their graft components and no pronounced proton conductivities have been observed for these membranes. The, detailed proton conductivity measurements have been carried out for ETFE-*g*-P4VP membranes to analyze its proton conductivity mechanism. It has been observed that its proton conductivity mechanism is similar to that of PBI membranes, and different than that of commercial Nafion® membrane. The membrane proton conductivity increases with increased temperature and high relative humidity does not have pronounced effect on the proton conductivity. The FTA operation of the ETFE-*g*-P4VP membrane in fuel cell shows that its voltage performance increases with increased temperature and comparable with PBI membrane. As an advantage, the ETFE-*g*-P4VP membrane does not requires the very high temperatures as the PBI membrane needs (T_{cell} >150 °C) and can operate at 120 °C and achieve the low temperature Nafion® membrane voltage by eliminating the water from the PEMFC.

The Greenlight® FC G50 PEMFC test station and single fuel cell were overhauled for the thesis study and are working properly for the future testing. The test station is in FTA operation mode and the initial single fuel cell tests started by using purchased MEAs with Nafion® membrane. After proper fuel cell performance has been observed for Nafion® and ETFE-*g*-P4VP membrane, the test station was modified according to DEA operation mode by including additional hardware such as solenoid valves to anode inlet and outlet in the study. The DEA test of Nafion® and high temperature ETFE-*g*-P4VP membranes were conducted. The transient time in DEa operation is the time between two purge cycle (such as voltage was 0.6 V at t=0 and decreases to 0.5 V at t=1000 s). The transient time of Nafion® and high temperature ETFE-*g*-P4VP were 650 seconds and 550 seconds respectively at 400 mA cm^{-2} current density. During the transient time of DEA operation it is expected that voltage is constant for a while, and then due to the accumulation of species on the electrode active areas, voltage start to decrease. Moreover, the flatter region in Nafion® membrane DEA operation cannot be observed for ETFE-*g*-P4VP membrane. This finding is interesting as it proves that the voltage decrease in DEA operation directly related with nitrogen accumulation since there is no water remains in the MEA structure in the high temperature DEA operation. On the other hand, it is obvious that the DEA operation performance of both membranes are comparable, but Nafion® exhibit longer DEA

transient time. The shorter transient and sudden decrease in the voltage indicates that synthesized high temperature ETFE-*g*-P4VP membrane has higher nitrogen permeation; another reason for the higher nitrogen permeation can be the high operation temperature (110 °C) since the gas permeability increases with increased temperature.

The degradation behaviors of both membranes are also different. The Nafion$^{®}$ membrane becomes thinner at the dry hydrogen inlet and thinning can leads to pinhole formation. Moreover, the accumulated water can oxidize the carbon structure of the electrodes. However, no detailed study has been completed for the electrode degradation. On the other hand, in the case of ETFE-*g*-P4VP membrane, the graft component is degraded due to the radicals that form due to the gas crossover. As the graft component worn out, the proton conductivity decreases and the cell voltage decreases. Hence, base film ETFE remains and no pinhole formation is observed.

The developed two phase water transport numerical model investigates the diffusion and the convection related mechanisms. In order to validate our numerical model, simulations of liquid water accumulation inside the anode/cathode gas channels and GDL are compared with neutron imaging of water in a DEA PEMFC for two load current densities, 3760 and 5660 A m^{-2} and results are agree well with experimental results in literature [8].

Based on model results; it can be concluded that two phase water transport take place as vapor water back diffuses from cathode to anode and saturates at the exit of anode and dragged from anode to cathode such as an equilibrium phenomena. Moreover, the accumulated liquid water at the anode exit contributes to the nitrogen back diffusion from anode to cathode and decreases the nitrogen blanketing effect. By using our model; the liquid water amount that is accumulated at anode/cathode GDL and gas channels can be estimated at different load conditions. Since accumulated liquid water has corrosive result on the expensive electrodes by oxidation of carbon support, it is vital to estimate the liquid water amount inside the gas diffusion electrodes. In our model it is found that onset of hydrogen starvation time is related with gas channel dimensions, i.e., channel length and channel depth. Thus, our model can be used to predict the optimum channel dimensions in a physical experiment.

CHAPTER 7

FUTURE WORK

Today there are three main barriers in front of the fuel cells to be placed in the industrial use: (a) durability, (b) cost, and (c) hydrogen supply transportation [161]. This thesis mainly addresses (b) in a very promising directions. Even though, the high temperature DEA operation is new in the literature, the results are very encouraging. On the other hand the following enhancements should be the subjects of the future study.

Gas Permeability

High temperature DEA operation of PEMFC is very critical to reduce the cost of the system while improving the cell performance for commercial automotive applications. The synthesized high temperature membrane ETFE-g-P4VP is very promising FTA and DEA performances. On the other hand, undesired reactions that have been linked to the degradation of membrane occur during the operations. It is observed that gas permeability is the main reason that is increasing the degradation of the membrane. Moreover, the nitrogen permeation of the membrane causes low transient time in DEA operation. In literature it is reported that the cross-linker addition to the graft structure enhancing both the durability and the gas permeation of the radiation grafted membrane. The synthesized high temperature ETFE-*g*-P4VP membrane DEA operation performance can be improved by enhancing its gas permeation by using cross-linker agents such as divinylbenzene (DVB), dichloromethyl phosphinic acid (DCMP) at high temperatures [102,160].

MEA Preparation

The MEA preparation methods are very well defined for Nafion$^®$ membrane that is operated at low temperature, and these methods are partly used for preparation of high temperature membranes as it is mentioned previously. On the other hand, it is evident with SEM images that there is delamination of the electrodes from membrane, so that the Nafion$^®$ ionomer solution that was used to glue the membrane and electrode interface are not lasting during high temperature operation since the T$_g$ of Nafion$^®$ is below 100 °C. Hence, the new ionomer binders to reduce internal resistance and prevent delamination should be explored.

Temperature Effects

Since, both high temperature DEA operation and high temperature operation of radiation induced grafted membranes have not been studied in literature before, the effect of high temperature on radiation induced grafted membrane. For instance, in the literature it is found that as the temperature increases the gas permeability of the phosphoric acid doped membrane increases, the same behavior is observed in our DEA operated PEMFC operation [80]. Hence, temperature vs. gas permeability can be investigated in detail and the study can fill an emerging gap in the literature.

Modeling

The one dimensional, along the channel, numerical model that is built in this thesis study firstly is used to investigate the two phase water transport between anode and cathode in DEA operation. Hence, it is well predicted the water amount that is accumulates on anode/cathode GDLs and gas channels. On this aspect the numerical model is important as it can be used to predict the water amount which is difficult to measure in the physical experiments. Moreover, the model defines the water dynamics during the DEA operation. Thus, one dimensional along the channel numerical model will be further extended to simulate high temperature DEA operation of PEMFC to investigate the mechanism that causes voltage declines during a transient of DEA operation.

IN PLANE FOUR POINT PROBE PROTON CONDUCTIVITY SET UP OF THE HIGH TEMPERATURE PROTON EXCHANGE MEMBRANES
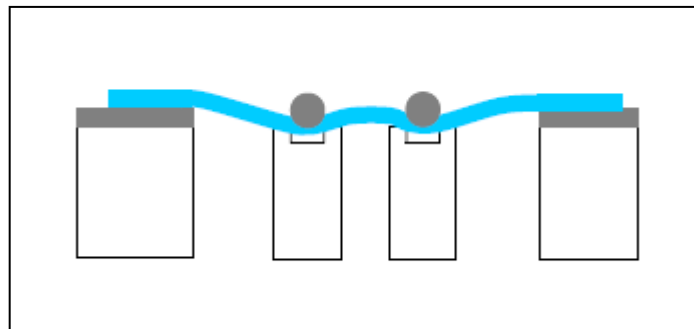
Figure A.1: Membrane Assembly Technique inside the conductivity cell. Placing membrane under platinum wires in the conductivity cell makes better contact with the membrane.
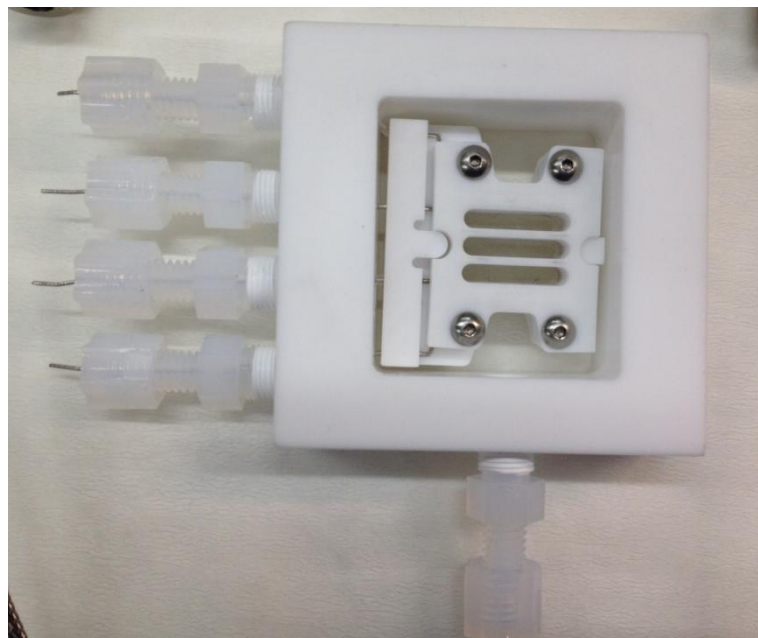
Figure A.2: Bekktech® four point probe conductivity cell
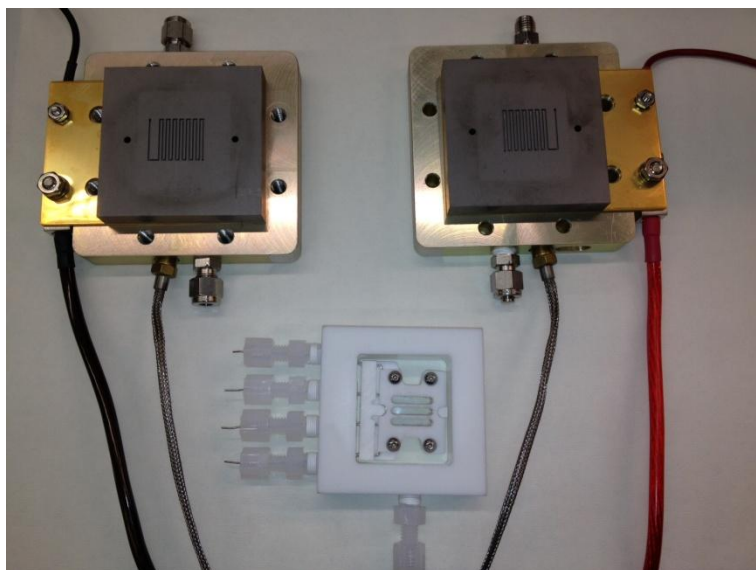
Figure A.3: Bekktech® conductivity cell assembly
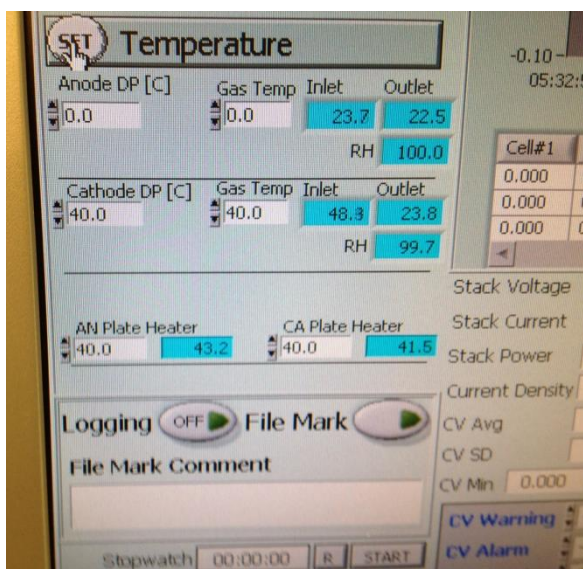
Figure A.4: Greenlight FC G50 test station maintains control on the cell temperature, relative humidity, pressure and the flow rate of the air
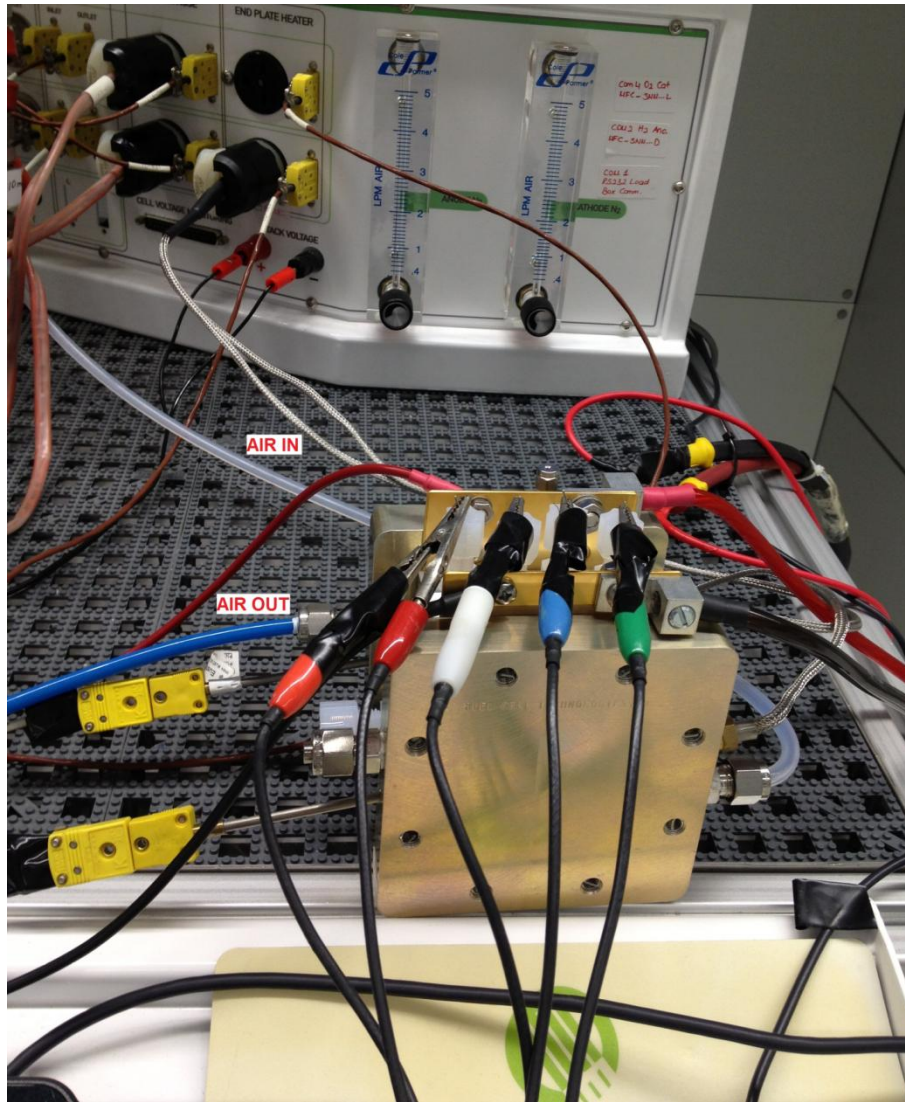
Figure A.5: Conductivity cell is controlled with Greenlight® FC G50 test station. Cell is heated with a cartridge type heater that is placed inside the metal end plates. According to dew point temperature and air stream temperature RH of the dry air was maintained.

EXPERIMENTAL SET UP OF DEA OPERATION
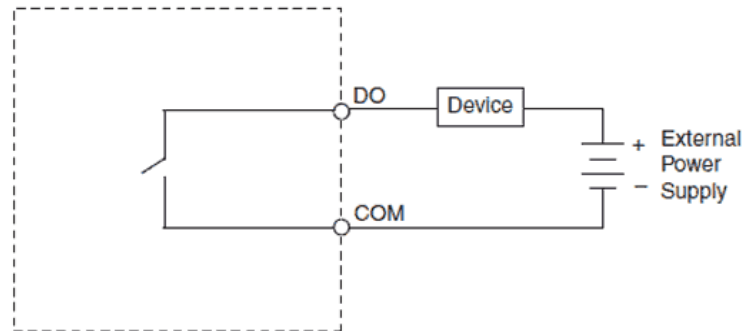
Figure B.1: Schematic of the solenoid valve control with an external power supply

Figure B.2: Connecting the solenoid valves to the NI 6220 Digital Output

MEA PREPARATION

Figure C.1: ETFE-*g*-4VP high temperature proton conducting membrane. Radiation dose:10 kGy, grafting solvent: *n*-propanol, GL: 42%
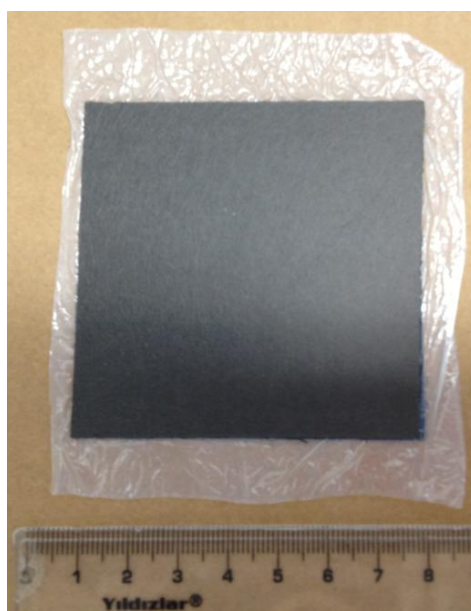
Figure C.2: Hot pressed MEA with ETFE-*g*-4VP high temperature proton conducting membrane. (10 MPa pressure, 90 seconds)

REFERENCES

1. O'Hayre R. P., Cha S-W., Colella W., and Prinz F. B., *Fuel Cell Fundamentals*. Hoboken, NJ: Wiley, (2006).

2. Shah A. A., Kim G. S., Gervais W., Young A., Promislow K., Li J., Ye S. "The effects of water and microstructure on the performance of polymer electrolyte fuel cells." *Journal of Power Sources* 160, no. 2 (2006): 1251-1268.

3. Barbir F., *PEM Fuel Cells: Theory and Practice*. Burlington, Ma: Elsevier, (2005).

4. Jixin C., Siegel J. B., and Stefanopoulou A. G. "Nitrogen blanketing front equilibria in dead end anode fuel cell operation." In *American Control Conference (ACC), 2011*, pp. 1524-1529. IEEE 2011

5. Muller E. A., Kolb F., Guzzella L., Stefanopoulou A.G., and McKay D.A. "Correlating nitrogen accumulation with temporal fuel cell performance." *Journal of fuel cell science and technology* 7, no. 2, (2010).

6. Karnik A. Y., and Jing S. "Modeling and control of an ejector based anode recirculation system for fuel cells." *ASME*, 2005.

7. Pekula N., Heller K., Chuang P. A., Turhan A., Mench M. M., Brenizer J. S., Ünlü K. "Study of water distribution and transport in a polymer electrolyte fuel cell using neutron imaging." *Nuclear Instruments and Methods in Physics Research Section A: Accelerators, Spectrometers, Detectors and Associated Equipment* 542, no. 1 (2005): 134-141.

8. Siegel J. B., McKay D. A., Stefanopoulou A. G., Hussey D. S., and Jacobson D. L. "Measurement of liquid water accumulation in a PEMFC with dead-ended anode." *Journal of the Electrochemical Society* 155, no. 11 (2008): B1168-B1178.

9. Mehta V., and Cooper J.S. "Review and analysis of PEM fuel cell design and manufacturing." *Journal of Power Sources* 114, no. 1 (2003): 32-53.

10. Scheirs J., *Modern Fluoropolymers*, Wiley, New York, (1997).

11. Ameduri B., and Boutevin B. "Update on fluoroelastomers:from perfluoroelastomers to fluorosilicones and fluorophosphazenes." *Journal of fluorine chemistry* 126, no. 2 (2005): 221-229.

12. Nasef M.M., and Hegazy E.A. "Preparation and applications of ion exchange membranes by radiation-induced graft copolymerization of polar monomers onto non-polar films." *Progress in Polymer Science* 29, no. 6 (2004): 499-561.

13. Chapiro A., Derai G., and Jendrychowska-Bonamour A-M "Grafting of acrylic acid and styrene on poly(tetrafluoroethylene) films preirradiated in air" *European Polymer Journal* 7, no. 11 (1971): 1595-1613.

14. Chen J., Asano M., Yamaki T. and Yoshida M., "Preparation of sulfonated crosslinked PTFE-*g*-poly (alkyl vinyl ether) membranes for polymer electrolyte membrane fuel cells by radiation processing." *Journal of Membrane Science* 256, no. 1-2 (2005):38-45.

15. Gupta B., and Scherer G. G. "Proton exchange membranes by radiation grafting of styrene onto FEP films. I. Thermal characteristics of copolymer membranes." *Journal of Applied Polymer Science* 50, no. 12 (1993): 2129-2134.

16. Rouilly M. V., Kötz E. R., Haas O., Scherer G. G., and Chapiro A. "Proton exchange membranes prepared by simultaneous radiation grafting of styrene onto Teflon-FEP films. Synthesis and characterization." *Journal of Membrane Science* 81, no. 1 (1993): 89-95.

17. Gupta B., Büchi F. N., and Scherer G. G. "Cation exchange membranes by pre-irradiation grafting of styrene into FEP films. I. Influence of synthesis conditions." *Journal of Polymer Science Part A: Polymer Chemistry* 32, no. 10 (1994): 1931-1938.

18. Büchi F. N., Gupta B., Haas O., and Scherer G.G. "Study of radiation-grafted FEP-g-polystyrene membranes as polymer electrolytes in fuel cells." *Electrochimica Acta* 40, no. 3 (1995): 345-353.

19. Nasef M. M., Saidi H., Nor M.H., Dahlan M., and Hashim K. "Cation exchange membranes by radiation induced graft copolymerization of styrene onto PFA copolymer films. I. Preparation and characterization of the graft copolymer." *Journal of Applied Polymer Science* 73, no. 11 (1999): 2095-2102.

20. Cardona F., George G. A., Hill D. J. T., and Perera S. "Spectroscopic study of the penetration depth of grafted polystyrene onto poly (tetrafluoroethylene-co-perfluoropropylvinylether) substrates. 1. Effect of grafting conditions." *Journal of Polymer Science Part A: Polymer Chemistry* 40, no. 19 (2002): 3191-3199.

21. Walsby N., Paronen M., Juhanoja J., Sundholm F. "Radiation grafting of styrene onto poly (vinylidene fluoride) films in propanol: the influence of solvent and synthesis conditions." *Journal of Polymer Science Part A: Polymer Chemistry* 38, no. 9 (2000): 1512-1519.

22. Hietala S, Maunu S.L., and Sundholm F."Structure of styrene grafted poly (vinylidene fluoride) membranes investigated by solid-state NMR." *Macromolecules* 32, no. 3 (1999): 788-791.

23. Brack, H. P., Buchi F. N., Huslage J., Rota M, and Scherer G. G. "Development of radiation-grafted membranes for fuel cell applications based on poly (ethylene-alt-tetrafluoroethylene)." In *ACS Symposium Series*, vol. 744, pp. 174-188. Washington, DC; American Chemical Society;2000.

24. Aricò A. S., Baglio V., Cretı P., Blasi Di A., Antonucci V., Brunea J., Chapotot A., Bozzi A., and Schoemans J. "Investigation of grafted ETFE-based polymer membranes as alternative electrolyte for direct methanol fuel cells." *Journal of Power Sources* 123, no. 2 (2003): 107-115.

25. Sugiyama S., Tsuneda S., Saito K., Furusaki S., Takanobu S., and Makuuchi K. "Attachment of sulfonic acid groups to various shapes of polyethylene, polypropylene and polytetrafluoroethylene by radiation-induced graft polymerization." *Reactive Polymers* 21, no. 3 (1993): 187-191.

26. Forsythe, J. S., and D. J. T. Hill. "The radiation chemistry of fluoropolymers." *Progress in Polymer Science* 25, no. 1 (2000): 101-136.

27. Clegg D. W. and Collyer A. A., "Irradiation effects on polymers", Elsevier,(1991)

28. Brack H-P., and Scherer G. G. "Modification and characterization of thin polymer films for electrochemical applications." *In Macromolecular Symposia*, vol. 126, no. 1, pp. 25-49. Hüthig & Wepf Verlag, 1998.

29. Horsfall J. A. and Lovell K. V. "Synthesis and characterization of sulfonic acid-containing ion exchange membranes based on hydrocarbon and fluorocarbon polymers." *European Polymer Journal* 38, no. 8 (2002): 1671-1682.

30. Qingfeng L. , He R., Jensen J. O., and Bjerrum N. J.. "Approaches and recent development of polymer electrolyte membranes for fuel cells operating above 100 C." *Chemistry of Materials* 15, no. 26 (2003): 4896-4915.

31. Qingfeng L., Jensen J. O., Savinell R. F., and Bjerrum N. J. "High temperature proton exchange membranes based on polybenzimidazoles for fuel cells." *Progress in Polymer Science* 34, no. 5 (2009): 449-477.

32. Gürsel Alkan S., Gubler L., Gupta B., and Scherer G. G."Radiation grafted membranes." In *Fuel Cells I*, pp. 157-217. Springer Berlin Heidelberg, 2008.

33. Gubler, L., Alkan Gürsel S., and Scherer G. G. "Radiation grafted membranes for polymer electrolyte fuel cells." *Fuel Cells* 5, no. 3 (2005): 317-335.

34. Gubler, L., Prost N., Alkan Gürsel S., and Scherer G.G. "Proton exchange membranes prepared by radiation grafting of styrene/divinylbenzene onto poly (ethylene-*alt*-tetrafluoroethylene) for low temperature fuel cells." *Solid State Ionics* 176, no. 39 (2005): 2849-2860.

35. Gürsel Alkan S., Yang Z., Choudhury B., Roelofs M. G., and Scherer G. G. "Radiation-grafted membranes using a trifluorostyrene derivative." *Journal of the Electrochemical Society* 153, no. 10 (2006): A1964-A1970.

36. Gubler L., Alkan Gürsel S., Wokaun A., and Günther G. Scherer. "Cross-linker effect in ETFE-based radiation-grafted proton-conducting membranes I. Properties and fuel cell performance characteristics." *Journal of the Electrochemical Society* 155, no. 9 (2008): B921-B928.

37. Schmidt C., and Schmidt-Naake G.. "Proton Conducting Membranes Obtained by Doping Radiation-Grafted Basic Membrane Matrices with Phosphoric Acid." *Macromolecular Materials and Engineering* 292, no. 10-11 (2007): 1164-1175.

38. Brack H.-P., Bührer H. G., Bonorand L., and Scherer G. G. "Grafting of pre-irradiated poly (ethylene-alt-tetrafluoroethylene) films with styrene: influence of base polymer film properties and processing parameters." *Journal of Materials Chemistry* 10, no. 8 (2000): 1795-1803.

39. Chapiro A., Radiation Chemistry of Polymeric Systems; Wiley-Interscience: New York, 1962.

40. Rabie A. M., Aly M. I., Hegazy E. S. A.; El-Awady N. I. "Radiation-induced graft polymerization of 4-vinylpyridine on polyethylene" Polymer Journal, 11, (1979): 359

41. Dessouki A. M., Hegazy E. S. A., El-Dessouky M. M., and El-Sawy N. M. "Anionic membranes obtained by radiation grafting of 4-vinylpyridine onto poly (vinyl chloride)." *Radiation Physics and Chemistry (1977)* 26, no. 2 (1985): 157-163.

42. Yang J-M., and Hsiue G.-H. "Radiation-induced graft polymerization of 4-vinyl pyridine to styrene–butadiene–styrene triblock copolymer." *Journal of Applied Polymer Science* 39, no. 7 (1990): 1475-1484.

43. Rath S. K., Palai A., Rao S., Chandrasekhar L., and Patri M. "Effect of solvents in radiation-induced grafting of 4-vinyl pyridine onto fluorinated ethylene propylene copolymer." *Journal of Applied Polymer Science* 108, no. 6 (2008): 4065-4071.

44. Dessouki A. M., Hegazy E. S. A., El-Dessouky M. M., and El-Sawy N. M. "Anionic membranes obtained by radiation grafting of 4-vinylpyridine onto poly (vinyl chloride)." *Radiation Physics and Chemistry* 26, no. 2 (1985): 157-163.

45. Hegazy E. A.; Mokhtar S. M, Osman M. B. S., Mostafa, A.E.B. Radiation Physics and Chemistry 1990, 36, 365.

46. Hegazy E. S. A., Mokhtar S. M., Osman M.B.S, Mostafa A. E. B. *Polymer* 33, no:22 (1992), 4230

47. Dessouki, A. M., Taher N. H., and El-Arnaouty M. B. "Synthesis of permselective membranes by radiation-induced grafting of N-vinylpyrrolidone onto poly (tetrafluoroethylene–hexafluoropropylene–vinylidene fluoride) (TFB) films." *Polymer international* 48, no. 2 (1999): 92-98.

48. Al Sagheer F. A., and El-Sawy N. M. "Investigation of radiation-grafted and radiation-modified N-vinyl-2-pyrrolidone onto polypropylene film." *Journal of applied polymer science* 76, no. 3 (2000): 282-289.

49. Kaur I., Kumar S., Misra B. N., Chauhan, G. S., *Material science and engineering*, no: A 270 (1990) , 137.

50. Kaur I., Kumar S., Chauhan G. S., Misra B. N., *Journal of applied polymer science* no: 99 (2006) , 1415.

51. Walsby N., Paronen M., Juhanoja J., Sundholm F., "Radiation grafting of styrene onto poly (vinylidene fluoride) films in propanol: the influence of solvent and synthesis conditions." *Journal of Polymer Science Part A: Polymer Chemistry* 38, no. 9 (2000): 1512-1519.

52. Nasef M. M., "Effect of solvents on radiation-induced grafting of styrene onto fluorinated polymer films." *Polymer International* 50, no. 3 (2001): 338-346.

53. Kang K., Kang P.H., and Nho Y. C. "Preparation and characterization of a proton-exchange membrane by the radiation grafting of styrene onto polytetrafluoroethylene films." *Journal of Applied Polymer Science* 99, no. 4 (2006): 1415-1428.

54. Kimura Y., Asano M., Chen J., Maekawa Y., Katakai R., Yoshida M., *Radiation Physics and Chemistry*, 77 (2008), 864.

55. Bozzi A., Chapiro A., *Radiation Physics and Chemistry,* 1988, 32,193.

56. Brandrup J., Immergut E. H. (eds). Polymer Handbook; Wiley Interscience Publications: New York, 1989.

57. Howard G. L., Lai S. H., *Journal of Polymer Science and Chemistry*, eds:1979, 17, 378

58. Gürsel, S. A., Ben youcef H., Wokaun A., Scherer G. G., *Nuclear Instrument and Methods in Physical Research B* , 265(1) (2006); 198

59. Rudin A, *The Elements of Polymer Science and Engineering*; Academic Press: New York, 1982.

60. Arichi, S., Matsurra, H.,Tanimoto, Y., Bull M., H., Chemical Society of Japan, 39, (1966): 434.

61. Nasef M. M., Saidi H., Dahlan K. M. Z., Radiation Physical Chemistry, 68 (2003), 875.

62. Socrates G. Infrared Characteristics Group Frequencies, Tables and Charts; John Wiley & Sons: Chichester, 1994.

63. Starkweather H. W. "Internal motions in an alternating copolymer of ethylene and tetrafluoroethylene." *Journal of Polymer Science: Polymer Physics Edition* 11, no. 3 (1973): 587-593.

64. Feng J., and Chan C.-M. "Compatibility and properties of alternating ethylene-tetrafluoroethylene copolymer and poly (methyl methacrylate) blends." *Polymer* 38, no. 26 (1997): 6371-6378.

65. Saarinen V., Karesoja M., Kallio T., Paronen M., and Kontturi K. "Characterization of the novel ETFE-based membrane." *Journal of Membrane Science* 280, no. 1 (2006): 20-28.

66. Stambouli A.B, Traversa E. "Solid oxide fuel cells (SOFCs): a review of an environmentally clean and efficient source of energy." *Renewable Sustainable Energy Rev* 6 , no. 5, (2002): 433–455

67. Wang J-T., Savinell R. F., Wainright J., Litt M., and Yu H. "A H_2O_2 fuel cell using acid doped polybenzimidazole as polymer electrolyte." *Electrochimica Acta* 41, no. 2 (1996): 193-197.

68. Gubler, L., Alkan Gürsel S., and Scherer G. G. "Radiation grafted membranes for polymer electrolyte fuel cells." *Fuel Cells* 5, no. 3 (2005): 317-335.

69. Li Q., Jensen J.O., Noye P.P., Pan C. and Bjerrum N. J., *Proceed. 26th Int. Symp. Mat. Sci.: Solid State Electrochem.*, (2005):267.

70. Schmidt C, and Schmidt-Naake G. "Proton Conducting Membranes Obtained by Doping Radiation-Grafted Basic Membrane Matrices with Phosphoric Acid." *Macromolecular Materials and Engineering* 292, no. 10-11 (2007): 1164-1175.

71. Nasef M. M., Shamsaei E., Saidi H., Ahmad A., and Dahlan K. Z. M. "Preparation and characterization of phosphoric acid composite membrane by radiation induced grafting of 4-vinylpyridine onto poly (ethylene-co-tetrafluoroethylene) followed by phosphoric acid doping." *Journal of Applied Polymer Science* 128, no. 1 (2013): 549-557.

72. Li, Q., He R., Jensen J. O., and Bjerrum N. J. "PBI-Based Polymer Membranes for High Temperature Fuel Cells–Preparation, Characterization and Fuel Cell Demonstration." *Fuel Cells* 4, no. 3 (2004): 147-159.

73. Teena S., and Rattana S. "Graft-copolymerization of N-vinyl-2-pyrrolidone onto isotactic polypropylene film by gamma radiation using peroxidation method." *Indian Journal of Pure & Applied Physics* 48 (2010): 823-829.

74. Kaur I, Kumar S., Misra B. N., and Chauhan G. S. "Graft copolymerization of 2-vinyl pyridine and styrene onto isotactic polypropylene powder by the preirradiation method." *Materials Science and Engineering: A* 270, no. 2 (1999): 137-144.

125

75. Skou E., Kauranen P., and Hentschel J. "Water and methanol uptake in proton conducting Nafion$^{®}$ membranes." *Solid State Ionics* 97, no. 1 (1997): 333-337.

76. Gürsel Alkan, S., Wokaun A., and Scherer G. G. "Influence of reaction parameters on grafting of styrene into poly (ethylene-*alt*-tetrafluoroethylene) films." *Nuclear Instruments and Methods in Physics Research Section B: Beam Interactions with Materials and Atoms* 265, no. 1 (2007): 198-203.

77. Nasef M. M. and Hegazy E.S.A. "Preparation and applications of ion exchange membranes by radiation-induced graft copolymerization of polar monomers onto non-polar films." Progress in Polymer Science 29, no. 6 (2004): 499-561

78. Gubler L., Prost N., Alkan Gürsel S., and Scherer G. G.. "Proton exchange membranes prepared by radiation grafting of styrene/divinylbenzene onto poly (ethylene-*alt*-tetrafluoroethylene) for low temperature fuel cells." *Solid State Ionics* 176, no. 39 (2005): 2849-2860.

79. Kaur I., Misra B. N., and Kohli A. "Synthesis of Teflon-FEP grafted membranes for use in water desalination." *Desalination* 139, no. 1 (2001): 357-365.

80. He, R., Li Q., Bach A., Jensen J. O., and Bjerrum N. J. "Physicochemical properties of phosphoric acid doped polybenzimidazole membranes for fuel cells." *Journal of Membrane Science* 277, no. 1 (2006): 38-45.

81. Kerres J., Ullrich A., Meier F., and Häring T. "Synthesis and characterization of novel acid–base polymer blends for application in membrane fuel cells." *Solid State Ionics* 125, no. 1 (1999): 243-249.

82. Staiti P., Lufrano F., Arico A. S., Passalacqua E., and Antonucci V. "Sulfonated polybenzimidazole membranes preparation and physico-chemical characterization." *Journal of Membrane Science* 188, no. 1 (2001): 71-78.

83. Li Q., Jensen J. O., Savinell R. F., and Bjerrum N.J. "High temperature proton exchange membranes based on polybenzimidazoles for fuel cells." *Progress in Polymer Science* 34, no. 5 (2009): 449-477.

84. Xing B., and Savadogo O. "The effect of acid doping on the conductivity of polybenzimidazole (PBI)." Journal of New Materials for Electrochemical Systems 2 (1999): 95-102.

85. Kawahara M., Morita J., Rikukawa M., Sanui K., and Ogata N., *Electrochim. Acta* 45, (2000):1395-1398.

86. Bouchet R., Miller S., Duclot M., and Souquet J. "A thermodynamic approach to proton conductivity in acid-doped polybenzimidazole." *Solid State Ionics* 145, no. 1 (2001): 69-78.

87. Kreuer K. D. "On the complexity of proton conduction phenomena." *Solid state ionics* 136 (2000): 149-160.

88. Kreuer K.-D. "On Solids with Liquidlike Properties and the Challenge To Develop New Proton-Conducting Separator Materials for Intermediate-Temperature Fuel Cells." *ChemPhysChem* 3, no. 9 (2002): 771-775.

89. Ma Y-L., Wainright J. S., Litt M. H., and Savinell R. F. "Conductivity of PBI membranes for high-temperature polymer electrolyte fuel cells." *Journal of the Electrochemical Society* 151, no. 1 (2004): A8-A16.

90. Glipa X., Bonnet B., Mula B., Jones D. J., and Rozière J. "Investigation of the conduction properties of phosphoric and sulfuric acid doped polybenzimidazole." *Journal of Materials Chemistry* 9, no. 12 (1999): 3045-3049.

91. Bouchet R., and Siebert E. "Proton conduction in acid doped polybenzimidazole." *Solid State Ionics* 118, no. 3 (1999): 287-299.

92. Wainright J. S., Wang J-T., Weng D., Savinell R. F., and Litt M. "Acid-Doped Polybenzimidazoles: A New Polymer Electrolyte." *Journal of the electrochemical society* 142, no. 7 (1995): L121-L123.

93. He R., Qingfeng L., Xiao G., and Bjerrum N. J. "Proton conductivity of phosphoric acid doped polybenzimidazole and its composites with inorganic proton conductors." *Journal of Membrane Science* 226, no. 1 (2003): 169-184.

94. Peron J., Mani A., Zhao X., Edwards D., Adachi M., Soboleva T., Shi Z., Xie Z., Navessin T., and Holdcroft S. "Properties of Nafion® NR-211 membranes for PEMFCs." *Journal of Membrane Science* 356, no. 1 (2010): 44-51.

95. Alkan Gürsel S., Yang Z., Choudhury B., Roelofs M. G., and Scherer G. G.. "Radiation-grafted membranes using a trifluorostyrene derivative." *Journal of the Electrochemical Society* 153, no. 10 (2006): A1964-A1970.

96. Yuyan S., Yin G., Wang Z., and Gao Y. "Proton exchange membrane fuel cell from low temperature to high temperature: material challenges." *Journal of Power Sources* 167, no. 2 (2007): 235-242.

97. Li Q., Hjuler A. H., and Bjerrum N. J. "Phosphoric acid doped polybenzimidazole membranes: physiochemical characterization and fuel cell applications." *Journal of Applied Electrochemistry* 31, no. 7 (2001): 773-779.

98. Donoso P., Gorecki W., Berthier C., Defendini F., Poinsignon C., and Armand M. B. "NMR, conductivity and neutron scattering investigation of ionic dynamics in the anhydrous polymer protonic conductor PEO (H3PO4) *Solid State Ionics* 28 (1988): 969-974.

99. Daniel M. F., Desbat B., and Lassegues J. C. "Solid state protonic conductors: complexation of poly (ethylene oxide) or poly (acrylic acid) with NH4HSO4*Solid State Ionics* 28 (1988): 632-636.

100. Grondin J., Rodriguez D., and Lassegues J. C. "Proton conducting polymer electrolyte-The Nylon 6–10/H_3PO_4 blends." *Solid State Ionics* 77 (1995): 70-75.

101. Yuichi A, and Sonai A. "Novel proton conducting polymer electrolytes based on polyparabanic acid doped with H_3PO_4 for high temperature fuel cell." *Journal of power sources* 163, no. 1 (2006): 60-65.

102. Ben youcef H., Alkan Gürsel, S., Buisson, A., Gubler, L., Wokaun, A. and Scherer, G. G. (2010), Influence of Radiation-Induced Grafting Process on Mechanical Properties of ETFE-Based Membranes for Fuel Cells. Fuel Cells, 10: 401–410

103. V. Shah, *Handbook of Plastics Testing and Failure Analysis*, John Wiley & Sons, New York, **2007**, 17-38

104. Gubler L., Beck N., Alkan Gursel S., Hajbolouri F., Kramer D., Reiner A., Steiger B. "Materials for polymer electrolyte fuel cells." *CHIMIA International Journal for Chemistry* 58, no. 12 (2004): 826-836.

105. Alkan Gürsel S., Gubler L., Gupta B.G., Scherer G. G., Radiation grafted membranes, *Fuel Cells 1*, Springer-Verlag, Berlin, **2008**, 157-217.

106. Tang Y., Karlsson A.M., Santare M. H., Gilbert M., Cleghorn S., and Johnson W. B. "An experimental investigation of humidity and temperature effects on the mechanical properties of perfluorosulfonic acid membrane." *Materials Science and Engineering: A* 425, no. 1 (2006): 297-304.

107. Nafion.can be found under www.dupont.com/FuelCells/en_US/products/nafion , 2012

108. Yeo R. S., Chan S. F., and Lee J. "Swelling behavior of Nafion and radiation-grafted cation exchange membranes." *Journal of Membrane Science* 9, no. 3 (1981): 273-283.

109. Rikukawa M., Inagaki D., Kaneko K., Takeoka Y., Ito I., Kanzaki Y., and Sanui K. "Proton conductivity of smart membranes based on hydrocarbon polymers having phosphoric acid groups." *Journal of molecular structure* 739, no. 1 (2005): 153-161.

110. Brack H.-P., Ruegg D., Bührer H., Slaski M., Alkan S., and Scherer G. G. "Differential scanning calorimetry and thermogravimetric analysis investigation of the thermal properties and degradation of some radiation-grafted films and membranes." *Journal of Polymer Science Part B: Polymer Physics* 42, no. 13 (2004): 2612-2624.

111. Gürsel Alkan S., Schneider J., Ben Youcef H., Wokaun A., and Scherer G. G. "Thermal properties of proton-conducting radiation-grafted membranes." *Journal of Applied Polymer Science* 108, no. 6 (2008): 3577-3585.

112. Pukrushpan J. T., Stefanopoulou A. G., and Peng H., *Control of Fuel Cell Power Systems: Principles, Modeling, Analysis and Feedback Design*. New York: Springer, 2000.

113. Kimball E, Whitaker T., Kevrekidis Y. G., and Benziger J.B. "Drops, slugs, and flooding in polymer electrolyte membrane fuel cells." *AIChE Journal* 54, no. 5 (2008): 1313-1332.

114. Zhang F. Y., Yang X. G., and Wang C. Y. "Liquid water removal from a polymer electrolyte fuel cell." *Journal of the Electrochemical Society* 153, no. 2 (2006): A225-A232.

115. Kumbur, E. C., Sharp K. V., and Mench M. M. "Liquid droplet behavior and instability in a polymer electrolyte fuel cell flow channel." *Journal of Power Sources* 161, no. 1 (2006): 333-345.

116. Bonville L. J., Kunz H. R., Song Y., Mientek A., Minkmas W., Ching A., and Fenton J.M. "Development and demonstration of a higher temperature PEM fuel cell stack." *Journal of power sources* 144, no. 1 (2005): 107-112.

117. Lee H.-J., Kim B. G., Lee D. H., Park S. J., Kim Y., Lee J. W., Henkensmeier D. "Demonstration of a 20 W class high-temperature polymer electrolyte fuel cell stack with novel fabrication of a membrane electrode assembly." *International Journal of Hydrogen Energy* 36, no. 9 (2011): 5521-5526.

118. Lobato J, Cañizares P., Rodrigo M. A., Linares J. J., and Pinar F. J. "Study of the influence of the amount of PBI–H_3PO_4 in the catalytic layer of a high temperature PEMFC." *International Journal of Hydrogen Energy* 35, no. 3 (2010): 1347-1355.

119. Matsuura T., Siegel J.B, Chen J., and Stefanopoulou A. G. "Multiple degradation phenomena in polymer electrolyte fuel cell operation with dead-ended anode." In *Proceedings of ASME 2011 5th International Conference on Energy Sustainability & 9th Fuel Cell Science, Engineering and Technology Conference, ESFuelCell2011-54344*. 2011.

120. Wu J., Yuan X. Z., Martin J. J., Wang H., Zhang J., Shen J., Wu S., and Merida W. "A review of PEM fuel cell durability: degradation mechanisms and mitigation strategies." *Journal of Power Sources* 184, no. 1 (2008): 104-119.

121. Zhai Y., Zhang H., Liu G., Hu J., and Yi B. "Degradation Study on MEA in H3PO4/ PBI High Temperature PEMFC Life Test." *Journal of the Electrochemical Society* 154, no. 1 (2007): B72-B76.

122. Liu G, Zhang H., Hu J., Zhai Y., Xu D., and Shao Z. "Studies of performance degradation of a high temperature PEMFC based on H_3PO_4 doped PBI." *Journal of Power Sources* 162, no. 1 (2006): 547-552.

123. Hu J, Zhang H., Zhai Y., Liu G., Hu J., and Yi B. "Performance degradation studies on PBI/H_3PO_4 high temperature PEMFC and one-dimensional numerical analysis." *Electrochimica Acta* 52, no. 2 (2006): 394-401.

124. Yu S., Xiao L., and Benicewicz B. C. "Durability Studies of PBI-based High Temperature PEMFCs." *Fuel Cells* 8, no. 3-4 (2008): 165-174.

125. Wannek C., Kohnen B., Oetjen H-F., Lippert H., and Mergel J. "Durability of ABPBI-based MEAs for High Temperature PEMFCs at Different Operating Conditions." *Fuel Cells* 8, no. 2 (2008): 87-95.

126. Mocoteguy Ph, Ludwig B., Scholta J., Nédellec Y., Jones D. J., and Rozière J. "Long-Term Testing in Dynamic Mode of HT-PEMFC H3PO4/PBI Celtec-P Based Membrane Electrode Assemblies for Micro-CHP Applications." *Fuel Cells* 10, no. 2 (2010): 299-311.

127. Lin H. L., Hsieh Y. S., Chiu C. W, Yu T. L., and Chen L. C. "Durability and stability test of proton exchange membrane fuel cells prepared from polybenzimidazole/poly (tetrafluoro ethylene) composite membrane." *Journal of Power Sources* 193, no. 1 (2009): 170-174.

128. Cheng X., Zhang J., Tang Y., Song C., Shen J., Song D., and Zhang J. "Hydrogen crossover in high-temperature PEM fuel cells." *Journal of power sources* 167, no. 1 (2007): 25-31.

129. Mattsson B., Ericson H., Torell L. M., and Sundholm F. "Degradation of a fuel cell membrane, as revealed by micro-Raman spectroscopy." *Electrochimica acta* 45, no. 8 (2000): 1405-1408.

130. Nasef M. M. and Saidi H."Post-mortem analysis of radiation grafted fuel cell membrane using X-ray photoelecton spectroscopy." *Journal of New Materials for Electrochemical Systems* 5 (2002).

131. Nasef M. M., and Saidi H."Post-mortem analysis of radiation grafted fuel cell membrane by XPS. New materials for electrochemical systems" IV. Extended abstracts of the fourth international symposium on new materials for electrochemical systems; (2001): 358–60.

132. Büchi F. N., Gupta B., Haas O., and Scherer G. G. "Study of radiation-grafted FEP-g-polystyrene membranes as polymer electrolytes in fuel cells." *Electrochimica Acta* 40, no. 3 (1995): 345-353.

133. Gubler L., Kuhn H., Schmidt T. J., Scherer G. G., Brack H-P., and Simbeck K. "Performance and durability of membrane electrode assemblies based on radiation-grafted FEP-g-polystyrene membranes." *Fuel Cells* 4, no. 3 (2004): 196-207.

134. Mathias S., Knöri T., Schneider A., and Gülzow E. "Degradation of sealings for PEFC test cells during fuel cell operation." *Journal of Power Sources* 127, no. 1 (2004): 222-229.

135. Ming C. H., and Chang M. H. "Effects of Assembly Pressure on the Gas Diffusion Layer and Performance of a PEM Fuel Cell." *Applied Mechanics and Materials* 110 (2012): 48-52.

136. McKay D. A., Stefanopoulou A G., and Cook J. "A membrane-type humidifier for fuel cell applications: Controller design, analysis and implementation." In *ASME Conference Proceedings*, no. 43181, pp. 841-850. 2008.

137. Wang C.-Y. "Fundamental models for fuel cell engineering." Chemical Reviews 104, no. 10 (2004): 4727-4766.

138. Bıyıkoğlu A. "Review of proton exchange membrane fuel cell models." *International Journal of Hydrogen Energy* 30, no. 11 (2005): 1181-1212.

139. Moçotéguy Ph., Druart F., Bultel Y., Besse S., and Rakotondrainibe A. "Monodimensional modeling and experimental study of the dynamic behavior of proton exchange membrane fuel cell stack operating in dead-end mode." *Journal of power sources* 167, no. 2 (2007): 349-357.

140. Dumercy L., Péra M-C., Glises R., Hissel D., Hamandi S., Badin F., and Kauffmann J-M. "PEFC stack operating in anodic dead end mode." *Fuel Cells* 4, no. 4 (2004): 352-357.

141. Kocha S., Yang D. J., and Yi J. S. "Characterization of gas crossover and its implications in PEM fuel cells." *AIChE journal* 52, no. 5 (2006): 1916-1925.

142. Ahluwalia R. K., and Wang X. "Fuel cell systems for transportation: Status and trends." *Journal of power sources* 177, no. 1 (2008): 167-176.

143. McKay D. A., Jason B. S., Ott W., and Stefanopoulou A. G. "Parameterization and prediction of temporal fuel cell voltage behavior during flooding and drying conditions." *Journal of Power Sources* 178, no. 1 (2008): 207-222.

144. Yeşilyurt S., Siegel J. B., and Stefanopoulou A.G. "Modeling and experiments of voltage transients of PEM fuel cells with the dead-ended anode." Journal of Fuel Cell Science and Technology (2011).

145. Bird R.B., Stewart W.E., Lightfoot E.N., Transport Phenomena, second ed., Wiley, New York, (2002).

146. Ge S., Li X., Yi B., and Hsing I.-M. "Absorption, desorption, and transport of water in polymer electrolyte membranes for fuel cells." *Journal of The Electrochemical Society* 152, no. 6 (2005): A1149-A1157.

147. Newman J., Thomas-Alyea K.E., Electrochemical Systems. 3rd edition, John Wiley & Sons, New York, (2004).

148. Springer T., Zawodzinski A., and Gottesfeld S., "Polymer electrolyte fuel cell model." *Journal of the Electrochemical Society* 138, no. 8 (1991): 2334-2342.

149. Gostick J. T., Fowler M. W., Ioannidis M.A., Pritzker M.D., Volfkovich Y. M., and Sakars A. "Capillary pressure and hydrophilic porosity in gas diffusion layers for polymer electrolyte fuel cells." *Journal of Power Sources* 156, no. 2 (2006): 375-387.

150. Pasaogullari U., and Wang C.-Y. "Two-phase transport and the role of micro-porous layer in polymer electrolyte fuel cells." *Electrochimica Acta* 49, no. 25 (2004): 4359-4369.

151. Wang X., and T. Van Nguyen. "Modeling the effects of the microporous layer on the net water transport rate across the membrane in a PEM fuel cell." *Journal of The Electrochemical Society* 157, no. 4 (2010): B496-B505.

152. Adachi M., Romero T., Navessin T., Xie Z., Shi Z., Mérida W., and Holdcroft S. "Water permeation through catalyst-coated membranes." *Electrochemical and Solid-State Letters* 13, no. 6 (2010): B51-B54.

153. Jixin C. "Experimental study on the two phase flow behavior in PEM fuel cell parallel channels with porous media inserts." *Journal of Power Sources* 195, no. 4 (2010): 1122-1129.

154. Wang Z. H., Wang C. Y., and Chen K. S. "Two-phase flow and transport in the air cathode of proton exchange membrane fuel cells." *Journal of Power Sources* 94, no. 1 (2001): 40-50

155. Benziger J., Nehlsen J., Blackwell D., Brennan T., and Itescu J. "Water flow in the gas diffusion layer of PEM fuel cells." *Journal of Membrane Science* 261, no. 1 (2005): 98-106.

156. Zhang L., Bi X. T., Wilkinson D. P., Anderson R., Stumper J., and Wang H. "Gas–liquid two-phase flow behavior in minichannels bounded with a permeable wall." *Chemical Engineering Science* 66, no. 14 (2011): 3377-3385.

157. Hartnig C., Manke I., Kuhn R., Kardjilov N., Banhart J., and Lehnert W. "Cross-sectional insight in the water evolution and transport in polymer electrolyte fuel cells." *Applied Physics Letters* 92, no. 13 (2008): 134106-134106.

158. Gurau V., and Mann J. A. "Effect of interfacial phenomena at the gas diffusion layer-channel interface on the water evolution in a PEMFC." *Journal of The Electrochemical Society* 157, no. 4 (2010): B512-B521.

159. Gauthier E., Duan Q., Hellstern T., and Benziger J. "Water Flow in, Through, and Around the Gas Diffusion Layer." *Fuel Cells* 12, no. 5 (2012): 835-847.

160. Noye P., Li Q., Pan C., and Bjerrum N. J. "Cross-linked polybenzimidazole membranes for high temperature proton exchange membrane fuel cells with dichloromethyl phosphinic acid as a cross-linker." *Polymers for advanced technologies* 19, no. 9 (2008): 1270-1275.

161. DOE, "Hydrogen and fuel cell activities, progress, and plans," DOE, Tech.Rep., 2009. [Online]. Available: http://www.hydrogen.energy.gov/pdfs/epact report sec811.pdf

162. Işıkel Şanlı, L., Alkan Gürsel S. "Synthesis and characterization of novel graft copolymers by radiation-induced grafting." *Journal of Applied Polymer Science*, no: 120 (2011): 2313-2323.